Transport phenomena in the presence of curvature and torsion: from cosmology to functional materials

Sébastien Fumeron

French habilitation thesis to supervise research

Université de Lorraine

Defended publicly on 04/03/2022, by :

Sébastien Fumeron

Transport phenomena in the presence of curvature and torsion

From cosmology to functional materials

Examined by a committee constituted of :

Oleg LAVRENTOVICH Trustees Research Professor, Kent State University, USA	**Referee**
Patrick PETER CNRS Senior Researcher, Institut d'Astrophysique de Paris, France	**Referee**
Silke WEINFURTNER Royal Society University Research Fellow, University of Nottingham, UK	**Referee**
Bertrand BERCHE Professor, Université de Lorraine, France	**Examiner**
Etienne BRASSELET CNRS Senior Researcher, Université de Bordeaux, France	**Examiner**
Karl JOULAIN Professor, Institut Pprime, France	**Examiner**
Fernando MORAES Professor, Universidade Federal Rural de Pernambuco, Brazil	**Invited**

Contents

Acknowledgements

First of all, my sincere thanks go to my two colleagues and friends, Fernando Moraes and Bertrand Berche. Fernando is probably my longest-term collaborator. Both his scientific background, his out-of-the-box creative thinking and his unfailing friendship have been essential to me and will continue to be. Bertrand welcomed me in the former Statistical Physics group of Institut Jean Lamour in 2018. We got along instantly and eversince, he has been my closest collaborator. His huge scientific culture, his insatiable curiosity and his many personal commitments are great sources of inspiration for me.

I would like to thank this committee for accepting to examine my works and for attending this defense, despite a particularly challenging context. Special acknowledgements to the rapporteurs, Pr and to Pr for their insightful comments on this manuscript.

I would also like to thank my fellow labmates, Christophe Chatelain, Thierry Gourieux and Dragi Karevski, for the stimulating discussions not only on physics, but on epistemology, history, martial arts, philosophy, politics... I have experienced no other place as nourishing for the mind as LPCT.

Last but not the least, I would like to thank my partner and my daughter for their love and comprehension all along these years. My final thoughts go to my beloved parents, who supported me and believed in me their whole life.

Notations

Einstein summation convention over repeated indices is used. Greek letters $\mu, \nu, \rho...$ are used for the holonomic indices and they run from 0 to 3: 0 is kept for the time component, $i, j, k... = 1, 2, 3$ are reserved for the remaining variables (space, angle...). Following the Schouten convention, we use the first latin letters $a, b, c... = 0, 1, 2, 3$ for the anholonomic indices. The metric signature is taken in the Pauli (or "East Coast") convention as $(-, +, +, +)$. Most of the time, we will also use units for which $c = 1$, as customary done in general relativity.

1 Introduction

In a famous article entitled *On the physical lines of forces* (1883), James Clerk Maxwell developed a mathematical model for what we now call field lines. He accounted that all along, his research was led by «*some method of investigation which allows the mind at every step to lay hold of a clear physical conception, without being committed to any theory founded on the physical science from which that conception is borrowed [...]. In order to obtain physical ideas without adopting a physical theory we must make ourselves familiar with the existence of physical analogies. By a physical analogy [we] mean that partial similarity between the laws of one science and those of another which makes each of them illustrate the other. [...] [We] find the same resemblance in mathematical form between two different phenomena* »[1]. Maxwell is not an isolated example and many contributions in modern physics have been steered by formal analogies, such as for instance

- Yukawa's theory on nuclear forces, built in direct analogy with quantum electrodynamics [2], the newborn meson substituting for the photon and the neutron-proton exchange current playing the role of the electric current,
- Fermi's theory on beta decay [3]-[4], where the emission of light particles from a nucleus was explained in analogy with the emission of photons from an excited atom returning to its fundamental state,
- Nambu and Jona-Lasinio's mechanism for nucleons [5], accounting how interacting fermionic systems induce spontaneous symmetry breaking and dynamically generate mass, in a similar fashion to the Bardeen-Cooper-Schrieffer mechanism in superconductors.
- Wilson's use of the renormalization group for the strong interactions, based on the self-similar behavior occurring near second-order phase transitions and the self-similar short-distance behavior of hadronic currents [6],
- De Gennes' analogy between liquid crystals and superconductors [7], where the free energy at the nematic-smectic A transition was shown to be formally identical to the Landau–Ginzburg Hamiltonian at the metal-superconductor transition, the Cooper pairs' wave function playing the role of the scalar density-wave order parameter,
- ...

In this manuscript, we will be concerned by analogue gravity, an emerging topic that intertwines cosmology, soft-matter physics and transport phenomena. Direct testing of cosmological models has always been a thorny issue, as it generally involves energy scales that are out of reach of any current or future apparatus on Earth: for instance, the question of the initial singularity (one Big-Bang or several Big Bounces ?) or that of any Planck-Scale phenomenon is likely to stay open for a long time. On the contrary, thermal Hawking radiation near a black hole is so weak that *in situ* detection seems almost impossible ought to crippling signal-to-noise ratios. One way out of these conundrums is precisely to find formal analogies with condensed matter. Ought to their large response functions, soft matter in general and liquid crystals in particular turn out to be playful and tunable systems, allowing to mimick almost any possible objects in cosmology.

This document sums up the results of a team effort, involving colleagues and students from France and from Brazil, without whom nothing would have been possible. The present manuscript is divided in four main parts. Chapter 2 establishes the conceptual framework for analogue gravity: it is aimed as a user's guide to differential geometry in the presence of curvature and torsion, illustrated by several examples taken from cosmology and condensed matter. A special emphasis is put on topological defects (cosmic strings, disclinations in nematics...), which will serve as an Ariadne's thread all along this work. The remaining chapters mainly deal with my personal contributions, which are referenced just after the title of each paragraph. Chapter 3 is dedicated to topics arising in a cosmological context, including transport phenomena in the presence of compact objects and in the primordial universe; potential condensed-matter analogs are discussed. The main idea driving Chapter 4 is to use the emerging curvature/torsion affecting transport phenomena in the presence of "terrestrial" topological defects to design functionalized materials, in particular thermal diodes. Engineering of geometry will also be discussed in the framework of electron transport in nanotubes. Chapter 5 focuses on classical electrodynamics formulated from exterior algebra. It is a personal attempt to address some recurring difficulties the students encounter when dealing with Maxwell's equations. Strictly speaking, its content is not new and at first sight, it may look a little bit disconnected from the two previous parts. This turns out to be inaccurate, as exterior calculus provides a purely topological formulation of electrodynamics, known as "premetric electrodynamics", more likely to single out the specific impact of geometry on the electromagnetic field. Finally, some research perspectives and miscellaneous information regarding my pedagogical activities are described in Chapter 6.

2

Eddington-Wheeler's program: «physics as geometry »

In Plato's *Timaeus*, an attempt was made to describe the world in terms of only five regular polyhedra and ever since, geometrization of physics has been a dream pursued by many figures in science, including René Descartes, Bernhard Riemann (for an updated account, see [8]), William K. Clifford [9], Henry A. Rowland [10]... A major step forwards in merging geometry and physics was made in the XX^{th} by Albert Einstein with the theory of general relativity: the gravitational interaction turns out to be nothing more than a manifestation of the spacetime curvature. The possible implications of that theory did not escape Eddington's attention. Arthur Stanley Eddington was one of the early masters of general relativity and he is known for conducting the first observational tests of Einstein's theory during the solar eclipse in 1919. The last chapter of Eddington's book *Space, Time and Gravitation* (1920) is entitled *On the nature of things* and he took in it a reversed point of view on Einstein field equations: "*When we perceive that a region contains matter we are recognizing the intrinsic curvature of the world; and when we believe we are measuring the mass and momentum of the matter (relative to some axes of reference) we are measuring certain components of world-curvature (referred to those axes)*". In other words, $\kappa T_{\mu\nu} = G_{\mu\nu}$ turns out to be a definition of matter in terms of pure geometry.

Eddington's ideas echoes those from Hermann Weyl [11] and were later given a broader purpose with John A. Wheeler's geometrodynamics program [12]. Wheeler introduced the idea of geons, that consist in hypothetical toroidal and spherical configurations of electromagnetic waves trapped by the spacetime curvature. As radiation carries energy and as energy gravitates, then a geon may exert a gravitational pull on neighboring objects. Seen from a distance, it behaves as an ordinary point mass... with no rest mass: thus, in geometrodynamics, mass originates from a localized curvature of spacetime. In the seminal paper *Classical physics as geometry* [13], Wheeler and Charles W. Misner borrow tools from cohomology, differential geometry, exterior algebra and topology to fully merge gravitation, electrodynamics and geometry: they obtain a system of equations in which the electromagnetic field, free of all charges and currents, is the source of the metric field. Or, put in Eddington's reversed point of view: the free electromagnetic field is a pure geometric entity. Provided spacetime is multiply-connected, Misner and Wheeler showed that similarly to mass, classical charge can also be seen as a byproduct of the spacetime geometry. The geometrization of physics project is still influential today: for instance, in Yang-Mills theories, the paradigm of

the standard model, gauge potentials are now understood as the components of the connection on a principal fiber bundle and a gauge choice simply corresponds to a section of the principal fiber bundle.

2.1 Einstein-Cartan theory in a nutshell

"Newton successfully wrote apple = moon, but you cannot write apple = neutron."
J.L. Synge

2.1.1 Gravity as a gauge theory

Theories of gravitation We are mainly concerned here with *Geometric theories of gravitation* that we can loosely define as theories in which spacetime (a manifold) is equipped with various *geometric objects*, like a connection or a metric tensor for the most popular ones. Among these geometric theories, General Relativity is the most famous. This is a *metric theory* which postulates first the existence of a symmetric metric tensor, the components of which are the unique degrees of freedom of the theory. They are solutions in the vacuum of Einstein equations which follow from a variational principle of an (Hilbert-Einstein) action w.r.t the metric tensor components and possibly coupled to matter via a minimal coupling prescription which relies on a connection. The curvature of the connection is thus determined by the conserved matter stress-energy tensor. These Einstein equations determine causally a unique metric tensor solution for any given matter stress-energy distribution.

In General Relativity, a torsionless connection compatible with the metric is assumed and is given by the Christoffel symbols. *Metric-affine theories* postulate, together with the metric tensor components, those of the connection as independent degrees of freedom. If the connection is assumed torsionless (Palatini action), one is led again to the Christoffel symbols and Einstein equations. *Einstein-Cartan theory* is an example of metric-affine theory in which the torsionless constraint is relaxed and which leads, together with the Einstein-equations, to a new set of equations of motion which couple the torsion of the connection to the matter spin density. More exotic geometric gravitation theories include for example those based on non symmetric metric tensors, non metric theories in which the metric-connection compatibility constraint is relaxed, and a bunch of theories which postulate additional fields, scalars, vectors, tensors, etc, not even mentioning higher dimensional theories.

Gauging Poincaré group All the interactions encompassed in the standard model of particle physics obey the same guiding principle: they are built as gauge theories. We will define a *gauge theory* as a theory which is invariant (covariant) under a Lie group, then called a gauge group. The action is gauge covariant under the local action of the gauge group, which demands the introduction of a connection (the gauge fields components) to define gauge covariant derivatives and render gauge covariant the matter Lagrangian through a minimal prescription scheme. For instance, the strong and electro-weak interactions are introduced by promoting global Lie symmetries of the Lagrangian to local symmetries: gauge invariance is restored provided that compensating fields are introduced.

Among the gauge theories, *Yang-Mills theories* are specific cases of central interest, since they are the building blocks of the Standard Model of electroweak and strong fundamental interactions. In Yang-Mills theories, the gauge group is a (compact) Lie group which acts on "internal" (i.e.

non spatio-temporal) degrees of freedom. An additional ingredient of Yang-Mills theories is that the action comprises in the usual (e.g. electrodynamics) manner a pure gauge field contribution proportional to the "square" of the curvature associated to the gauge connection plus the minimally coupled matter-gauge contribution. In this perspective, gravitation can be understood as a gauge theory, not of the Yang-Mills type, but which exhibits conceptual similarities with these latter theories.

Quantization of the gauge fields provides with the different gauge bosons that mediate the interactions: for the standard model based on the symmetry group $SU(3) \times SU(2) \times U(1)$, there are 12 gauge bosons: 1 photon, 3 weak bosons and 8 gluons. However, the gravitational interaction, classically described by Einstein's general relativity, has been reluctant to such quantization procedure up to now. To perform it, the first step is to express gravity as a gauge theory, which means to seek what is the right symmetry group that should be promoted from global to local. In the absence of gravity, geometry is described by the Minkowski spacetime M_4. The isometry group of M_4 is the global 10-parameter Poincaré group which consists in space-time rotations (Lorentz group $SO(1,3)$) and translations (group T_4). Promoting those (external) non compact symmetries to be local results in the gravitational interaction, provided that 10 gauge potentials are introduced: 6 rotational gauge potentials, the Lorentz connection field 1-form $\Gamma^b{}_a = \Gamma^b_{\mu a} dx^\mu$, and 4 translation gauge potentials, the tetrad field 1-form $e^a = e^a{}_\mu dx^\mu$. Those two sets of gauge potentials are treated as independent degrees of freedom.

The Γ symbols "connect" (co)tangent spaces at different points, whereas the tetrads (or vierbeins) cover the manifold with frames of orthonormal vectors. The tetrad field is commonly used to switch between holonomic and anholonomic coordinates and it defines $g_{\mu\nu}$ the metric tensor in the holonomic (or coordinate) basis as

$$g_{\mu\nu} = \eta_{ab}\, e^a{}_\mu e^b{}_\nu \tag{2.1}$$

where $\eta_{ab} = (-1, +1, +1, +1)$ is the Minkowski metric associated to the anholonomic basis. But what is the physical ground of η_{ab} which does not appear as a degree of freedom of the gravitational interaction ? An elegant explanation for the emergence of that structure has been formulated by Obukhov and Hehl in the framework of premetric electrodynamics [14]: the Minkowski metric would come out not as a consequence of gravity but of the topology of the electromagnetic field.

Field equations From the gauge potentials, two gauge field strengths, the Riemann curvature 2-form $R_a{}^b$ and the Cartan torsion 2-form T^a can be defined:

$$R^b{}_a = D\Gamma^b{}_a = d\Gamma^b{}_a + \Gamma^b{}_c \wedge \Gamma^c{}_a = R^b{}_{\mu\nu a} dx^\mu \wedge dx^\nu \tag{2.2}$$

$$T^a = De^a = de^a + \Gamma^a{}_b \wedge e^b = T^a{}_{\mu\nu} dx^\mu \wedge dx^\nu \tag{2.3}$$

These are known as Maurer-Cartan structure equations. Physically, the curvature field is generated by the mass-energy distribution (General Relativity), whereas the torsion field is generated by the

spin[1]. In terms of holonomic components, these quantities are expressed more explicitly as:

$$R^{\rho}{}_{\sigma\mu\nu} = \partial_\mu \Gamma^{\rho}{}_{\sigma\nu} - \partial_\nu \Gamma^{\rho}{}_{\sigma\mu} + \Gamma^{\rho}{}_{\lambda\mu}\Gamma^{\lambda}{}_{\sigma\nu} - \Gamma^{\rho}{}_{\lambda\nu}\Gamma^{\lambda}{}_{\sigma\mu} \tag{2.4}$$

$$T^{\rho}{}_{\mu\nu} = \Gamma^{\rho}{}_{\mu\nu} - \Gamma^{\rho}{}_{\nu\mu} \tag{2.5}$$

where

$$\Gamma^{\rho}{}_{\mu\nu} = e^{a}{}_{\nu} e_{b}{}^{\rho}\, \Gamma^{b}{}_{\mu a} - e_{b}{}^{\rho}\, \partial_\mu e_{\nu}{}^{b} \tag{2.6}$$

The geometry of spacetime is shaped by $R^{\rho}{}_{\sigma\mu\nu}$ and $T^{\rho}{}_{\mu\nu}$. The corresponding field equations were obtained by Kibble [19] and Sciama [20] to be [21, 22]:

$$G_{\mu\nu} = R_{\mu\nu} - \frac{1}{2} R^{\rho}{}_{\rho} g_{\mu\nu} = \frac{8\pi G}{c^4} t_{\mu\nu} \tag{2.7}$$

$$P_{\rho\mu\nu} = T_{\mu\rho\nu} + 2 g_{\mu[\rho} T^{\alpha}{}_{\nu\alpha]} = \frac{8\pi G}{c^4} s_{\rho\mu\nu} \tag{2.8}$$

where $G_{\mu\nu}, t_{\mu\nu}, P_{\rho\mu\nu}$ and $s_{\rho\mu\nu}$ are respectively the (asymmetric) Einstein tensor, the canonical stress-energy tensor, the Palatini tensor and the spin density tensor. (2.7) is a set of partial differential equations that dictates the dynamics of curvature, whereas (2.8) is purely algebraic: hence, torsion is bound to matter and it does not propagate. The main outcome is that the field equations (2.7)-(2.8) reduce to Einstein's equation in free space.

Comparison to general relativity The set (L_4, g) with the most general metric compatible linear connection Γ is called a Riemann–Cartan spacetime U_4. When the torsion vanishes, the U_4 spacetime identifies with the Pseudo-Riemannian spacetime V_4 of general relativity. When the curvature vanishes, the U_4 theory degenerates into Weitzenböck's teleparallelism T_4 that is equivalent to general relativity. Finally, when both curvature and torsion vanish, the simple flat (gravitationless) Minkowski M_4 spacetime is recovered.

As spin plays no role in general relativity, the number of degrees of freedom required is different than in Einstein-Cartan theory. While the affine connection Γ is independent of the metric in the U_4 theory, the Levi-Civita connection $\tilde{\Gamma}$ depends on the first derivatives of the metric g (or equivalently of the tetrad field) in V_4:

$$\tilde{\Gamma}^{\rho}{}_{\mu\nu} = \frac{1}{2} g^{\rho\sigma} \left(\partial_\mu g_{\nu\sigma} + \partial_\nu g_{\sigma\mu} - \partial_\sigma g_{\mu\nu} \right) \tag{2.9}$$

The general relation connecting the affine and the Levi-Civita connection is supplied by

$$\Gamma^{\rho}{}_{\mu\nu} = \tilde{\Gamma}^{\rho}{}_{\mu\nu} + K^{\rho}{}_{\mu\nu} \tag{2.10}$$

where the contortion tensor derives from the torsion tensor as

$$K^{\rho}{}_{\mu\nu} = \frac{1}{2} \left(T^{\rho}{}_{\mu\nu} - T_{\mu}{}^{\rho}{}_{\nu} - T_{\nu}{}^{\rho}{}_{\mu} \right) \tag{2.11}$$

[1]Torsion is a requirement of superstring theories, which call for the existence of torsion with a non-minimal coupling to scalar fields and fermions. Moreover, an unexpected asset of U_4 is that Dirac equation is turned into the Hehl-Datta equation (quadratic in spinor fields) for which ultraviolet divergences vanish from QED (for detailed references see [15]). However, it must be remarked that the Einstein-Cartan road is not mandatory to deal with spinors: general relativity can handle parallel transport of spinors through the (local) torsionless Fock-Ivanenko connection [16].

So when the Γ symbols are symmetric with respect to their last two indices, the torsion vanishes: the Levi-Civita connection is recovered and only the symmetric part of (2.7) remains, which corresponds to Einstein's equation.

Moreover, it must be emphasized that Einstein's 1915 formulation of general relativity was not built on the recipes of gauge theories à la Yang–Mills. Indeed, as pointed out by Hehl [23], Einstein considered that gravity is coupled to the (symmetric) energy-momentum current, which is the Noether current associated to T_4, but the (antisymmetric) spin angular momentum current associated to the Lorentz group was totally left aside. Therefore, general relativity is not *stricto sensu* a gauge theory for the Lorentz group: according to Tom Kibble, «*starting from special relativity and applying the gauge principle to its Poincaré-group symmetries leads most directly not precisely to Einstein's general relativity, but to a variant, originally proposed by Elie Cartan, which instead of a pure Riemannian space-time uses a space-time with torsion.* »(cited in [24])

2.1.2 Autoparallels and extremals

Geodesics of V_4 JA Wheeler summed up general relativity by the catchphrase: "*Matter tells spacetime how to curve and spacetime tells matter how to move*". Whereas the first part refers to Eqs. (2.7)-(2.8), the second part is related to the geodesic equation, which provides the trajectories followed by free-falling test particles:

$$\frac{d^2x^\rho}{dl^2} + \tilde{\Gamma}^\rho{}_{\mu\nu}\frac{dx^\mu}{dl}\frac{dx^\nu}{dl} = 0 \tag{2.12}$$

Here, l is an affine parametrization of the geodesic and $\tilde{\Gamma}^\rho{}_{\mu\nu}$ are the Christoffel symbols associated to the Levi-Civita connection. In V_4, geodesics are the curves of extremal proper time that parallel transport their own velocity along themselves: hence (2.12) can equivalently be derived either from the least action principle or from the principle of equivalence.

The intrinsic curvature of spacetime is linked to the failure of Euclid's fifth postulate: the Riemann curvature tensor characterizes the failure of initially parallel geodesics to remain parallel. Equivalently, parallel-transporting a vector along a small closed loop results in orientational misfits that are governed by $R^\rho{}_{\sigma\mu\nu}$ (see figure 2.1).

Trajectories in U_4 In U_4, finding the equations of motion is much more tricky. Indeed, the definition of a V_4-geodesic merges two different classes of curves: extremals and autoparallels. The former result from the extremisation of the proper time between two events: the derivation of Euler-Lagrange equations leads to (2.12), as the skew-symmetric part of the connection cancels out from the calculations.

The case of autoparallel curves (or straightest lines) is pretty much different. Coming from the principle of equivalence, an autoparallel is a trajectory such that its tangent vector is parallel-transported along itself with respect to the connection on the spacetime manifold. It obeys the differential equation:

$$\frac{d^2x^\rho}{dl^2} + \Gamma^\rho{}_{\mu\nu}\frac{dx^\mu}{dl}\frac{dx^\nu}{dl} = 0 \tag{2.13}$$

or equivalently

$$\frac{d^2x^\rho}{dl^2} + \tilde{\Gamma}^\rho{}_{\mu\nu}\frac{dx^\mu}{dl}\frac{dx^\nu}{dl} = -K^\rho{}_{\mu\nu}\frac{dx^\mu}{dl}\frac{dx^\nu}{dl} \tag{2.14}$$

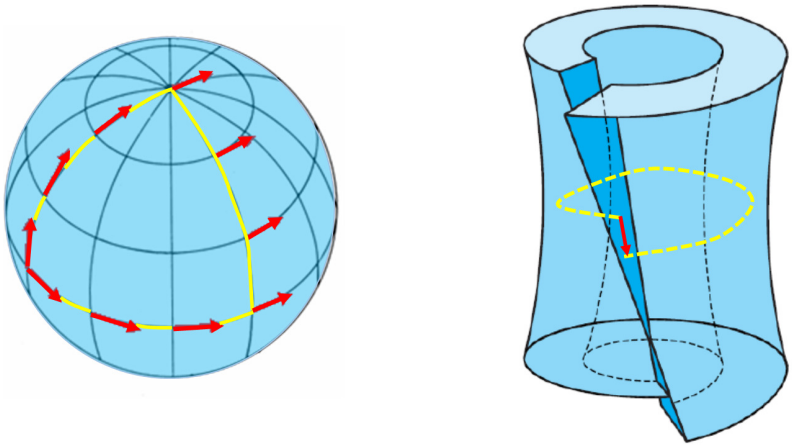

Figure 2.1: *Left:* Example of orientational misfit caused by curvature. *Right:* Example of closure failure caused by torsion.

which can be understood as a force equation. As stated in [21], when torsion does not vanish, autoparallels and extremals do not coincide, but more importantly, the trajectory of a test body generally coincides with none of them: spinning matter is indeed likely to undergo spin-curvature couplings that lead to nongeodesic motion (see for example Eq. 203 in [25], which obviously violates the principle of equivalence stricto sensu). In the pole-dipole approximation (only the mass monopole and spin dipole are considered, multipoles of higher orders are ignored), the general relativistic dynamics of spinning particles obey the Mathisson-Papapetrou equations [26, 27].

This is because the correct method to derive the equations of motion is not to postulate the least action principle or the equivalence principle, but to combine the field equations with either Bianchi identities or Noether identities [25]. However, a spinless particle will only experience the symmetric part of the connection and will remain totally insensitive to the torsion in the geometry, as shown by Yasskin and Stoeger [28], Ne'eman and Hehl [29] and Puetzfeld and Obukhov [30]: hence, it will still move on standard geodesics (2.12).

2.1.3 All that U_4 geometries can do for you

Geometrization of the dark sector The existence of the dark matter has been considered since Fritz Zwicky's 1933 article reporting higher than expected radial velocities of galaxies in the Coma cluster. Nowadays, cold dark matter (CDM) is assumed to account for about 25% of the total mass-energy content of our universe and to play a key role in the formation of cosmic structures: the CDM haloes act as gravitational wells that cluster neighboring galaxies together, which in return left other regions of space devoid of matter (for a review, see [31]). Several works [32]-[35] showed that Einstein-Cartan theory may successfully account for all these effects without introducing exotic CDM particles (WIMPs, axions...). In particular, Belayev et al. [35] proved that if the torsion field mass comes from both the Higgs mechanism and an assumed symmetry breaking at a GUT energy

scale, there is a region in the parameter space where torsion is responsible for 100% of the dark matter contribution to the universe.

The dark energy (or equivalently the cosmological constant) was originally introduced by Einstein in 1917 to keep the universe static. Nowadays, dark energy is assumed to account for about 70% of the total mass-energy content of our universe and it causes the rate of expansion of the universe to accelerate over time (for a review, see [36]). Similarly to dark matter, the physical origin of dark energy (vacuum energy, chameleon particles...) is still a thorn in standard cosmology's side. Several cosmological models [32],[37]-[41] investigated the possibility that torsion may account for effects assigned to dark energy. In particular, Popławski used a spare four-fermions-based model derived from the Hehl-Datta equation to retrieve the cosmological constant: calculations lead to a positive constant that was only 8 times larger than the observed value [39] which is nothing in comparison with the cosmological constant problem [42].

Bouncing cosmologies Modern cosmology is still struggling to explain why the observable universe is statistically homogeneous (the horizon problem), flat and isotropic. At the turn of the 1980s, Alexei Starobinsky, Alan Guth and Andrei Linde independently postulated the mechanism of cosmic inflation: just after the Big-Bang, the very early universe underwent a phase of sustained accelerated expansion at an exponential rate (its size grew of a factor 10^{75}), that is presumedly steered by new scalar particles (inflatons, curvatons...). However, despite intensive search at the LHC, no experimental support has been found for any of them yet.

The U_4 theory provides an alternate framework to account for a phase of accelerated expansion, but without resorting to *ad hoc* additional fields. Indeed, the high spin density of the quarks-leptons soup filling the early Universe couples strongly to torsion. In the semiclassical Weyssenhoff fluid approximation[2], torsion appears to be responsible for a repulsive effect and the temporal evolution of the spin-density tensor dictates the accelerated expansion, as discussed for instance in [44]-[49],[15]. This turns out to forbid any initial singularity at the Big Bang [17],[18] and replaces it by a non-singular Big Bounce.

The spin-driven accelerated expansion was therefore preceded by a Big Crunch of the Universe down to a minimal radius and the inflationary epoch thus fits into in the broader picture of cyclic cosmology, where the universe periodically transitions from contraction to expansion [50],[46, 47],[51]-[53],[15]. Some authors also mentioned that the Einstein-Cartan-Sciama-Kibble theory may replace the usual Big-Bang singularity by a continuous signature transition from a Euclidean spacetime to a Lorentzian spacetime [54]. Bouncing cosmologies are nowadays considered as credible alternatives to the inflationnary paradigm and they are fostering active research (for comprehensive reviews, see [55], [56]).

A taylor-made framework for cosmic strings As a result of the inflationary phase, the universe undergoes a Joule-Thomson expansion that cools it down. The drop in temperature gave rise to a series of phase transitions from the GUT high energy scales down to the Standard Model energy scale, during which cosmic defects - such as domain walls, cosmic strings or monopoles - may form, depending on the spontaneous symmetry breaking patterns. Domain walls are generally ruled out on cosmological grounds: their tremendous energy density would overclose the universe. Cosmic point defects (also called 't Hooft-Polyakov monopoles) possess both a mass and a magnetic charge. They

[2]In Weyssenhoff's phenomenological model, the standard cosmological fluid is treated as a continuous macroscopic medium characterized by a spin density tensor. This property results from an averaging on microscopic scales of the spin contributions of the fermionic fields [43].

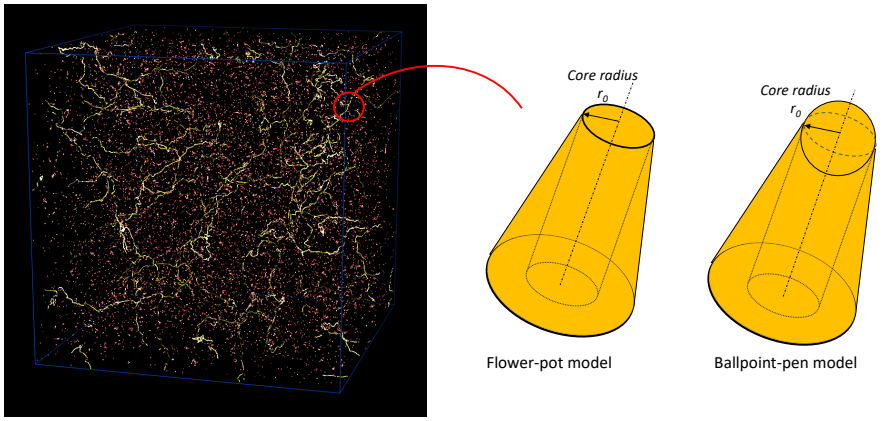

Figure 2.2: Left: Simulation of a cosmic strings network in radiation era (Cambridge cosmology group). Right: Close-up shots of possible string cores.

are relics of any phase transition such that $G \to H \times U(1)$. Like domain walls, their huge energy content may cause the universe to close on itself[3]. However in their case, several mechanisms are likely to decrease the number density of monopoles (inflation, Langacker-Pi mechanism [60]-[61]...) down to a sustainable value.

Above all, cosmic strings are probably the most studied of cosmic relics. The formation of linear defects was shown to be unavoidable [62] in the framework of supersymmetric GUTs. In the simplest models, strings are taken as infinitely thin objects[4], with no internal structure. They exist either as stable infinite straight lines (their equation of state simply equates the string mass-energy density to its tension $\mu = T$) or as closed loops that radiate away gravitational waves until they vanish[5]. Cosmic strings in motion happens to distort spacetime such that at all scales, matter accretes along its wake into sheet-like structures. They may account for the formation of large-scale structures in our universe (including the Great Wall) and they have several observable signatures such as the Kaiser-Stebbins effect (an asymmetric Doppler shift giving rise to anisotropies of the cosmic microwave background), gravitational lensing (not in the form of an Einstein ring, but as a double image instead), geometric phase (Aharonov-Bohm effect but with a cosmic string replacing the flux tube [66])... In 2014, datas collected by the PLANCK mission only settle upper bounds on the string mass-energy content [67] and in 2020, observations of the stochastic gravitational wave background (NANOGrav experiment) may provide with first evidences for cosmic strings [68].

[3]Yet their respective geometries have been investigated. The metric of plane cosmic domain wall can be found in several works such as [57]-[58], whereas for that of a cosmic monopole see for instance [59].

[4]In that case, they are generally called (maybe improperly) Nambu-Goto strings as their dynamics is also obtained from the Nambu-Goto action.

[5]This mechanism does not only hold for current-carrying loops. As discussed in [63]-[65], such defects can reach rotating states called vortons, which may be involved in high energy cosmic rays and dark matter. The centrifugal force then balances the string tension, which may stabilize the loop.

The geometry of cosmic strings can only be investigated in the framework of U_4 theory: the action of the Poincaré group $SO(1,3)\rtimes T_4$ deforms the Minkowski spacetime into 10 different Riemann-Cartan spacetimes, which respectively corresponds to 10 elementary defects. The $SO(1,3)$ part accounts for six of them, which correspond to cosmic strings (for extensive reviews, see [69]-[70]). They are solutions of Einstein's field equations when the energy-momentum tensor is distributional

$$T^{\alpha\beta} = \mu \,\mathrm{diag}\,(-1,0,0,1)\,\delta(x)\delta(y) \tag{2.15}$$

where μ is the linear mass density of the defect. This means that a cosmic string carries curvature that is concentrated along its axis [71, 72]. These cosmic strings may additionally have a chiral structure. The T_4 part of the Poincaré group accounts for the last four Riemann-Cartan spacetimes, which correspond to cosmic dislocations (twisted strings) [73]. They are solutions of Einstein-Cartan-Sciama-Kibble field equations when the spin density tensor is distributional, such that a dislocation carries torsion that is concentrated along an axis. For instance, the line element for the spinning twisted cosmic string was found to be [74],[75]:

$$ds^2 = -\left(4GJ^0 d\theta + dt\right)^2 + dr^2 + (1-4G\mu)^2\, r^2 d\theta^2 + \left(4GJ^z d\theta + dz\right)^2 \tag{2.16}$$

where J^0 is the angular momentum and J^z is the twist of the string.

A final word must be said about the zero-width approximation of cosmic strings we will use thereafter. A string is indeed an extremely thin object: its core radius is $r_0 \approx 10^{-30}$ cm for defects formed during a GUT-scale phase transition [79]. The linear distribution of mass-energy (2.15) leads to a δ-distribution of curvature along the defect axis [76] and one may wonder if such singularity is just a mathematical artefact coming from a too coarse model or if it does correspond to real physics. Hiscock [77] and independently Gott [78] suggest to smoothen this singularity by introducing two string models with a core structure of constant curvature: the flower-pot model (with zero curvature) and the ballpoint-pen model (with non-vanishing curvature). In the Gott-Hiscock thick cosmic string spacetime, the metric tensor is piecewise-defined (see Eqs 7 and 10-12 in [79] for instance) and it must obey matchings conditions at the core radius: the extrinsic curvature of the boundary should be the same whether measured in the interior or exterior region (O'Brien-Synge-Lichnerowicz jump condition).

The next section is aimed at showing U_4 theory is also relevant in other branches of physics besides cosmology. Indeed, it happens that cosmic defects have condensed-matter counterparts (especially in liquid crystals). They belong to the realm of analogue gravity, an emerging branch of physics the main features of which will be discussed after a short overview.

2.2 Analogue gravity in condensed matter

«And I cherish more than anything else the analogies, my most trustworthy masters. They know all the secrets of nature, and they ought to be least neglected in geometry.»
J. Kepler

2.2.1 Example 1: Defects in elastic media

Geometric theory of defects The first gauge theory of continuous defects dates back to the pioneering works by Bilby [80] and Kröner [81] in the 1950s [6] and ever since, this approach has been extensively developped [83]-[91]. In the noteworthy set of works [92]-[94], Katanaev proposed a Riemann-Cartan based model for dislocations and disclinations but only considered the strain tensor field as a relevant degree of freedom. In essence, the geometric theory of elasticity models a body submitted to internal stresses as a three dimensional continuum that can assume two possible states [95]:

- *the ground state* corresponds to the situation where the material is not deformed and as it is, it is maximally symmetric (invariance under translations and rotations). In such state , the medium is associated to a flat manifold equipped with an orthonormal coordinate system x^i. Lengths are given by the usual form of Pythagoras theorem:

$$dl_g^2 = \delta_{ij} dx^i dx^j = dx^2 + dy^2 + dz^2 \tag{2.17}$$

- *the deformed state*: anytime a stress is applied or in then presence of a defect, some of the symmetries mentioned hereinbefore are broken and the medium changes in size and/or in shape: as the points are moving with respect to each other, distances between them are changing as well and so is the associated metric g_{ij}.

An expression of the effective metric g_{ij} in the medium rest-frame can be obtained in the case of linear elasticity from the displacement field $u^i(\mathbf{x})$. For a point M originally at position x^i in the ground state, that same point is shifted to the position $y^i = x^i + u^i(\mathbf{x})$ in the deformed state. The distance between any pair of points after deformation then writes:

$$dl^2 \quad = \quad \delta_{ij} dy^i dy^j = \left(\delta_{ij} + \partial_i u_j + \partial_j u_i + \delta_{kl} \partial_i u^k \partial_j u^l\right) dx^i dx^j \tag{2.18}$$

Therefore, the elastic strain metric is obtained as

$$g_{ij} = \delta_{ij} + \partial_i u_j + \partial_j u_i + \delta_{kl} \partial_i u^k \partial_j u^l = \delta_{ij} + 2\varepsilon_{ij} \tag{2.19}$$

where ε_{ij} denotes the strain tensor. Compared to ordinary elasticity theory (OET), the geometric theory of defects is in principle more accurate (OET only reproduces the first-order approximation of the geometric theory of defects [94]) and it is more versatile (changing the kind of defect only requires changing the metric, instead of a complicated set of boundary conditions in OET).

[6] "Continuous" is meant here in relation to the continuous symmetries associated to gauge groups. Note that Kröner questioned the significance of such approach very soon: «*Although the field theory of defects has found many applications, the early hope that it could become the basis of a general theory of plasticity has not been fulfilled. Among various reasons we mention first of all, that the defects namely the dislocations that above all are responsible for plastic flow, do not form smooth line densities that can well be described by a dislocation density tensor field. Direct observation of dislocations in crystals, for instance by means of electron microscopy, shows that dislocations rather form three dimensional networks that are interconnected in practically immobile nodes and other often complex local arrangements... These networks have a strong statistical component, a fact that shows that a real physical understanding of plasticity requires also considerations in the frame of statistical physics. However, a statistical theory of interacting deformable lines that can be created, annihilated and change their length, has never been worked out* »(cited in [82]).

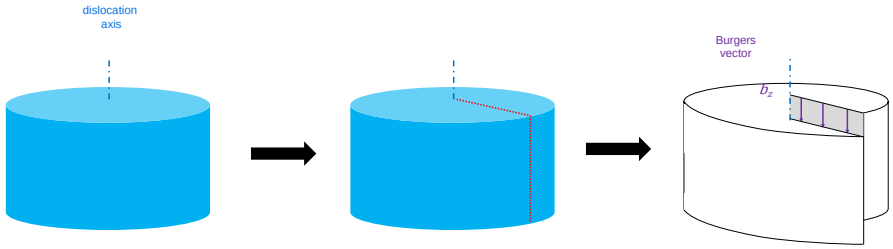

Figure 2.3: Volterra cut-and-weld process for a screw dislocation along z.

Screw dislocations Screw dislocations are defects related to shear stress that are very common in crystalline solids (they have close relatives in amorphous solids as well [96]) and in smectic liquid crystals (soap-like mesophases). They are associated to a breaking of the translational symmetry group and can be easily pictured by a Volterra cut-and-weld process (see figure 2.3). In this example, the magnitude and the direction of the crystal lattice distortion resulting from a screw dislocation of axis z is encompassed in the Burgers vector $\mathbf{b} = b\,\mathbf{e}_z$. In real crystals, b is a small parameter that is usually of the same order as the unit cell length: for example, Vogel [97] used optical methods to measure $b = 4\,\text{Å}$ in Germanium and studies mentioning large Burgers vectors report values around $1000\,\text{Å}$ [98]. Hence, the displacement field at equilibrium obeys the two relations:

$$\Delta u_z = 0 \tag{2.20}$$

$$\oint_{\mathcal{C}} du_i = -b_i \tag{2.21}$$

where C is a Burgers circuit enclosing the dislocation line clockwise. Solutions to these equations were found in 1907 by Volterra to be [95]:

$$u_z = \frac{b}{2\pi}\theta = \beta\theta \tag{2.22}$$

Computing the components of the strain tensor leads straightforwardly to

$$dl^2 = g_{ij}dx^i dx^j = dr^2 + r^2 d\theta^2 + (\beta d\theta + dz)^2 \tag{2.23}$$

This line element can be understood as follows: by performing clockwise a complete turn around the axis, one moves up by one unit of Burgers vector b. This can be summed up by the condition $\theta \to \theta + 2\pi \;\Rightarrow\; z \to z + b$.

The torsion tensor has only one non-vanishing component given by

$$T^z_{r\theta} = 2\pi\beta\delta^2(r) \tag{2.24}$$

whereas the curvature tensor is identically zero. Here and after, we will use the shorthand notation $\delta^2(r) = \delta(x)\,\delta(y)$. Hence, a screw dislocation must be described in terms of a Riemann-Cartan manifold, for which torsion is only located on the dislocation axis and vanishes everywhere else.

Disclinations Nematic liquid crystals are mesophases in-between the crystalline state and the isotropic fluid state. They are made of self-organized rod-shaped molecules and they are characterized by a long-range orientational order (for more details on the physics of liquid crystals, see [200]-[203]). Many materials such as ferromagnets or spin glasses possess a spin structure as well: at each point, a preferred average orientation can be defined[7]. Inside such medium (called a Cosserat continuum), a breaking of the rotational symmetry group is associated to a disclination, which is a second family of elementary elastic defects (for a historical reviews on defects in liquid crystals, see [204], [205] and more recently [206]). A disclination is generally not isolated: it is generally associated to other disclinations within dipoles (edge dislocations), amorphous networks (blue phases), etc

The equilibrium configuration of a Cosserat medium such as a nematic liquid crystal is obtained by minimizing Frank-Oseen free energy (and alike). For planar distorsions, the local average orientation points in the direction

$$\boldsymbol{n} = \begin{pmatrix} \cos(m\theta + \psi_0) \\ \sin(m\theta + \psi_0) \\ 0 \end{pmatrix}_{(x,y,z)} \tag{2.25}$$

where the value of the topological charge m is restricted to integer or half-integer numbers[8].

As the elastic energy is linear in m^2, only line defects corresponding to low winding numbers are observed in practice. Among them, the $(m = 1, \psi_0 = 0)$-disclination is probably the simplest: the local average orientation is radial and the elastic distortion field is fully encompassed in the Frank vector $\mathbf{f} = \frac{1}{2}\sin\Omega\,\mathbf{e}_z$ (the Frank angle $\Omega = 2\pi(1-\alpha)$ is positive when a wedge of material is removed, negative otherwise). In the medium rest-frame, the resolution of elasticity equations [99, 82] leads after some algebra to the following line element:

$$dl^2 = dr^2 + \alpha^2 r^2 d\theta^2 + dz^2 \tag{2.26}$$

Therefore, the Ricci scalar is obtained as

$$R = \frac{2\pi(1-\alpha)}{\alpha r}\delta^2(r) \tag{2.27}$$

whereas the torsion tensor is identically zero. In the case of a removal disclination of axis z, the geometry surrounding the defect is conical and can be easily pictured by the Volterra cut-and-weld process of figure 2.4. Hence, a disclination can be described in terms of a Riemann manifold, for which curvature is only located on the disclination axis and vanishes everywhere else.

[7] Hence, the rotational symmetry group is smaller than $SO(3)$: for instance, in nematics, this group is $O(2)$.

[8] These two families of defects correspond to the two equivalence classes of first homotopy group associated to the isotropic-nematic phase transition (see section 2.2.3 below).

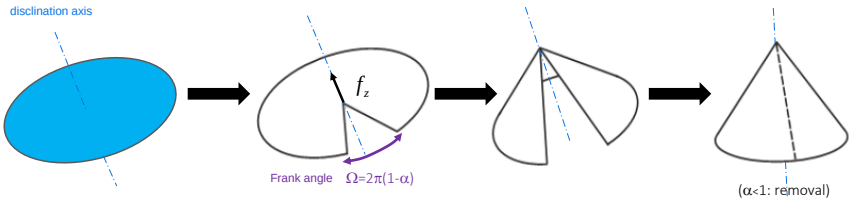

Figure 2.4: Volterra cut-and-weld process for a (wedge) disclination along z.

Discussion This short overview of the continuum theory of defective crystals calls for three remarks. First, a solid crystal consists in a discrete lattice of atoms and modeling it as a continuous medium is not self-explanatory. Rigorously, the continuum limit for elasticity should come as a coarse grained approximation of molecular dynamics and it should fail at the atomic scale (for attempts to push these limits down, see for instance [100]). This is obvious when examining the concept of elastic strain, which is defined as an average value over an domain containing a sufficiently large number of unit cells, but that remains sufficiently smaller than the bulk size. The continuum approach is thus relevant when the characteristic length scale is large enough compared to interatomic distances: as noticed by Davini [101], this holds for instance in X-rays devices, which provide information at scales where defects are smoothed out.

The same line of reasoning also holds for liquid crystals. Nematics are made of rod-like molecules (called nematogens) that self-assemble to minimize the Frank-Oseen free energy. This results in a long-range orientational order, characterized by a director field $\boldsymbol{n}(\mathbf{r})$ with a variable orientation. $\boldsymbol{n}(\mathbf{r})$ is defined statistically, as the average common direction of the nematogens at each "point" in space. The "point" actually refers to a small volume of space that includes enough molecules for the avering process to be physically significant. Hence, in practice, it means that the "point-volume" has to be large enough compared to molecular dimensions a (typically $a \approx 20$Å) and that the variations of the director field must occur at much larger scales than a. Then, the distorted liquid crystal can be described as a continuous medium, as discussed by Oseen [102], Zöcher [103] and Frank [104].

The second remark is related to the status of (2.19), which obviously possesses non-vanishing curvature and/or torsion, as in three-dimensional gravity. Yet, the deformed solid actually lives in a three-dimensional euclidean space, which means that the geometry is flat. How to reconcile these two standpoints? As suggested by De Wit[105], the state described by (2.19) cannot exist in the flat space, but only in an imaginary space where the solid is relaxed: g_{ij} comes from the projection of this imaginary space onto the physical flat space, in a similar way as a stereographic map projection

transfers the geometric properties on a 2-sphere (the Earth, with its meridians and parallels) onto a flat plane while deforming them (Wulff net). It turns out that the geometric description of solids thus requires two metrics: 1) The physical flat metric, δ_{ij}, will be used to perform operations on tensors such as raising/lowering indices... 2) The effective metric g_{ij}, which contains the elastic information, will be used to determine the kinematics of low energy perturbations (geodesics, first integrals...).

Third, one may naturally wonder what really happens on the defect axis and how to refine our zero-width model. In hard matter, the high-strained core region is of atomic width and as such, the continuum approximation breaks down: classical elasticity gets burdened by singularities (as illustrated by the delta functions in Eqs. 2.24 and 2.27) and it must be dropped in favor of atomistic calculations (empiric potentials or ab-initio simulations). Yet, for dislocations, all the singularities can be removed by considering an extended tubular core with an isotropically-distributed Burgers vector about every point on the defect axis [106]. For soft matter and more especially nematics, defect cores are very narrow as well but they still belong to the realm of continuum mechanics. As discussed in [203], a disclination line can accurately be described by a "two-phase model": the core consists in a tubular region, filled with the nematogens in isotropic phase (vanishing order-parameter), and surrounded by the nematic phase (non-zero order parameter). This approach is consistent with exact solutions obtained from the minimization of the Landau-Ginzburg-De Gennes free energy. Yet, the last word has probably not been said about disclination cores: observations made on lyotropic chromonic liquid crystals revealed that the core region has several unexpected features (asymmetric non-circular interfaces between the nematic and the isotropic phases, azimuthal and radial dependencies for the phase and amplitude of the order parameter...) compared to classic two-phase models [107].

2.2.2 Example 2: Optics in dielectric media

Light-cone condition Electromagnetic waves and their low-wavelengths limit, geometrical optics, can also be geometrized in a very natural way. Consider first a plane electromagnetic wave propagating in free space. The wavevector $\mathbf{k}$ and the angular frequency ω of that wave are related by the dispersion relation:

$$k^2 = \frac{\omega^2}{c^2} \tag{2.28}$$

Using units where $c = 1$, this can be rewritten in a covariant form using the 4-wavevector $k^\mu = (\omega, \mathbf{k})$:

$$-\omega^2 + k^2 = k^\mu \eta_{\mu\nu} k^\nu = k_\mu \eta^{\mu\nu} k_\nu = 0 \tag{2.29}$$

where $\eta_{\mu\nu}$ is the flat Minkowski metric. (2.29) is the so-called light-cone condition and it makes explicit use of the metric experienced by the wave.

Now consider the same kind of wave but propagating inside a dielectric medium (refractive index n) in its comoving frame. The dispersion relation now becomes:

$$k^2 = n^2\omega^2 \Leftrightarrow -\omega^2 + k^2 + \left(1 - n^2\right)\omega^2 = 0 \tag{2.30}$$

This time, getting a covariant form for the dispersion relation is not as straightforward as in free space, as

$$k_\mu \eta^{\mu\nu} k_\nu + \left(1 - n^2\right)\omega^2 = 0 \tag{2.31}$$

As testified by the extra-term in n^2, the wave propagating in the dielectric does not couple to the Minkowski metric but instead, it couples to an effective metric that incorporates the optical properties of matter. Using the identity $k_\mu v^\mu = -\omega$ where v^μ is the 4-velocity, then (2.31) can be rewritten as a light-cone condition $k_\mu g^{\mu\nu} k_\nu = 0$ provided that the metric is taken to be

$$g^{\mu\nu} = \eta^{\mu\nu} + \left(1 - n^2\right) v^\mu v^\nu \tag{2.32}$$

$$g_{\mu\nu} = \eta_{\mu\nu} + \left(1 - \frac{1}{n^2}\right) v_\mu v_\nu \tag{2.33}$$

(2.33) was originally found in 1923 by Walter Gordon and it is called after him as the Gordon optical metric [9] [108]. It is made of two terms: the first one $\eta_{\mu\nu}$ is the physical background metric whereas the second one, in $(1 - 1/n^2)$, is interpreted as a Fresnel-Fizeau dragging coefficient[10]. Ever since, several authors have clarified Gordon's insight [110]-[114]: any gravitational field can be modeled by an equivalent optical medium, under the Dicke's constraint that $\varepsilon = \mu$.

Fermat's principle as a geodesic equation Geometrical optics can also be reinterpreted from the standpoint of differential geometry, because the null geodesics of the Gordon metric identify with the light paths. Indeed, for any affine parametrization q of the optical paths, the geodesic equation writes as

$$0 = g_{\mu\nu} \frac{d^2 x^\mu}{dq^2} + g_{\mu\nu} \Gamma^\mu_{\ \rho\sigma} \frac{dx^\rho}{dq} \frac{dx^\sigma}{dq} \tag{2.34}$$

where $\Gamma^\mu_{\ \rho\sigma}$ are the Christoffel symbols associated to the Gordon metric (Levi-Civita connection). If the parametrization is chosen to be t, then the geodesic equation becomes [115]:

$$-\frac{d^2 t/dq^2}{(dt/dq)^2} \frac{dx^\mu}{dt} = \frac{d^2 x^\mu}{dt^2} + \Gamma^\mu_{\ \rho\sigma} \frac{dx^\rho}{dt} \frac{dx^\sigma}{dt} \tag{2.35}$$

For a static metric, (2.35) can be rearranged after some algebra as [116]

$$\gamma_{jk} \frac{d^2 x^k}{dt^2} + \tilde{\Gamma}_{jkl} \frac{dx^k}{dt} \frac{dx^l}{dt} = 0 \tag{2.36}$$

where $\gamma_{ij} = -\frac{g_{ij}}{g_{00}}$ and

$$\tilde{\Gamma}_{jkl} = \frac{1}{2} \left(\frac{\partial \gamma_{jk}}{\partial x^l} + \frac{\partial \gamma_{jl}}{\partial x^k} - \frac{\partial \gamma_{kl}}{\partial x^j} \right) \tag{2.37}$$

This corresponds to the geodesic equation with respect to t on the three dimensional submanifold described by the metric γ_{ij}.

(2.36) also happens to be the Euler-Lagrange equation that is obtained when extremizing the time between two points a and b:

$$S_{ab} = \int_a^b dt \tag{2.38}$$

[9] The same Gordon left his name to the famous Klein-Gordon equation, $\Box\psi + m^2\psi = 0$, which he built in 1926 with Oskar Klein to describe the dynamics of spinless massive relativistic particles.

[10] In 1822, Augustin Fresnel investigated the possibility that light may be dragged by matter in motion. That prediction was later confirmed by observations performed by Hippolyte Fizeau in 1851. More details can be found on this topic in [109].

Indeed, as null geodesics are concerned, $dt^2 = \gamma_{ij} dx^i\, dx^j$ so that

$$0 = \delta S_{ab} = \delta \left(\int_a^b \sqrt{\gamma_{ij} \frac{dx^i}{dq} \frac{dx^j}{dq}}\, dq \right) \tag{2.39}$$

Elementary variational calculations for the action S_{ab} leads along any virtual path δx^i to

$$0 = \int_a^b \left(\gamma_{ji} \frac{d^2 x^i}{dt^2} + \frac{1}{2} \left[\frac{\partial \gamma_{ji}}{\partial x^k} + \frac{\partial \gamma_{jk}}{\partial x^i} - \frac{\partial \gamma_{ik}}{\partial x^j} \right] \frac{dx^i}{dt} \frac{dx^k}{dt} \right) \delta x^j dt \tag{2.40}$$

which is equivalent to equations (2.36)-(2.37).

Now, in the comoving frame, the Gordon metric is static and from (2.33), it comes readily that

$$\gamma_{ij} = n^2 \eta_{ij} \tag{2.41}$$

Plugging into (2.39) finally gives

$$0 = \delta \left(\int_a^b \sqrt{\gamma_{ij} dx^i\, dx^j} \right) = \delta \left(\int_a^b n\, dl \right) \tag{2.42}$$

which is the integral form of Fermat's principle [117]. Hence, the null geodesics of Gordon's metric are the extremal curves followed by light in geometrical optics. This equivalence has been successfully used to investigate optics in the presence of compact objects in [118]-[119].

Anisotropic media Light propagating inside an anisotropic medium does not comply to the usual Fermat principle. As a matter of fact, the electric constitutive relation involves a permittivity tensor that may have two different eigenvalues (uniaxial media, such as simple nematics, calcite, ice...) or three different ones (biaxial media, such as oxadiazole bent-core nematics, chlorite, gypsum, ...). The harmonic analysis of propagating waves inside uniaxial crystal gives rise to the Fresnel equation:

$$\left(n^2 - \varepsilon_\perp\right) \left(\varepsilon_\perp [n_x^2 + n_y^2] + \varepsilon_\parallel n_z^2 - \varepsilon_\perp \varepsilon_\parallel\right) = 0 \tag{2.43}$$

where $\varepsilon_\parallel$ is the permittivity eigenvalue along the local average orientation (degeneracy 1) and $\varepsilon_\perp$ is the permittivity eigenvalue orthogonal to the local average orientation (degeneracy 2). Fresnel's equation implies that two different modes can propagate:

- an ordinary wave experiencing an isotropic refractive index $n = \sqrt{\varepsilon_\perp}$.
- an extraordinary wave experiencing an anisotropic refractive index mixing $\varepsilon_\perp$ and $\varepsilon_\parallel$.

In 1919, Grandjean extended the least action principle to extraordinary modes. Paths of extraordinary rays are obtained from the extremization of the extraordinary energy index N_e:

$$0 = \delta \left(\int_a^b N_e(\boldsymbol{r})\, dl \right) = \delta \left(\int_a^b \sqrt{\varepsilon_\perp \cos^2 \beta(\boldsymbol{r}) + \varepsilon_\parallel \sin^2 \beta(\boldsymbol{r})}\, dl \right) \tag{2.44}$$

where β is the local angle between the director field $\boldsymbol{n}$ and the tangent vector $\boldsymbol{T}$ to the extraordinary light path[11]. In polar coordinates, straightforward algebra shows that angle β is defined from

$$\cos\beta = \boldsymbol{n}.\boldsymbol{T} = \dot{r}\cos(\psi-\theta) + r\dot{\theta}\sin(\psi-\theta) \quad (2.45)$$

$$\sin\beta = |\boldsymbol{n}\times\boldsymbol{T}| = -\dot{r}\sin(\psi-\theta) + r\dot{\theta}\cos(\psi-\theta) \quad (2.46)$$

where $\dot{}$ denotes the derivative with respect to curvilinear abscissa l.

Plugging into (2.44) and considering a nematic liquid crystal with a $(m=1,\psi_0=0)$-disclination as before, it comes in each $z=C^{st}$ slice that

$$N_e^2(\boldsymbol{r})\,dl^2 = \left(\varepsilon_\perp\dot{r}^2 + \varepsilon_\parallel r^2\dot{\theta}^2\right)\,dl^2 = \varepsilon_\perp dr^2 + \varepsilon_\parallel r^2 d\theta^2 \quad (2.47)$$

Rescaling the radial coordinate as $\rho=\sqrt{\varepsilon_\perp}r$, it finally comes that the three-dimensional line element writes as

$$ds^2 = d\rho^2 + \alpha^2\rho^2 d\theta^2 + dz^2 \quad (2.48)$$

A comparison with (2.26) shows that the topological defect distorts in a similar way the geometry experienced by the elastic field and the electromagnetic field. Note that the ordinary rays will not experience such optical disclination.

More generally, as reported by Tamm [121], linear anisotropic media creates an artificial geometry for light as well. In the geometrical optics limit, Satiro and Moraes [122, 123] showed that the presence of a disclination in a nematic always gave rise to lensing effects (see Figure 2.5). Eversince, several authors highlighted the peculiarities of defects in liquid crystals for optics and their relevance for applications [203]-[124].

Discussion Light experiences dielectric media as non-euclidean geometries, whether the material is isotropic or anisotropic, whether it is linear or nonlinear [125, 114]... A thorough examination shows that the empty-space Maxwell equations in arbitrary coordinates and geometries are fully equivalent to the Maxwell equations in an anisotropic impedance-matched media [126]: if one finds a medium for which the permittivity tensor equals the permeability tensor $\bar{\bar{\varepsilon}}=\bar{\bar{\mu}}$ (in agreement with Dicke's constraint), then one may expect to mimic optics in a non-euclidean geometry. Ordinary materials do not fulfill such condition, but fortunately, metamaterials do.

Metamaterials are artificial media devised in the 2000s. Following a pioneering idea of Victor Veselago on negative refraction [127], John Pendry [128] and David Smith [129] developed subwavelength-structured media, the optical properties of which can almost be taylored at will[12]. The advent of metamaterials prompted the birth of transformational optics: the capability to distort light paths as in gravitational lensing, to mimick the outside of a black hole [130]-[131] and more generally to recreate *any kind of spacetime curvature* from electromagnetic medium is now within reach (see in particular the section dedicated to "spacetime transformation optics" in [132]). The differential geometry methods used to designing optical metamaterials have now been extended to control wave propagation in many other problems [133, 134][13].

[11] Fermat's principle also holds for extraordinary sound rays in elastodynamics [120], with elastic constants playing the role of refractive indices. Its application to acoustics in liquid crystals will be discussed later in Chapter 4.

[12] There are still some limitations. For instance, to work efficiently at a given wavelength λ, the elementary components of the metamaterial have to be at least an order of magnitude smaller than λ.

[13] The list now encompasses: acoustics [135]-[137], elasticity (from laboratory scale up [138]-[136] to the geophysical scale [140]-[142]), fluid mechanics (protection against sea waves [143]-[144]), heat transfer [145]-[146]... and even quantum mechanics (cloaking of matter waves [147]-[148]).

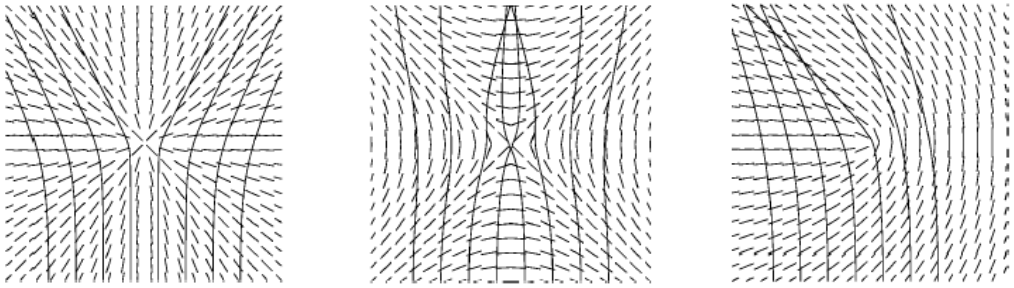

Figure 2.5: *Left*: Light paths in the presence of a radial disclination ($m = 1, \psi_0 = 0$). *Middle*: Light paths in the presence of a disclination ($m = -1, \psi_0 = \frac{\Pi}{2}$)-disclination. *Right*: Light paths in the presence of a half-integer disclination ($m = \frac{1}{2}, \psi_0 = \frac{\Pi}{4}$). Taken from Satiro et al. (2006).

Effective background geometries in optics may also be hidden in much more subtle ways. For instance, in Haller's approximation, the hydrodynamics of a nematic liquid crystal flowing radially is experienced as a Schwarzschild's metric (in isotropic coordinates) by light beams [149][14]. More generally, the realm of liquid crystals offers an ideal playground to look for optical effective geometries and to tune them for electromagnetic transport [151]: ought to their high sensitivity towards external constraints, they can be put in almost countless different configurations and they are generally transparent in the visible range. Besides, soft matter systems can also exibit a metamaterial-like feature: a host liquid crystal doped with coated core-shell nanospheres becomes hyperbolic in the near infrared range [152] (for a review on soft matter metamaterials see [153]).

2.2.3 Lessons and pitfalls

Kinematics vs dynamics The preceding examples testify that in many condensed matter systems, the effective degrees of freedom are represented by specific field excitations that propagate over effective Riemann-Cartan manifolds[15]. This idea has spread out to the point where it has become an area of research on its own: analogue gravity (for an extensive review, see [155] and more recently

[14] Another example taken from soft matter is the jammed state of granular media, which could also share analogies with the exterior of a black hole [150].

[15] Interestingly, Cartan proceeded the converse way and introduced torsion into gravity, bearing in mind the mechanics of elastic media [154].

[156]). However, despite appealing to classical and quantum physics, analogue gravity is tricky and must be handled with great care. Indeed, it relies simultaneously on two different manifolds:

- the background gravitational metric, which is experienced by all fields (generally Minskowski's), is the outcome of Einstein-Cartan equations (2.7)-(2.8). It is a tensor, used for instance to raise and lower indices of tensors, and as such, it is a covariant quantity.
- the effective metric, which is experienced only by the fields coupled to matter, does not obey Einstein-Cartan equations. Its purpose is limited (for instance, to determine the geodesics followed by the coupled-fields excitations, as it is not a covariant quantity: indeed, the effective metric is derived from physical quantities 1) which are defined in a privileged frame, the medium rest-frame, and 2) that are not Lorentz invariant.

As can be seen explicitly on (2.33), the effective metric is the sum of the background Minkowski metric plus a corrective term due to couplings between the electromagnetic field and the moving dielectric matter. In the original experiment led by Hippolyte Fizeau, the changes in the velocity field of water (and hence of the Gordon metric itself) were obviously ruled by the Navier-Stokes equations (for the velocity field) instead of Einstein-Cartan equations: in other words, effective spacetimes are generally stationary. [186] pointed out that textures in nematic liquid crystals can indeed be described by the space sector of an Einstein-like equation, with the elastic-stress tensor replacing the energy-momentum tensor.

The relevance of the effective metric is therefore restricted to calculations of properties related to the *kinematic properties* of the fields coupled to matter. This encompasses the geodesics of low-energy excitations but also the less obvious cases of Unruh effect or Hawking radiation which are purely kinematic phenomena [157]. Therefore, the analogy between gravitation and condensed matter is strictly kinematic but not dynamical. To rephrase Wheeler, *analog spacetime tells matter how to move... but matter does not tell analog spacetime how to curve.*

As condensed matter physics can duplicate some effects of true gravity, but not all of them, this raises a question: for what purpose shall models of analogue gravity be used ? The answer is twofold:

1. to design laboratory analogs of cosmic objects, from which experimental investigations can be carried out. This is sometimes referred to as the "cosmology in the laboratory" game plan and it covers topics such as classical black holes [158]-[163], Hawking radiation [164]-[176], wormholes [177]-[180] and of course expanding cosmological backgrounds [181]-[191].
2. to use the toolbox of differential geometry to model the complex couplings of particles to surrounding matter. This is extensively used in the emerging field of transformation optics, which aims at tayloring light propagation by means of metamaterials [126], [192]-[195]. This is now spreading to (aero)acoustics [196]-[197] and to elasticity (for instance [198]), with one subtlety: it is not the classical elastodynamic equations that are invariant under a curvilinear coordinate transformation, but those of Willis [199].

The case for topological defects [16] Among all analog phenomena, investigations related to topological defects received a particularly sustained attention, probably because here the analogy between

[16] Strictly speaking, a defect is topological when the singular configuration of the order parameter cannot be transformed continuously into a uniform configuration. This process depends not only on the order parameter configuration but also on the dimensionality of the embedding space (as will be discussed in section 4.1, this is the well-known "escape in the third dimension" of nematic liquid crystals). Therefore, there is also a more flexible use

cosmology and condensed matter - especially with nematic liquid crystals - is deeper than everywhere else [207]-[210]. Cosmic strings and disclinations in nematics are both formed during thermally-driven phase transitions. In the framework of GUT, the universe rapidly cools down (quench) as it expands: cosmic phase transitions occur during which the high-energy gauge group G spontaneously breaks down. For all eligible gauge groups G (such as $SO(10), SO(14), SU(5), SU(6)....$), the homotopy group analysis shows that the formation of cosmic strings is generic [62]. Likewise, isotropic - nematic phase transition also corresponds to a non-trivial content for the first homotopy group π_1. The symmetry breaking pattern is indeed $SO(3) \rightarrow O(2)$, which leads to $\pi_1(SO(3)/O(2)) = \pi_1(\mathbb{R}P^2) = \mathbb{Z}_2$: disclination lines or loops may form (for more details on homotopy theory and defects in soft matter, see [212].

A detailed mechanism for the formation of cosmic strings has been initially proposed by Tom Kibble in the 1970s [213]. This occurs in three main steps:

1. Protodomains form, inside which symmetries are spontaneously broken. The breaking of symmetry triggers a Higgs mechanism. At high temperatures, the order parameter vanishes[17], but below the transition temperature, the potential term adopts a Mexican-hat shape, causing the order parameter to randomly take a non-zero value.

2. As the temperature decreases, ordered domains grow in size. As initially distant protodomains may not be in causal contact, the values of their order parameter are not correlated.

3. When the domains eventually meet each other, they merge. But as the values of the order parameters across a frontier may not match, relics of the high temperature phase are left in the form of cosmic strings.

The Kibble mechanism was refined in 1985 by Zurek to take into account the characteristics of the quench and it makes several quantitative predictions such as the scaling dynamics of the string network, the average density of defects, correlations between defects and antidefects...

Since the 1990s, several works showed that the formation of line defects in nematics obeys the Kibble-Zurek mechanism as well [216]-[220][18]. But the family resemblance goes further. Networks of cosmic strings and networks of disclinations also share similar intersection processes: 1) when two line defects intertwine, they may reconnect the other way as they cross (intercommutation) [222], [216] and 2) when one line defect self-intersects, it creates a loop [223], [224]. Last but not least of these common points: the metric around a regular cosmic string - without chirality or spinning -, has exactly the same form as the metric around a disclination: that of a conical geometry corresponding to a removed Frank angle[19] (typically, for a GUT scale string, this angle is a few seconds of arc).

Yet, there are discrepancies between cosmic and elastic defects that one must bear in mind to avoid fallacies. Dissipation mechanisms for cosmic strings are due to radiation of gravitational waves, while those in liquid crystals are friction-dominated. What is the outcome on the dynamics of the defects? In cosmology, a network of monopoles is supposed to annihilate slowly and to rapidly

for the terminology "topological defect", referring to the singularity associated to any non-trivial homotopy content of the order parameter manifold, whatever its topological stability is. In the remainder of this document, we will stick to that latter meaning.

[17] In the cosmological context, the order parameter corresponds to the vacuum expectation value of the Higgs field.

[18] Experiments led on other laboratory analogs (such as superfluid ^{4}He) have also supported the scenario for the formation of several kinds of topological defects (monopoles, strings, textures...) [207],[221]

[19] However, no isolated cosmic string corresponds to the case of an added Frank angle (saddle-like geometry). To our knowledge, the existence of a negative-mass cosmic string has been considered only when the defect is associated to a wormhole [225, 226].

dominate the universe. On the contrary, elastic hedgehogs in a nematic annihilate rapidly according to a scaling law. At a more fundamental level, this is linked to the fact that in high energy physics, broken symmetries are gauged (or internal) whereas in liquid crystals, they are no gauge fields at all and broken symmetries are geometrical: in the first case, one is dealing with "gauged defects" and in the second case, one is dealing with "global defects".

3

Cosmology inside and outside the lab

In astrophysics and in cosmology, putting a theory into test is always a thorny challenge. In 1994, the great epistemologist Karl Popper already pointed out that the "*major theoretical problem in cosmology is how the theory of gravitation may be further tested and how unified field theories may be further investigated*" [227]. If the plentiful harvest of low-energy observations (baryonic oscillation spectroscopy, gravitational wave interferometry, mapping of the cosmic background ...) answered many questions, theoretical models involving (trans)planckian scales bloomed even faster, for which experimental confirmations seem almost impossible - even in principle - to reach.

A possible way out of this conundrum is to take advantage of the richness and flexibility of condensed matter. Within certain limits, analogues of gravity can be used to simulate different types of cosmological objects (signature transitions events, cosmic strings...) and to investigate the transport of bosonic and fermionic quasiparticles in nontrivial spacetimes. This chapter reviews of series of articles dealing with compact objects and non-standard cosmological models. Each time a discussion suggests possible laboratory analogs to test their predictions.

3.1 Compact objects

3.1.1 Radiative transfer in stellar photospheres

From optical trapping [228]... In the core of a star, nuclear reactions release the thermal energy that diffuses to the outer layers, crosses the stellar photosphere and finally comes out in the form of observable radiation. During their journey through the star, the outgoing photon beams exert a radiative pressure that balances the hydrostatic pressure (in supergiants and Wolf-Rayet stars, the radiative pressure is even larger than the gaseous pressure). The understanding of stellar evolution, as well as the estimate of stellar ages through radiometric measurements, thus strongly depends on the accuracy of radiative transfer models.

In 1906, Karl Schwarzschild showed that radiative transfer by itself also ensures the stability of the photosphere against convective motions [229]. From the standpoint of radiative properties, the

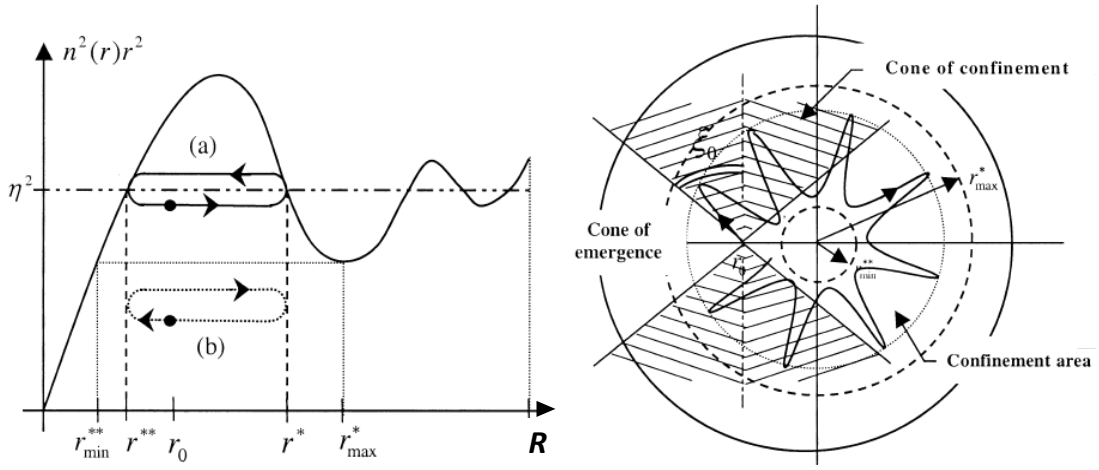

Figure 3.1: *Left*: Potential well associated to a varying refractive index. *Right*: Confinement of light rays by total internal reflections.

photosphere is a participating medium: radiation is both absorbed (Beer-Lambert law) and thermally emitted (Kirchhoff-Planck law) by this layer. However, most of the time, strong simplifying assumptions are made: corrections due to the gravitational field are often overlooked as well as spatial variations of the optical properties[1]. The Schwarzschild-Milne equations and the Eddington moments come as approximates of the radiative transfer equation (RTE), written in its simplest form as [231]:

$$\frac{DI_\nu}{Ds} + \kappa_\nu I_\nu = \kappa_\nu I_\nu^0(T) \tag{3.1}$$

where I_ν is the specific intensity, s is the arc length along a light path, κ_ν is the frequency-dependent absorption coefficient and $I_\nu^0(T)$ is the Planck function. Despite being historically built from phenomenological grounds, the RTE turns out to be a Boltzmann equation for the photons fluid with a collision term (due to matter) and no external force.

In fact, a rigorous treatment of stellar interiors should at least take into account the inhomogeneities of the refractive index $n(\mathbf{r})$ (due to the variations of density) and incorporate the pertaining non-Euclidean effects. Indeed, the variations of n have two main outcomes:

1. from the standpoint of optics, a varying refractive index curves light paths and as in the well-known mirage effect, it may even confine light paths within spherical domains owing to total internal reflections (see Figure 3.1).

[1] To our knowledge, the only work including both kinds of effects is [230].

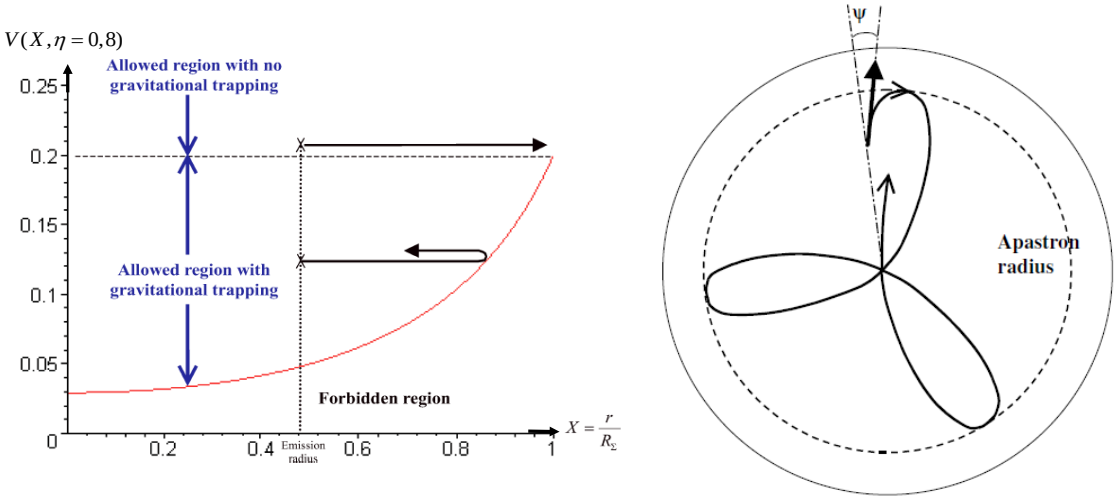

Figure 3.2: *Left*: Potential well associated to the Schwarzschild interior close to Buchdhal's limit ($\eta < 8/9$). *Right*: Depending on the impact parameter, the ray may be reflected on the potential barrier and pulled back toward the center of the star.

2. from the standpoint of energy, the RTE is modified accordingly by replacing the specific intensity by the more general Clausius invariant I_ν/n^2.

To date, the thermal and mechanical consequences of the optical trapping inside stars are still not well understood: if this confinement is probably responsible for local overheating, the effects on the radiative pressure and on the stability of the stellar atmosphere remain to be investigated.

... to gravitational trapping [232]. Refined models of radiative transfer inside compact objects usually rely on numerical recipes to compute emergent spectra or effective temperatures (see for instance [234]). But ought to the complexity of the equations, computational simulations are prickly and no qualitative understanding is really provided by such models. This is precisely where analog gravity becomes worthy. Indeed, if one inverts Gordon's perspective, it should be possible to mimic the gravitation field inside a star with an appropriate refractive medium. Hence, all the numerical methods developed in mechanical engineering (Discrete Ordinates, Finite Volume, Monte-Carlo, Ray-Tracing [233]...) can be implemented and physical insight can be gained from what is known inside graded-index materials.

In the case of a Schwarzschild interior (non-rotating star of constant mass density), light rays propagate along curved paths and depending on the shooting conditions, they can even stay gravitationally trapped inside the star, as in the case of the graded-index medium (see Fig. 3.2). From a thermal standpoint, the trapped rays cannot convey their energy outside the star and they thus warm up the surrounding matter through absorption processes. Therefore, omitting the effects of

gravitation on radiation transport leads to an underestimation of the temperature field inside the star.

This suggests that an appropriate graded-index dielectric can be used to reproduce both the geometrical optics and the radiation transport in the Schwarzschild interior:

$$n_{eff}(r) = \frac{re^{-\alpha(r)}}{\sqrt{e^{-2\beta(r)}r^2 + b^2e^{2\alpha(r)}\left(1 - e^{-2\beta(r)}\right)}} \tag{3.2}$$

where

$$\alpha(r) = \ln\left[\frac{3}{2}\sqrt{1 - \frac{R_s}{R_\Sigma}} - \frac{1}{2}\sqrt{1 - \frac{R_s r^2}{R_\Sigma^3}}\right] \tag{3.3}$$

$$\beta(r) = -\frac{1}{2}\ln\left[1 - \frac{R_s r^2}{R_\Sigma^3}\right] \tag{3.4}$$

This effective refractive index associated to a ray depends on the star parameters (Schwarzschild radius R_s and star surface radius R_Σ), as well as on the shooting conditions (impact parameter b). Plugging it in Clausius invariant and writing the corresponding RTE, the spacetime curvature appears to play an active role in the radiative balance: when the effective index decreases with r, the optical thickness along the ray is enhanced by gravity, which increases the star temperature.

3.1.2 Wiggly strings

The six differences game Cosmic strings are structured on a length scale related to the phase transition at which they are formed. In the case of a GUT string, this length is about 10^{-30} cm, which is so small that is seems fair to use a model of structureless straight strings (or Nambu-Goto strings). In that case, the Ricci scalar is a 2-dimensional δ-function, which means that curvature is located only on the string axis $r = 0$. A remarkable outcome is that such defect does not gravitate, as the linear mass-energy density content μ_0 is perfectly balanced by the string tension T. There are still detectable outcomes due to the conical geometry, such as the Kaiser-Stebbins effect [236] when the string is moving.

In fact, such model is too coarse to account for a realistic string, which may present small-scale perturbations such as cusps, kinks and wiggles. The averaged effect of these perturbations increases the linear mass density μ and decreases the string tension T, as prescribed by the equation of state $\mu\, T = \mu_0^2$. Using a distributional energy-momentum tensor such as $T^\mu_\nu = \delta(x)\delta(y)\,(\mu, 0, 0, T)$, the resolution of Einstein's equation in the weak field gives the following metric [69]:

$$ds^2 = -\left(1 + 8\varepsilon \ln\left[\frac{r}{r_0}\right]\right)dt^2 + dr^2 + \alpha^2 r^2 d\theta^2 + \left(1 - 8\varepsilon \ln\left[\frac{r}{r_0}\right]\right)dz^2 \tag{3.5}$$

where $\alpha^2 = 1 - 4G(\mu + T)$, ε is the excess of mass-energy density $2\varepsilon = G(\mu - T)$ and r_0 is a cut-off radius introduced to avoid the logarithmic divergences. Compared to straight string, the geometry remains conical but the deficit angle is larger than in the straight string case. Moreover, the excess of mass-energy density, represented by the parameter ε, leads to a a far away gravitational pull on neighboring objects, which could be responsible for the elliptical distortion in the shape of background galaxies [237] or for the accretion of dark energy around the defect [238].

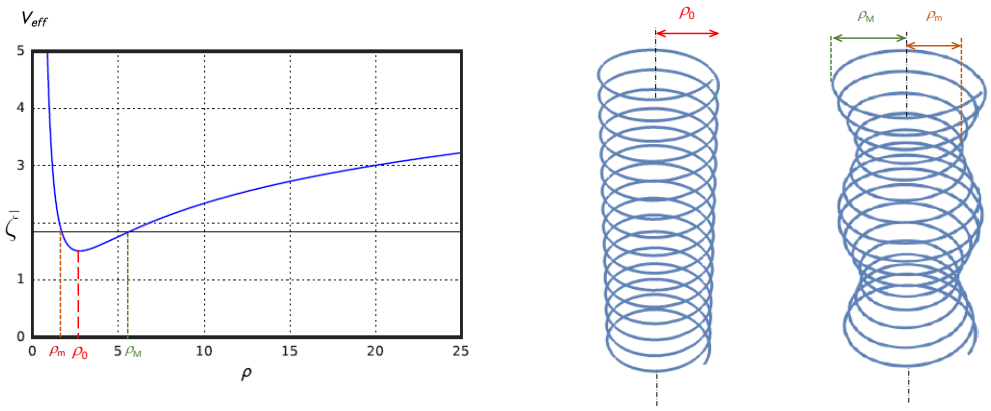

Figure 3.3: *Left*: Effective potential profile $V_{eff}(\rho) = \frac{l^2}{\alpha^2\rho^2} + \ln\frac{\rho}{\rho_0}$. *Right*: Possible bounded trajectories in the WKB approximation.

Transport of massless fields [235] In the vicinity of the wiggly string, the propagation of a massless field Φ obey the Laplace-Betrami wave equation:

$$\frac{1}{\sqrt{-g}}\partial_\mu(\sqrt{-g}g^{\mu\nu}\partial_\nu)\Phi = 0 \tag{3.6}$$

Using the ansatz $\Phi(r,\theta,z,t) = e^{il\theta}e^{i(\omega t-kz)}R(r)$, the wave equation turns out to be analog to the Schrödinger equation that describes the 2D hydrogen atom [239][2]:

$$-\frac{1}{\rho}\frac{d}{d\rho}\left(\rho\frac{dR}{d\rho}\right) + \left(\frac{l^2}{\alpha^2\rho^2} + \ln\frac{\rho}{\rho_0}\right)R = \bar{\zeta}R \tag{3.7}$$

where $\rho = r/\gamma$, $\rho_0 = r_0/\gamma$, $\gamma = \left[8\varepsilon\left(\omega^2+k^2\right)\right]^{-1/2}$ and

$$\bar{\zeta} = \frac{1}{8\varepsilon}\frac{\omega^2-k^2}{\omega^2+k^2}. \tag{3.8}$$

A consequence of the effective potential term in (3.7) is that in the geometrical optics limit, trajectories are radially confined helices around the string. As discussed before for stellar interior,

[2]The logarithmic potential is the correct form for the 2D Coulomb potential as it satisfies the Gauss' theorem in two dimensions.

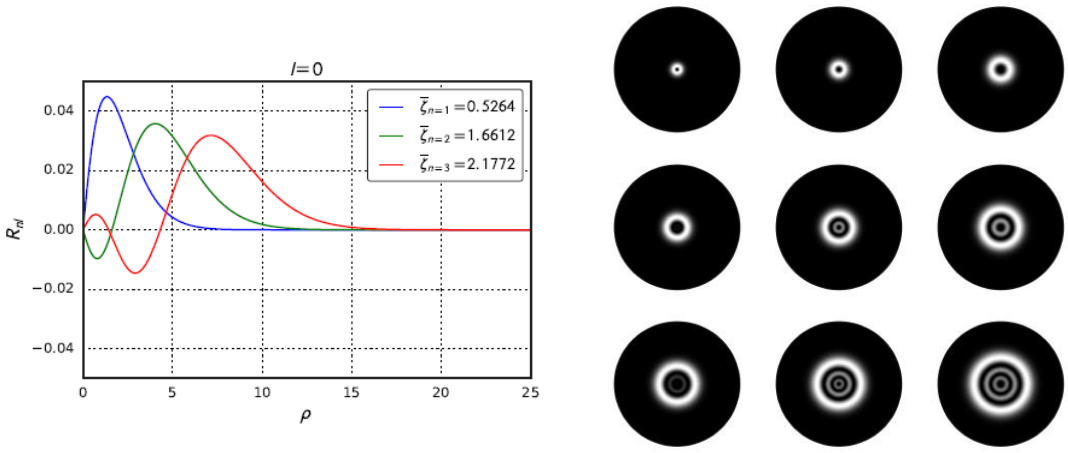

Figure 3.4: *Left*: Radial solutions for $n = 1, 2, 3$ and $l = 0$. *Right*: Radial intensity profiles with $n = 1, 2, 3$ and $l = 0, 1, 2$. The profiles are disposed as in a matrix where n and l give the line and column numbers respectively.

there is a gravitational trapping of the massless field, giving rise to bound states (see Fig. 3.3). The different states of energy $\bar{\zeta}$ are labeled by two integers n and l. In Figure 3.4, the numerical solutions of 3.7 are plotted from a finite difference algorithm for several values of these pseudo-quantum numbers. A similar work can be performed for massive fields, the main difference being the introduction of a cut-off frequency due to the mass term. The number of propagating modes turn out to be finite they explicitly depend on the mass of the particles.

As suggested by Figure 3.4, such cosmic structures with a non-vanishing gravitational potential behave as waveguides: the number of propagating modes along the defect axis is limited by the constraint $\bar{\zeta}_{nl}^{-1} < 4G(\mu - T)$. It is then possible to mimic them in the laboratory from a cylindrical graded-index optical fiber: when $l = 0$, the propagating electromagnetic modes also obey (3.7) when a refractive index is tuned as

$$n(r) = \left(1 - \Omega \ln \frac{r}{r_0}\right)^{1/2}, \tag{3.9}$$

with the dimensionless parameter $\Omega \ll 1$ in order to be consistent with the wiggly string parameter ε. The radial solution and the intensity profiles are similar to the plots on Figure 3.4 (intensities are restricted to the first column).

3.2 Kleinian universes

3.2.1 Klein-Gordon transport at a signature transition

A sign of the times [240] A metric signature change from Euclidean $(+,+,+,+)$ to Lorentzian $(-,+,+,+)$ might have happened in the early Universe as a theoretical consequence of the "no-boundary proposal" from Hartle and Hawking [241]. Another possibility suggested by Sakharov [242] is that of a transition to a Kleinian signature $(-,+,+,-)$. Mechanisms accounting for metric signature transitions are investigated in the framework of quantum gravity [243]-[245] and in Einstein-Cartan theory as well: in that case, the repulsive effect due to the spinning matter gives rise to a regular transition from Euclidean to the Lorentzian region [54].

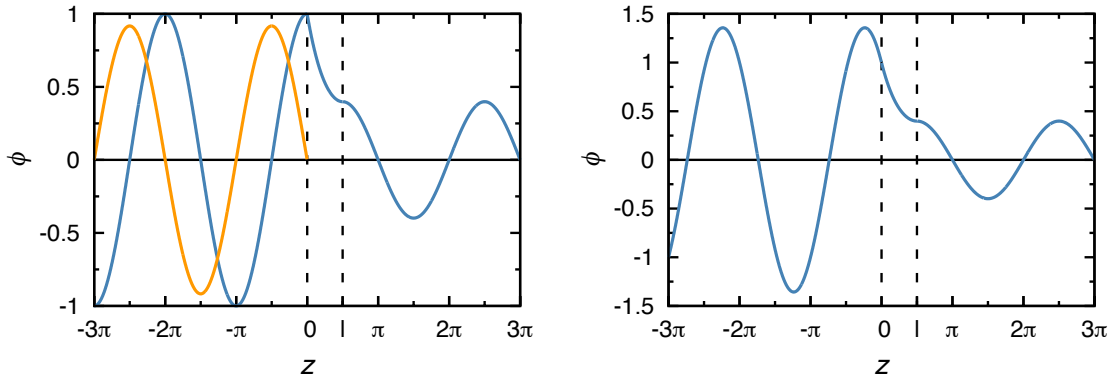

Figure 3.5: *Left*: Tunneling of the wave function ϕ (real part) through a Kleinian slab of length l: the blue line represents the incident and transmitted waves while the orange line denotes the reflected one. *Right*: Graph showing the total wave function for $z<0$ (incident+reflected). The probability current is conserved since in Eq. (3.12) we have $|r|^2+|t|^2=1$. In both graphs, z is given in units of k_z^{-1}.

The effects of a Lorentzian to Kleinian transition on matter and electromagnetic waves were studied in details by Alty [246] from the following geometry:

$$ds^2=\begin{cases}-c^2dt^2+dx^2+dy^2+dz^2 & \text{for } z<0\\ -c^2dt^2+dx^2+dy^2-dz^2 & \text{for } 0<z<l\\ -c^2dt^2+dx^2+dy^2+dz^2 & \text{for } z>l.\end{cases} \tag{3.10}$$

Solving the Klein-Gordon equation $\left[\Box-\mu^2\right]\phi=0$ in such background gives

$$\phi(t,x,y,z)=e^{i(k_x x+k_y y-\omega t)}\begin{cases}e^{ipz}+re^{-ipz} & \text{for } z<0\\ ae^{pz}+be^{-pz} & \text{for } 0<z<l\\ te^{ipz} & \text{for } z>l.\end{cases} \tag{3.11}$$

Here, p is the z-component of the wavevector, a and b are complex amplitudes and r and t are the reflected and transmitted amplitudes obtained from conditions of continuity at the boundaries [246]

$$\begin{aligned} a &= \left(\frac{1+i}{2}\right)\frac{e^{-pl}}{\cosh(pl)} \\ b &= \left(\frac{1-i}{2}\right)\frac{e^{pl}}{\cosh(pl)} \\ t &= \frac{e^{-ipl}}{\cosh(pl)} \\ r &= -i\text{tanh}(pl) \end{aligned} \tag{3.12}$$

Thus, there is tunneling across the Kleinian slab and it is easily verified that the probability current is conserved by summing the squared modulus of the amplitude of the incident, reflected and transmitted waves (see Fig. 3.5).

An analog: the electronic metamaterial [240] Electronic metamaterials are analogs of optical metamaterials in the sense 1) that the effective mass m^* and the difference $(E-V)$ are the electronic counterparts of the dielectric permittivity ε and the magnetic permeability μ, respectively and 2) that a positive (negative) effective mass corresponds to a positive (negative) permittivity (similarwise for $(E-V)$ and μ) [247]. As an example, the electronic analogue for the permittivity tensor of a hyperbolic metamaterial[3] is the effective mass tensor:

$$\varepsilon_{ij} = \begin{pmatrix} \varepsilon_1 & 0 & 0 \\ 0 & \epsilon_1 & 0 \\ 0 & 0 & -|\varepsilon_2| \end{pmatrix} \longleftrightarrow \left[\frac{1}{m^*}\right]^{ij} = \begin{pmatrix} m_1^{-1} & 0 & 0 \\ 0 & m_1^{-1} & 0 \\ 0 & 0 & -|m_2|^{-1} \end{pmatrix} \tag{3.13}$$

The energy levels of spinless electrons in anisotropic semiconductors are given by the time-independent effective mass Schrödinger equation:

$$-\frac{\hbar^2}{2}\left[\frac{1}{m^*}\right]^{ij}\partial_i\partial_j\Psi + V\Psi = E\Psi \tag{3.14}$$

Comparing with the Schrödinger equation for electrons propagating in a non-euclidean geometry

$$-\frac{\hbar^2}{2m_e}\frac{1}{\sqrt{g}}\partial_i\left(\sqrt{g}g^{ij}\partial_j\right)\Psi + V\Psi = E\Psi, \tag{3.15}$$

shows that the effective mass tensor generates an hyperbolic geometry, whose metric is

$$g^{ij} = m_e\left(\frac{1}{\hbar^2}\frac{\partial^2 E}{\partial k_i \partial k_j}\right)_{\mathbf{k}=0} = \begin{pmatrix} m_e/m_1 & 0 & 0 \\ 0 & m_e/m_1 & 0 \\ 0 & 0 & -m_e/|m_2| \end{pmatrix} \tag{3.16}$$

Resolution of (3.14) shows that the wavefunction $\Psi(\boldsymbol{x}, z, t)$ is given by

$$\Psi(t,x,y,z) = e^{i(\boldsymbol{k}\cdot\boldsymbol{x}-\omega t)}\begin{cases} e^{ipz} + re^{-ipz} & \text{for } z<0 \\ ae^{pz} + be^{-pz} & \text{for } 0<z<l \\ te^{ipz} & \text{for } z>l \end{cases} \tag{3.17}$$

[3] That is a material for which the permittivity eigenvalues are of different signs.

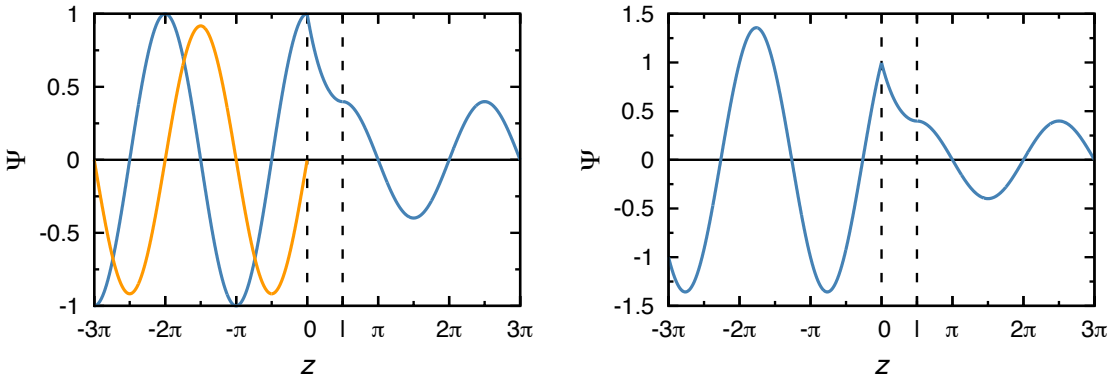

Figure 3.6: *Left*: Tunneling of the wave functions Ψ and ϕ (real part) through a metamaterial (Kleinian spacetime) sandwich of length l: comparison with Fig. 3.5 shows a phase shift of π between the two reflected waves (orange lines). *Right*: Graph of the total wave function with a sharp peak at $z = 0$. In both graphs, z is given in units of k_z^{-1}.

which is formally analog to (3.11). Applying the conditions of continuity at the boundaries gives

$$\begin{aligned} a &= \left(\frac{1-i}{2}\right) \frac{e^{-pl}}{\cosh(pl)} \\ b &= \left(\frac{1+i}{2}\right) \frac{e^{pl}}{\cosh(pl)} \\ t &= \frac{e^{-ipl}}{\cosh(pl)} \\ r &= i\tanh(pl) \end{aligned} \tag{3.18}$$

Eqs. (3.18) are very close to eqs. (3.12): the differences arise because of the discontinuity of $\partial\Psi/\partial z$ at the boundaries, which shifts the reflected wave by a phase of π and produces a sharp peak at $z = 0$ in the wave function Ψ (Fig. 3.6).

3.2.2 Particle dynamics in a bouncing cosmology

Big Bang or Big Bounces ? [187],[248] Understanding cosmology at transplanckian scales is a thorny problem, but today, most of the high-energy physics theories[4] call for cyclic universe models, that is an endless repetition of big crunches followed by big bounces, along the same line of thought as the Stoics' concept of palingenesia. Recently, a safe transition has been proposed [250, 251], where the singularity is nothing more than the temporary collapse of a fifth dimension. The three space dimensions remain large and time keeps flowing smoothly.

A toy model for the geometry of this transition is the compactified 2D Milne universe $\mathcal{M}_C$ [252, 253]. The Milne universe metric is given by

$$ds^2 = -dt^2 + t^2 d\chi^2 + t^2 \sinh^2\chi \left(d\theta^2 + \sin^2\theta d\phi^2\right) \tag{3.19}$$

[4]This a natural outcome in quantum loop gravity but it is also considered in superstring theory [249].

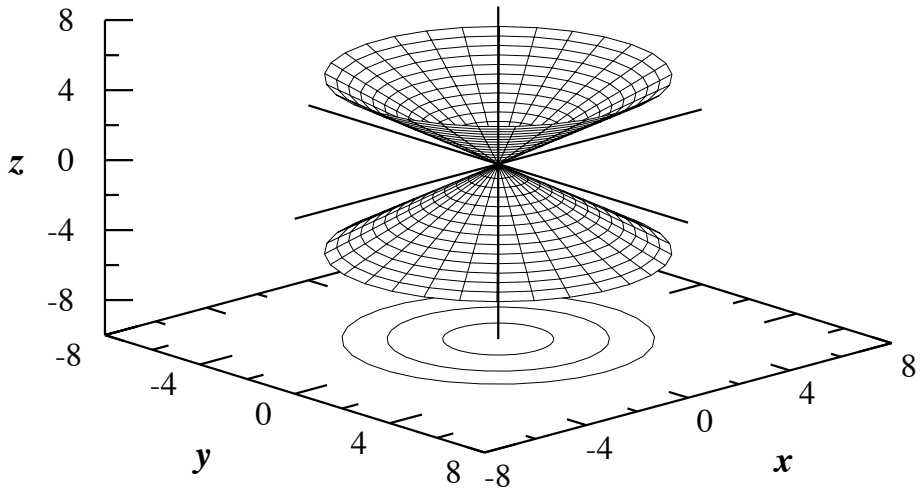

Figure 3.7: Double cone surface corresponding to the geometry of a compactified Milne universe with $(x = t\sinh\theta\cos\phi, y = t\sinh\theta\sin\phi, z = t\cosh\theta)$. The upper half part corresponds to $t > 0$ while the lower one is for values of $t < 0$.

and it was proposed by E.A. Milne in 1933. It represents a homogeneous, isotropic and expanding model for the universe with a negative curvature [254] which grows faster than those simple cold matter dominated or radiation dominated universes.

In order to compactify the Milne universe on hypersurfaces of fixed solid angle, we follow the usual approach [250]-[252],[255] and let the variable χ acquire some period denoted as $2\pi\kappa$: here, $0 < \kappa \in \mathbb{R}^1$ is a constant parameter for compactifications that is related to the rapidity $\tanh^{-1} v = 2\pi\kappa$ of a finite Lorentz boost [256, 257]. After reparametrization, the line element corresponding to the compactified Milne universe finally writes as

$$ds^2 = -dt^2 + \kappa^2 t^2 d\phi^2 \tag{3.20}$$

where $t \in \mathbb{R}^1$. As can be seen from the disclination line element (2.26), the presence of κ^2 in the above metric indicates a conical singularity of the curvature at the origin (see Fig. 3.7). As we will see below, this has important implications to the geodesics and wavefunctions of particles approaching the singularity, which acts as a filter for classical particles and a phase-eraser for quantum ones.

Transport of classical and quantum particles [187],[248] For classical particles, the resolution of the geodesic equations lead after some algebra to the following expression:

$$t = \pm\frac{t_0}{|\sinh\kappa\Delta\phi|}, \tag{3.21}$$

where the angular momentum $\kappa^2 J = C^{st}$, $t_0 = \kappa\,|J|$ and $\Delta\phi = \phi - \phi_0$. This trajectory is known to be a Poinsot spiral [258], with the $+$ $(-)$ sign corresponding to the upper (lower) cone. For $J \neq 0$ one can see that depending on the choice of the signal (or sheet of the cone), the particle

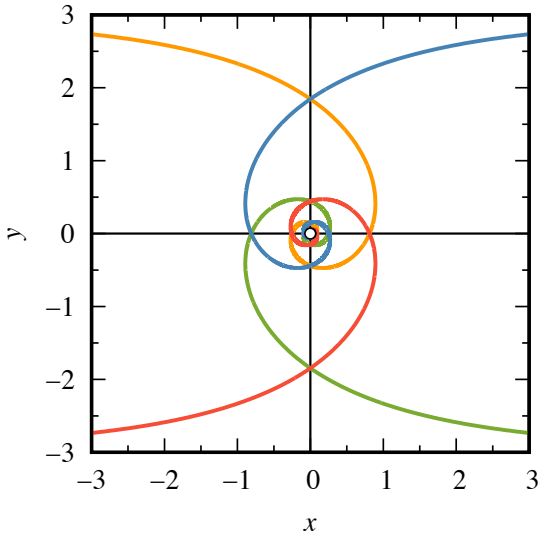

Figure 3.8: Timelike geodesics with the radial time t given in units of t_0 and $\kappa = 1/3$, corresponding to (3.21). The blue and green (orange and red) lines are moving away (towards) from (to) the singularity. Furthermore, particles following the trajectories in the first (third) and second (fourth) quadrants are spinning clockwise (counterclockwise). The blank point at the origin is just to emphasize that the curves do not reach the singularity.

always remains in the upper or lower region with no link between those regions of spacetime, but for $J = 0$, which corresponds to $\phi = \phi_0$ and $t = \pm\,\Delta\lambda$, the geodesics are straight lines crossing the singularity. As a result, the particle can travel from one cone to the other, but such trajectories are very unstable since small perturbations in the value of $J = 0$ causes large deviations on the trajectories. A similar result was found for a classical particle in a double cone in Ref. [259], where a classical non-relativistic particle constrained to a double cone only crosses the vertex through straight lines.

The treatment of quantum particles is based on the resolution of Klein-Gordon equation on the same background manifold (here in natural units $c = \hbar = 1$):

$$\left[-\frac{1}{t}\frac{\partial}{\partial t}\left(t\frac{\partial}{\partial t}\right) + \frac{1}{\kappa^2 t^2}\frac{\partial^2}{\partial \phi^2} - m^2\right]\varphi = 0. \tag{3.22}$$

Separating variables according to $\varphi(t,\phi) = f(t)g(\phi)$, the solutions of (3.22) are obtained as:

$$f(t) = A\tilde{J}_{l/\kappa}(mt) + B\tilde{Y}_{l/\kappa}(mt) \tag{3.23}$$

$$g(\phi) = Ce^{il\phi} + De^{-il\phi} \tag{3.24}$$

where A, B, C, D are constants of integration and $\tilde{J}_{l/\kappa}$, $\tilde{Y}_{l/\kappa}$ are linearly independent modified Bessel

functions defined in Ref. [260] as

$$\tilde{J}_{l/\kappa}(mt) = \operatorname{sech}\left(\frac{\pi l}{2\kappa}\right) \operatorname{Re} J_{il/\kappa}(mt) \tag{3.25}$$

$$\tilde{Y}_{l/\alpha}(mt) = \operatorname{sech}\left(\frac{\pi l}{2\kappa}\right) \operatorname{Re} Y_{il/\kappa}(mt) \tag{3.26}$$

An interesting feature arises for $l \neq 0$: Eqs. (3.25)-(3.26) are indeed not continuous through the origin, which is similar to the classical geodesics that in general do not cross the singularity. In [253] it was given an interesting interpretation for this fact constructing a Hilbert space $\mathcal{H} = \mathcal{H}^{(-)} \oplus \mathcal{H}^{(+)}$ as a direct sum of two Hilbert spaces $\mathcal{H}^{(-)}$, $\mathcal{H}^{(+)}$. The elements of $\mathcal{H}^{(-)}$ are solutions of Eq. (3.22) in the pre-singularity era ($t < 0$) while the ones of $\mathcal{H}^{(+)}$ are solutions in the post-singularity era ($t > 0$). That is, $\mathcal{H} = \mathcal{H}^{-} \oplus \mathcal{H}^{+}$ is a vector space whose elements φ have the following form [261]

$$\varphi = \left(\varphi^{(-)}, \varphi^{(+)}\right) \in \mathcal{H}^{(-)} \times \mathcal{H}^{(+)}, \tag{3.27}$$

with an inner product

$$\langle \varphi | \psi \rangle = \left\langle \varphi^{(-)} \middle| \psi^{(-)} \right\rangle + \left\langle \varphi^{(+)} \middle| \psi^{(+)} \right\rangle. \tag{3.28}$$

Hence, vectors like $(\varphi^{(-)}, 0)$ and $(0, \varphi^{(+)})$ describe states of annihilation and creation of particles at the singularity $t = 0$, respectively. By Eq. (3.28) an inner product between those kinds of states yields zero, which means no correlation between them. This reflects the loss of phase of the wave function due to the strong oscillations around the singularity.

An analog: the hyperbolic disclination [187],[248] Probing how particles behave in $\mathcal{M}_C$ can be tested in the laboratory from hyperbolic liquid crystal metamaterials (HLCM): this means that the permittivity along the director axis $\varepsilon_{\parallel} < 0$ and the permittivity perpendicular to the director axis $\varepsilon_{\perp} > 0$ are of opposite sign. Such media can be made from a host nematic liquid crystal that includes an admixture of metallic nanorods [262] or coated core-shell nanospheres [152]. To retrieve the Kleinian double-cone geometry, the HCLM must be endowed with an hyperbolic disclination, which is a line defect described by the geometry:

$$ds^2 = \varepsilon_{\perp} d\rho^2 - \varepsilon_{\parallel} \rho^2 d\phi^2 + \varepsilon_{\perp} dz^2 \tag{3.29}$$

or more simply, after a rescaling:

$$ds^2 = dr^2 - \gamma^2 r^2 d\phi^2 + dz^2 \tag{3.30}$$

This line element is relevant only by the extraordinary modes. For radial injection conditions (planar trajectories $z = C^{st}$), the geometry experienced by extraordinary rays is perfectly identical to that of the compactified Milne universe.

A stable configuration for the director field may be obtained from a cylindrical shell of HLCM with homeotropic anchoring at the boundaries (see Fig. 3.9). In the geometrical optics limit, extraordinary light paths turn out to be Poinsot's spirals as for the compactified Milne universe. The practical realization sets limits to the efficiency of such analog device for the classical particles. First, the analysis holds only within a limited frequency bandwidth due to the resonant nature of the used core-shell spheres. Second, as previous phenomena concerns the extraordinary mode, an

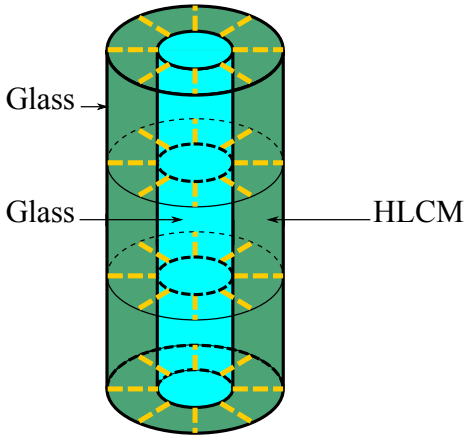

Figure 3.9: Director configurations for HLCM in a cylindrical shell, with optical axis represented in cylindrical coordinates (ρ, ϕ, z) as $\hat{\mathbf{n}} = \hat{\boldsymbol{\rho}}$. The walls of the inner and outer cylinder are made of glass, while the liquid crystal together with metallic nanorods (aligned in the direction of $\hat{\mathbf{n}}$) fills the space in between.

efficient optical absorber should include a filter to shut off the ordinary wave. Finally, it should be noticed that the present model concerns optics inside a bulk hyperbolic material: to design a perfect optical analog, the hyperbolic medium must be impedance matched to avoid sizable reflections at the interfaces. The analogy was also extended to quantum particles by investigating light in the scalar wave approximation in the same device.

Another solution to avoid difficulties related to the inner cylinder is to fill a capillary with an HLCM (homeotropic anchoring as well) having its optical properties depending on the radial variable:

$$\varepsilon_{\parallel}(r) = \epsilon_{\parallel}\left(1 + \frac{\delta^2}{r^2}\right), \tag{3.31}$$

$$\varepsilon_{\perp}(r) = \epsilon_{\perp}\left(1 + \frac{\alpha^2\delta^2}{r^2 + \delta^2}\right), \tag{3.32}$$

where $\epsilon_{\parallel}$, $\epsilon_{\perp}$ are the previous values of the permittivities, $\alpha^2 = |\epsilon_{\parallel}|/\epsilon_{\perp}$ and δ is the radius of the inner core, which is a small value. This regularization was suggested in [263] and, in fact, used in [253] to remove the Cauchy problem at the singularity. However, none of these two solutions take into account explicit gravitational backreaction calculations in the spirit of [264]-[265].

4

Geometry-driven functionalization of materials

In a famous lecture given in 1959, Feynman stated that "*there's plenty of rooms at the bottom*" [266]. Nowadays, the advent of nanoscience and nanoengineering seemed to have completely fulfilled Feynman's foresight. In photonics, metamaterials are artificial media structured at a subwavelength scale. Originally intended for imaging below the diffraction limit, they are now used to design not only passive negative-index systems (phase compensators, invisibility cloaks, superlenses [267]) but also metadevices, i.e. tunable, switchable and nonlinear active systems with sensing functionalities [268, 269]. In a similar fashion, the emerging field of thermotronics now opens the possibility to design the thermal analogs of usual electronic components (such as thermal logic gates [274] thermal diodes and transistors [270]-[273]) and to manage heat flux at an unprecedented level [275]-[278]. Last but not least, low-dimensional systems such as carbon nanotubes, graphene and more recently silicene have shown unseen chemical, electrical, mechanical and thermal properties which are expected to incent a wide spectrum of applications, ranging from to biochemistry [279] to energy generation [280] and storage [281].

The common thread between these examples is their reliance on curvature. Indeed, transformation optics uses conformal mappings to predict the physical properties a metamaterial must have, such that light propagates along predesigned curved paths: stated otherwise, the metamaterial is taylored in order to mimic a desired curvature of space. Likewise, the honeycomb structure of graphene is known to exibit pentagonal and heptagonal defects (generally associated in Stone-Wales dipoles), which are line sources of curvature that generate small bumps (generally of a few Angstrom of height) in graphene sheets. As the shape of graphene plays a crucial role in determining its physical properties [282, 283], it is expected that the physical properties of graphene can be taylored from distributions of topological defects: this is the promising field of defect engineering, now invading soft matter systems [284].

Soft-matter systems, in particular liquid crystals, are well-renowned contenders to build functionalized devices. Contrary to metamaterials, they have a high flexibity, which makes their physical properties and even their topology [285] easily tunable for the visible range. Several proposals have been made in optics to design q-plates [286]-[290], non-reciprocal devices [292]-[293]... The forthcoming sections are dedicated to transport phenomena in condensed matter, and how curvature/torsion can be taken advantage of to taylor outgoing fluxes in a wide range of problems (acoustics, electronics, thermotronics, optics...).

4.1 Defect engineering in hard and soft matter

4.1.1 Electrodynamics

Generation of optical vorticity [294] In classical electrodynamics, it is well known that light carries linear as well as angular momentum. This latter can be divided into two parts: a spin contribution, associated to the polarization of the wave, and an orbital contribution. During the last decades, the interaction of the orbital angular momentum of light with matter has become a very active research field due to its large number of potential applications such micromachines, microscopy and imaging, optical tweezers, terabit communications...(for a review, see [295]).

A possible way of generating orbital angular momentum states in light beams is to use non-chiral line defects such as disclinations [296], or chiral line defects (screw dislocations), as these latter are likely to imprint their torsion onto wavefronts and light paths. This can be confirmed from the differential form of Maxwell's equations, which provides a natural framework to include the coupling of the field to a background geometry (for further details on exterior calculus, see part 5 below). In the presence of a screw dislocation, the source-connected equations (Maxwell-Gauss and Maxwell-Ampère) write as:

$$\frac{1}{r}\frac{\partial}{\partial r}(rE^{\hat{r}}) + \frac{1}{\sqrt{r^2+\beta^2}}\frac{\partial E^{\hat{\phi}}}{\partial r} + \frac{\partial E^{\hat{z}}}{\partial z} = \rho \tag{4.1}$$

$$\frac{1}{r}\left[\left(\frac{\beta}{\sqrt{r^2+\beta^2}}\frac{\partial}{\partial\phi} - \sqrt{r^2+\beta^2}\frac{\partial}{\partial z}\right)B^{\hat{\phi}} + \left(\frac{\partial}{\partial\phi} - \beta\frac{\partial}{\partial z}\right)B^{\hat{z}}\right] = J^{\hat{r}} + \frac{\partial E^{\hat{r}}}{\partial t} \tag{4.2}$$

$$\frac{\sqrt{r^2+\beta^2}}{r}\left[\frac{\partial B^{\hat{r}}}{\partial z} - \frac{\partial}{\partial r}\left(B^{\hat{z}} + \frac{\beta}{\sqrt{r^2+\beta^2}}B^{\hat{\phi}}\right)\right] = J^{\hat{\phi}} + \frac{\partial E^{\hat{\phi}}}{\partial t} \tag{4.3}$$

$$\frac{1}{r}\left[\frac{\partial}{\partial r}\left(\sqrt{r^2+\beta^2}B^{\hat{\phi}} + \beta B^{\hat{z}}\right) - \frac{\partial B^{\hat{r}}}{\partial\phi}\right] = J^{\hat{z}} + \frac{\partial E^{\hat{z}}}{\partial t} \tag{4.4}$$

The source-free equations (Maxwell-Thomson and Maxwell-Faraday) can be derived from a similar procedure, or more rapidly by using the electric-magnetic duality:

$$\rho \to 0 \quad J^{\hat{i}} \to 0 \quad E^{\hat{i}} \to -B^{\hat{i}} \quad B^{\hat{i}} \to E^{\hat{i}} \tag{4.5}$$

Except for the plane wave, most of the propagating solutions of Maxwell's equations are of quite complicated form. They are usually described as superpositions of plane waves or, depending on the coordinate system, special functions or polynomial expansions. Nevertheless, the essential physics of the system can be retained with the following ansatz for the fields:

$$\boldsymbol{E} = \boldsymbol{E}_0(r)\exp\left(ikz + i\beta k\phi - i\omega t\right) \tag{4.6}$$

$$\boldsymbol{B} = \boldsymbol{B}_0(r)\exp\left(ikz + i\beta k\phi - i\omega t\right) \tag{4.7}$$

assorted with the constraint $k\beta = m \in \mathbb{Z}$, since the point (r, ϕ, z) is the same as $(r, \phi + 2\pi, z - 2\pi\beta)$. This implies that the solutions allowed near the defects are the modes of discrete wavenumbers

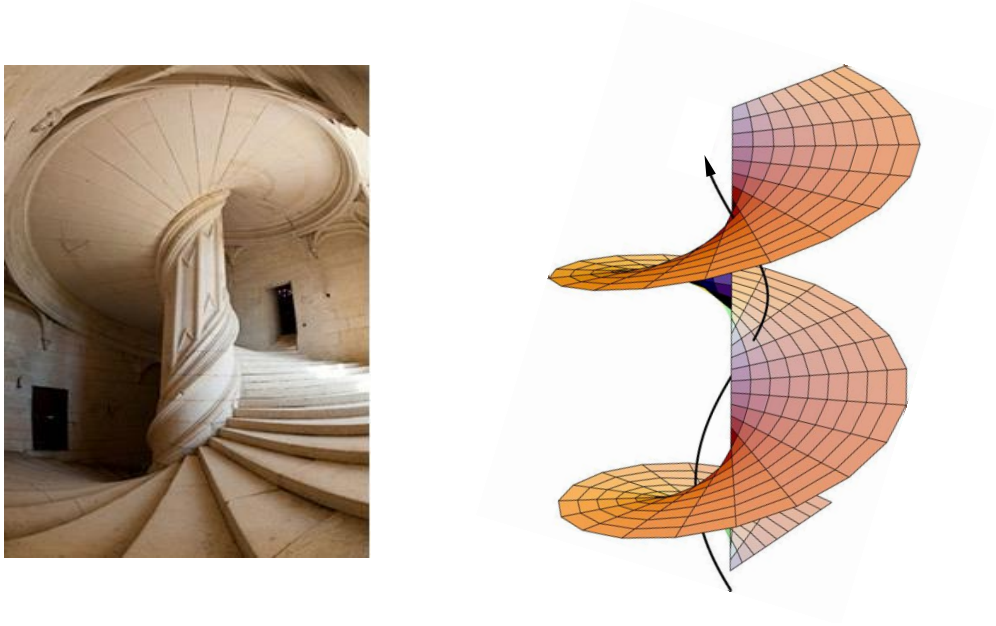

Figure 4.1: *Left*: A giant screw dislocation in Da Vinci's spiral stairway (Chambord). *Right*: The screw dislocation imprints an optical vorticity on the electromagnetic wavefronts.

$k_m = m/\beta$. Usually, values of the Burgers vector in smectic liquid crystals range from one layer thickness (typically 3 nm, the most common family of screw dislocations) up to hundreds of layers (typically 300 nm for giant screw dislocations, which are more seldom and less stable): therefore, couplings of electromagnetic waves with the defect are expected to occur in a spectrum ranging from soft X-rays to ultraviolet. This brings about interesting applications such as using the medium endowed with a defect as a filter in that range of frequencies.

Plugging (4.6)-(4.7) gives the following amplitudes:

$$\boldsymbol{E}_0(r) = \frac{a}{r}\hat{\boldsymbol{e}}_r - \frac{a\sqrt{r^2+\beta^2}}{r^2}\hat{\boldsymbol{e}}_\phi + \frac{\beta a}{r^2}\hat{\boldsymbol{e}}_z \tag{4.8}$$

$$\boldsymbol{B}_0(r) = \frac{a}{r}\hat{\boldsymbol{e}}_r + \frac{a\sqrt{r^2+\beta^2}}{r^2}\hat{\boldsymbol{e}}_\phi - \frac{\beta a}{r^2}\hat{\boldsymbol{e}}_z \tag{4.9}$$

where the parameter a sets the intensity of the fields.

The mean Poynting vector can now be determined as

$$\boldsymbol{S} = \mathrm{Re}\left(\frac{1}{2}\boldsymbol{E}\times\boldsymbol{B}^*\right) = \frac{\beta a^2}{r^3}\hat{\boldsymbol{e}}_\phi + \frac{a^2\sqrt{r^2+\beta^2}}{r^3}\hat{\boldsymbol{e}}_z \tag{4.10}$$

This expression means that the Poynting vector spirals along the direction of propagation. Now,

the volume density of orbital angular momentum being defined as

$$\boldsymbol{M} = \boldsymbol{r} \times \boldsymbol{S} = -\frac{z\beta a^2}{r^3}\hat{\boldsymbol{e}}_r - \frac{a^2\sqrt{r^2+\beta^2}}{r^2}\hat{\boldsymbol{e}}_\phi + \frac{\beta a^2}{r^2}\hat{\boldsymbol{e}}_z \tag{4.11}$$

Computing the ratio between the flux of angular momentum to that of energy across the surface $z = C^{st}$ finally leads to

$$\frac{L}{P} = \frac{\int_\delta^{+\infty}\int_0^{2\pi} M_z r dr d\phi}{\int_\delta^{+\infty}\int_0^{2\pi} S_z r dr d\phi} = \beta = \frac{m}{k} \tag{4.12}$$

where the ultraviolet cut-off δ was introduced to include a possible core structure for the defect (in smectic liquid crystals, δ is of the order of the average thickness of a layer). The electromagnetic field has therefore a well-defined orbital angular momentum, which provides an alternate approach to design optical tweezers from a simple (and tunable) waveguide effect[1].

Spintronics [297] The torsion generated by a dislocation also couples to the spin of the particles, and in a way similar to an applied external magnetic field. This form of this coupling is obtained by writing the action for a fermion field in the presence of gravity with torsion [25]-[299] In the non-relativistic limit, the Dirac operator results in the low-energy Pauli Hamiltonian

$$H = \frac{1}{2m}\left(\boldsymbol{p} + \frac{\eta_1}{c}A_0\boldsymbol{\sigma}\right)^2 - \frac{1}{mc^2}\eta_1^2 A_0^2 - \eta_1 c\boldsymbol{\sigma}\cdot\boldsymbol{A} \tag{4.13}$$

where $A_\mu = (A_0, -\boldsymbol{A})$ is the axial part of torsion[2], η_1 is material-dependent constant due to the magneto-elastic interaction and $\boldsymbol{\sigma}$ is the vector of Pauli matrices. The time-like part of axial torsion, A_0, couples to the electron spin via a minimal coupling to the kinematic momentum in Eq. (4.13)[3]. The presence of the second term in Eq. (4.13) plays the role of a mass term for torsion (it is quadratic in A_0) [301]. It adds to the gauge invariant form of the minimally coupled term of the kinetic energy [301]. Finally, the last term is analogous to a Zeeman interaction which couples the spatial part of torsion to the spin. In the case of the screw dislocation, we only have an axial term remaining (called the axitor) whose unique component is:

$$A^z = \frac{\kappa}{r_0^2}K_0(r/r_0). \tag{4.14}$$

where K_0 is the modified Bessel function of the second kind of order zero and r_0 is a characteristic core length scale of the defect. It follows from Eq. (4.13), that the Hamiltonian reduces to the simple form

$$H = \frac{1}{2m}\boldsymbol{p}^2 - \frac{2\eta_1 c}{\hbar}\boldsymbol{S}\cdot\boldsymbol{A} \tag{4.15}$$

where $\boldsymbol{S} = \frac{\hbar}{2}\boldsymbol{\sigma}$ is the spin angular momentum of the electron.

[1] Even if this result is derived from a simple solution of Maxwell's equations, it corresponds to what is obtained for realistic laser modes (Laguerre–Gaussian beams).

[2] Torsion can be written as the sum of its irreducible parts [300]: tensor, trace and axial.

[3] It is worth noting that the coupling is similar to the way spin-orbit interactions are included into the kinetic energy through a non-Abelian gauge field in the Pauli equation.

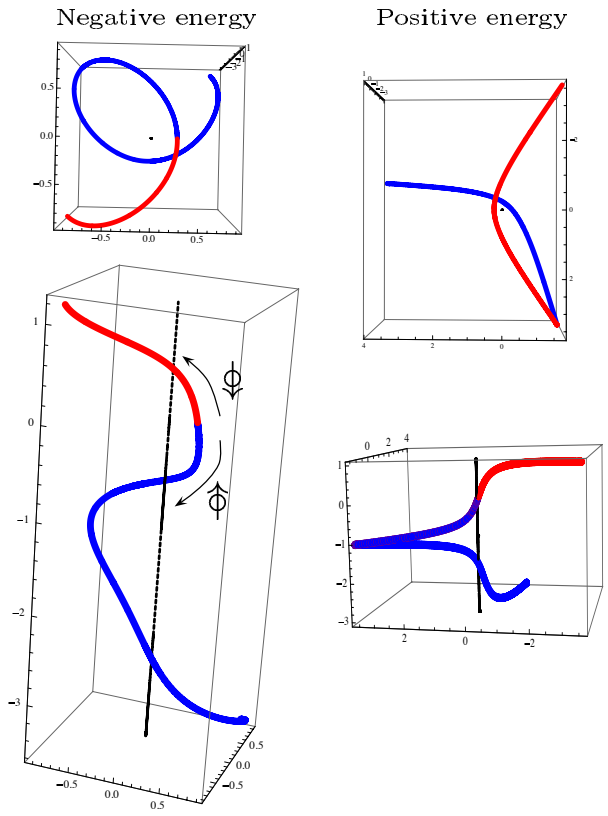

Figure 4.2: Trajectories around the defect line (straight line along $z-$axis) for a bound state of total energy $A = -0.5$ (left) and an asymptotically free state $A = 0.5$ (right). For $A = -0.5$ the trajectories are bounded in the perpendicular plane (upper pannel), but the potential does not allow for closed orbits. The trajectories follow channels along the defect (lower pannel), downwards when the angular momentum is positive ($B = +0.447$, blue part, symbolized by the uparrow) and upwards otherwise ($B = -0.447$, red part). A particle orbiting in the perpendicular plane will automatically scatter along the defect in one direction or the other, depending on the particle's angular momentum, leading to spin and orbital momentum-dependent conducting channels. For $A = 0.5$, and more generally for free states, the defect can be used to select orbital momentum in the $z-$direction lower pannel, which is a peculiarity of spaces with torsion.

Following [302], the quasi-classical equations of motion for a fermion corresponding to Hamiltonian (4.15) are:

$$m\frac{d\boldsymbol{v}}{dt} = +\frac{2\eta_1 c}{\hbar}\boldsymbol{\nabla}\left(\boldsymbol{S}\cdot\boldsymbol{A}\right) \tag{4.16}$$

$$\frac{d\boldsymbol{S}}{dt} = -\frac{2\eta_1 c}{\hbar}\left(\boldsymbol{A}\times\boldsymbol{S}\right) \tag{4.17}$$

Since $\eta_1 < 0$, according to Eq. (4.16), the most favorable spin orientation is parallel to the Burger's

vector: if the gradient of torsion is negative, the force will be attractive when the spin is parallel to it and repulsive otherwise. This gives the screw dislocation the ability to attract spins with a specific polarisation. If the captured carriers are able to move along the defect, this gives rise to a spin-polarized current, an important resource for spintronics. In what follows, we focus the classical motion of the carriers attracted by the defect. Euler-Lagrange equations of motions can then be obtained explicitly as

$$\dot{r}^2 + \frac{B^2}{r^2} - \frac{2|\eta_1|\kappa c}{m r_0^2} K_0(r/r_0) = A \tag{4.18}$$

$$r^2\dot{\phi} = B \tag{4.19}$$

$$z + \kappa\phi = Ct + D \tag{4.20}$$

where A, B, C and D are integration constants. Examples of attractive (bound state) and asymptotically free trajectories are depicted in Fig. 4.2. The classical picture may then be summarized as follows[4]:

1. The defect line selectively captures in the positive $z-$direction particles with spin polarized antiparallel to the Burgers vector.

2. Particles are directed to the defect core and, depending on their angular momentum as explained in the caption of Fig. 4.2, they propagate along the defect which acts as a conducting channel.

3. Asymptotically free particles are just scattered out of their initial plane of injection towards the defect, which acts as a spin splitter.

Since the captured spins are polarized antiparallel to $\boldsymbol{b}$, the defect induces a two-way channel with opposing helicity. With the eventual inclusion of the spin-orbit interaction, the channel corresponding to $\ell < 0$ will be favoured and therefore the dominant spin-polarized current will be in this direction $(-\hat{\vec{z}})$. Torsion due to dislocations thus provides a pathway for spin circuitry design and spin current control in the absence of a real external magnetic field.

Omnidirectional concentrators [304] Concentration of light has become a major issue in a large number of applications ranging from solar energy harvesting to optical sensing. For a long time, diffraction phenomena forbid beam sizes below half of a wavelength and most of the attempts to focus light have consisted in overcoming the diffraction limit using superlenses [305].

Another possibility to efficiently concentrate light is to use an hyperbolic liquid crystal metamaterial (HLCM), obtained from an admixture of metallic nanoobjects to nematics[5]. As seen in section 3.2, the permittivity along the director axis $\varepsilon_{\parallel}$ and the permittivity perpendicular to the

[4] In the same reference [297], we refined this analysis by investigating the quantum behavior of the particles near the dislocation. Bound states can exist only if the minimum distance scale is such that $\hbar/\sqrt{m\alpha} < 0.681 r_0$. Moreover, the attraction by the dislocation depends on the angular momentum and the latter is intimately linked to the linear momentum along the defect core: hence the linear momentum along the z-axis must be quantized, $\hbar k = \ell\hbar/\kappa$, for the same reason. Finally, the results show that the particle, in its bound state, is always within the defect core r_0.

[5] The losses due to metallic components do not jeopardize the performances of the device, as they might be offset by using gain media as pointed in (highly doped oxides with lower dissipation levels have also been considered). The low-loss limit for metamaterials has also been recently reached by working within the terahertz waveband [12].

director axis $\varepsilon_\perp$ have opposite signs. For an orthoradial director field, the effective metric writes as[6]:

$$g_{ij} = \begin{pmatrix} 1 & 0 & 0 \\ 0 & -\alpha^2\rho^2 & 0 \\ 0 & 0 & 1 \end{pmatrix}. \tag{4.21}$$

The constants of motion are given by energy conservation and the Killing equations

$$K^i g_{ij} \frac{dx^j}{d\lambda} = 0 \tag{4.22}$$

where K^i are Killing vectors, which correspond to the cyclic variables of the metric, and λ is an affine parameter. A quick examination of Eq. (4.21) reveals two Killing vectors, $(\partial_\phi)^i = (0,1,0)^{\mathrm{T}}$ and $(\partial_z)^i = (0,0,1)^{\mathrm{T}}$ (here $^{\mathrm{T}}$ denotes the transposition operation used to represent column vectors), associated with the covectors:

$$(\partial_\phi)_i = g_{ij}(\partial_\phi)^j = (0, -\alpha^2\rho^2, 0), \tag{4.23}$$
$$(\partial_z)_i = g_{ij}(\partial_\varsigma)^j = (0,0,1). \tag{4.24}$$

Equations of motions are quickly obtained as:

$$\frac{dz}{d\lambda} = A \tag{4.25}$$
$$\rho^2 \frac{d\phi}{d\lambda} = C \tag{4.26}$$
$$\frac{1}{2}\left(\frac{d\rho}{d\lambda}\right)^2 - \frac{\alpha^2 C^2}{2\rho^2} = E \tag{4.27}$$

Integration leads after some algebra to solutions having the form of Poinsot spirals:

$$\rho(z) = \frac{\rho_M}{\cosh\left[\alpha\phi(z)\right]} \tag{4.28}$$
$$\text{with} \quad \phi(z) = \frac{1}{\alpha}\mathrm{argth}\left(\frac{Kz - \sqrt{\rho_M^2 - \rho_0^2}}{\rho_M}\right) \tag{4.29}$$

where ρ_0 is the injection radius, ρ_M and K are constants depending on α, A, C and E. Trajectories are confined within regions of maximum radius ρ_M (see Fig. 4.3). The smaller the value of α, the stronger is the spiraling behavior: indeed, $1/\alpha$ corresponds to the spiraling strength (or vorticity) of the defect.

The hyperbolic defect behaves as a sink for light paths. Is that property robust beyond the geometrical optics limit ? In the scalar wave approximation, the complex amplitude Φ of the wave is governed by the generalized form of the d'Alembert equation

$$\nabla_i \nabla^i \Phi - \frac{1}{c^2}\frac{\partial^2 \Phi}{\partial t^2} = 0, \tag{4.30}$$

[6]Despite the orientation of $\hat{\boldsymbol{n}}$ being different, the metric looks identical to (3.30). The identity is only apparent, as the rescalings are different in the two problems.

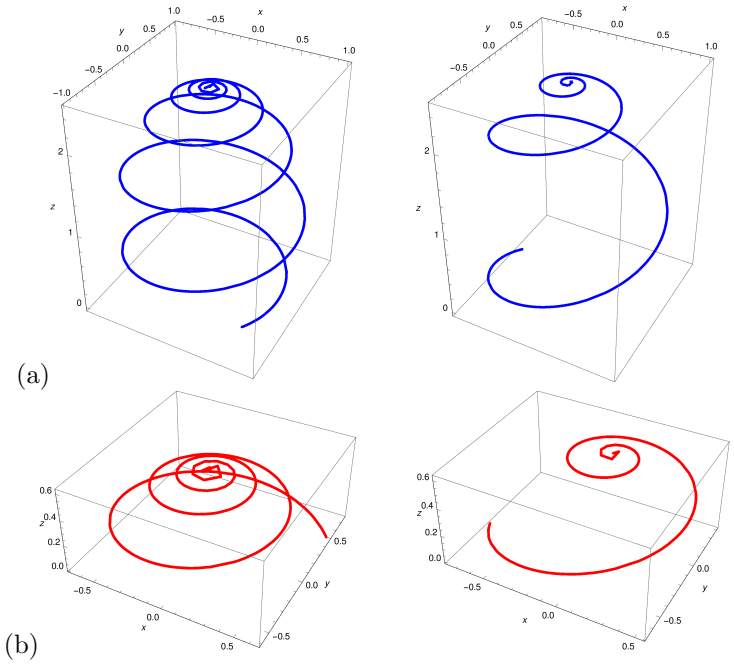

Figure 4.3: Light paths in three dimensions for $\rho_M = 1$, $\rho_0 = 0.8$ and $K = 0.64$. The figures on the left (resp. right) side refer to $\alpha = 0.1$ (resp. $\alpha = 0.2$). (a) Rays of increasing radius starting at $\rho_0 = 0.8$. (b) Rays of decreasing radius starting at $\rho_0 = 0.8$.

where $\nabla_i \nabla^i$ is the Laplace-Beltrami operator

$$\nabla_i \nabla^i \Phi = \frac{1}{\sqrt{|g|}} \partial_i \left(\sqrt{|g|} g^{ij} \partial_j \Phi \right). \tag{4.31}$$

Using the ansatz

$$\Phi(\rho, \phi, z) = F_{\ell,k_z}(\rho) e^{\pm i\ell\phi} e^{-i\omega t} e^{\pm i k_z z} \tag{4.32}$$

the wave equation writes as a modified Bessel differential equation of imaginary order $i\ell/\alpha$

$$\rho^2 \frac{d^2 F_{\ell,k_z}}{d\rho^2} + \rho \frac{dF_{\ell,k_z}}{d\rho} - \left[\left(\frac{\omega^2}{c^2} + k_z^2 \right) \rho^2 - \frac{\ell^2}{\alpha^2} \right] F_{\ell,k_z} = 0 \tag{4.33}$$

Solutions of this equation are of the form

$$F_{\ell,k_z}(\rho) = e_\ell \tilde{I}_{\ell/\alpha}(\bar{\omega}\rho) + f_\ell \tilde{K}_{\ell/\alpha}(\bar{\omega}\rho), \tag{4.34}$$

where $\bar{\omega}$ is given by

$$\bar{\omega} = \sqrt{k_z^2 + \omega^2/c^2} \tag{4.35}$$

with e_ℓ, f_ℓ being constants of integration. The functions $\tilde{I}_{\ell/\alpha} = \mathrm{Re} I_{i\ell/\alpha}$ and $\tilde{K}_{\ell/\alpha} = K_{i\ell/\alpha}$ are linearly independent solutions of Eq. (4.33), with $I_{i\ell/\alpha}, K_{i\ell/\alpha}$ being the modified Bessel functions

of first and second kind, respectively. At large distances, the asymptotic behavior allows to dismiss $\tilde{I}_{\ell/\alpha}$ and to retain only

$$\tilde{K}_{\ell/\alpha}(\bar{\omega}\rho) = \left(\frac{\pi}{2\bar{\omega}\rho}\right)^{1/2} e^{-\bar{\omega}\rho}\left[1 + O\left(\frac{1}{\bar{\omega}\rho}\right)\right] \tag{4.36}$$

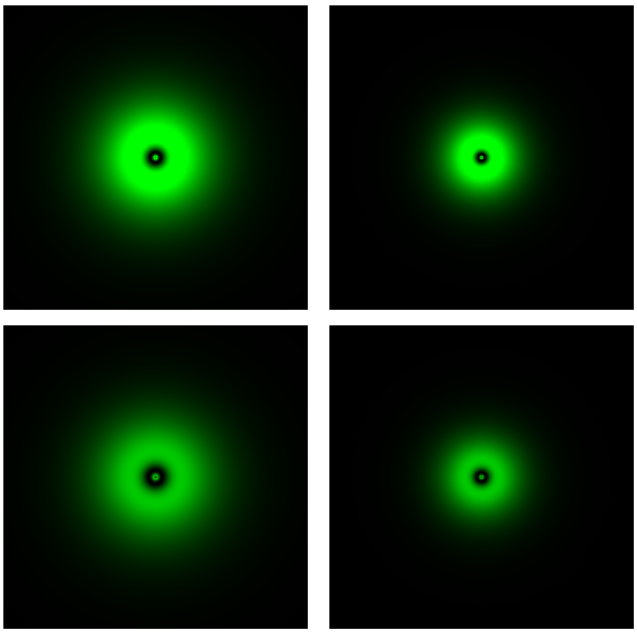

Figure 4.4: $|\tilde{K}|^2$ intensity profiles, representing the transverse field distributions. All plots are in the same scale and with $\ell = 1$. The ones on the left (right) correspond to $\bar{\omega} = 0.67$ ($\bar{\omega} = 1$). The top (bottom) ones correspond to $\alpha = 0.90$ ($\alpha = 0.83$).

The intensity distribution for the propagating fields shows 1) that the electromagnetic field concentrate along the axis of the device, and 2) that the bigger the value of $\bar{\omega}$, the smaller the light rings are (see Fig. 4.4). Thus, geometrical optics and wave optics treatments agree that light is concentrated while propagating in the HLCM medium: no matter how the rays are injected, they will fall down onto the defect core with or without being reflected in the outer layer of the cylindrical concentrator.

4.1.2 Acoustics

Analog model [306] Analogue models in acoustics have been developed most notably by Matt Visser [307] to investigate vorticity effects in isotropic fluids. Nematics are anisotropic fluids, which allows two kinds of acoustic waves to exist (similarly to sound in solid crystals): the ordinary wave, that behaves as inside an isotropic medium, and the extraordinary one that depends on the angle between the direction of the propagation and the director field $\mathbf{n}$. For the extraordinary wave, the

group index N_g, associated to acoustic energy transport, has the same structure as the energy index in optics (2.44):

$$N_g^2(\beta) = \frac{\rho v^2}{C_{11}} \sin^2 \beta + \frac{\rho v^2}{C_{33}} \cos^2 \beta \tag{4.37}$$

where ρ is the mass density, v is the velocity of sound in the isotropic phase, C_{33} and C_{11} are elastic constants respectively along the director's direction and in directions orthogonal to it.

Using the coordinates of the tangent vector in Frenet-Serret frame as we did in (2.45)-(2.46), one gets a line element from the orientation of the director field. For the planar horizontal configuration (2.25), this gives

$$\begin{aligned} ds^2 = Ng^2 dl^2 = &\left(\frac{\rho v^2}{C_{33}} \cos^2 \chi + \frac{\rho v^2}{C_{11}} \sin^2 \chi \right) dr^2 \\ &+ \left(\frac{\rho v^2}{C_{33}} \sin^2 \chi + \frac{\rho v^2}{C_{11}} \cos^2 \chi \right) r^2 d\theta^2 + \sin 2\chi \left(\frac{\rho v^2}{C_{33}} - \frac{\rho v^2}{C_{11}} \right) r dr d\theta \end{aligned} \tag{4.38}$$

with $\chi(\theta) = m\theta + \psi_0$.

In the case of a planar vertical configuration ($\mathbf{n} = (\sin \xi, 0, \cos \xi)$), similar calculations lead to [308]

$$\begin{aligned} ds^2 &= \left(\frac{\rho v^2}{C_{33}} \cos^2 \xi + \frac{\rho v^2}{C_{11}} \sin^2 \xi \right) dr^2 + \left(\frac{\rho v^2}{C_{33}} \sin^2 \xi + \frac{\rho v^2}{C_{11}} \cos^2 \xi \right) dz^2 \\ &+ \frac{\rho v^2}{C_{33}} r^2 d\theta^2 + \sin 2\xi \left(\frac{\rho v^2}{C_{33}} - \frac{\rho v^2}{C_{11}} \right) dr dz \end{aligned} \tag{4.39}$$

Here the angle ξ depends on anchoring conditions (weak, strong) at the boundaries. For weak anchoring, in the one-constant approximation,

$$\xi(r) = 2 \arctan \left(\frac{r}{R} \tan \left(\frac{1}{2} \arccos \frac{1}{\sigma} \right) \right) \tag{4.40}$$

where σ is the anchoring parameter. The case of strong anchoring is obtained in the limit $\sigma \to +\infty$.

The escaped radial disclination [308] When a nematic medium is confined inside a capillary tube (radius R) with homeotropic boundary conditions, the director field tends to be radially oriented everywhere but on the central axis where an orientational singularity lies: this is the disclination line, associated to a singular distribution of curvature (see Figure 4.5). To reduce the elastic energy of this configuration, the director field can switch from a planar configuration to a three dimensional involving point defects (radial and hyperbolic hedgehogs): this phenomenon is called the "escape in the third dimension"[309]-[310].

In the limit of infinitely long cylinders (large aspect ratios of the capillary), this configuration becomes metastable. Indeed, as opposite directions along the capillary axis are energetically equivalent, point defects always come in pairs of opposite topological charge and like opposite electric charges, they attract and annihilate one another[7] (similarly, similar topological charges repel and migrate at infinity). Eventually, the nematic relaxes into a funnel-shaped configuration, known as

[7] Strictly speaking, this happens when the defects are close enough, i.e. their distance d obey $d < 0,25R$ [311].

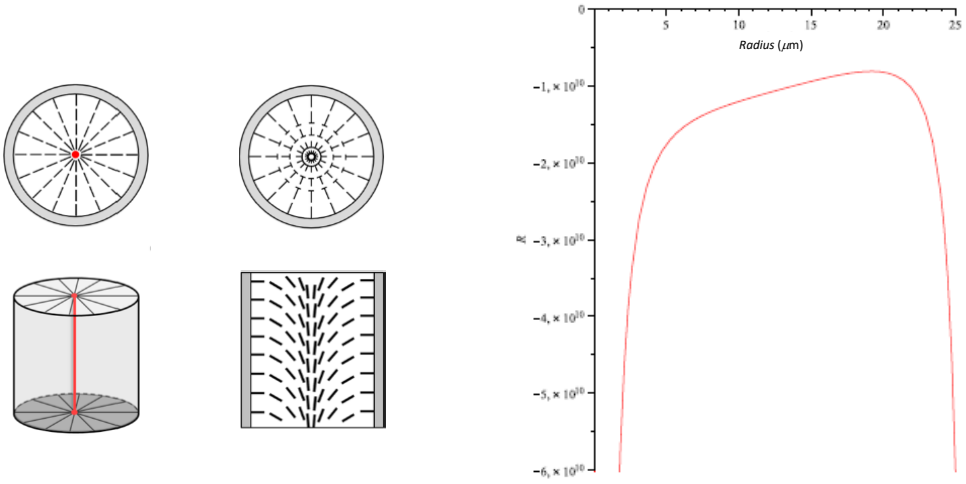

Figure 4.5: *Left*: A regular unstable disclination in a capillary. *Middle*: The stable escaped radial disclination in a capillary. *Right*: Ricci scalar for the escaped radial disclination in a capillary tube with radius $R = 25\ \mu$m filled with weakly-anchored liquid crystal E7 [308].

the escaped radial disclination (ERD) possessing lower energy than three-dimensional distortions with point defects (depending on the boundary conditions, this can also hold for cylinders of finite length) [312]: form the geometrical standpoint, this configuration replaces the delta-distributed Ricci scalar by an extended smooth one (see Figure 4.5).

Acoustic rectification [314] Acoustic rectification can be obtained from mechanisms: for instance, nonreciprocal effects can be obtained from an acoustic circulator in analogy with electromagnetic nonreciprocity based on the Zeeman effect [313]. In the spirit of a low-cost soft-matter-based solution, we propose a liquid crystal-based device using an ERD filling a conical frustum of varying radius $R(z)$. The inner surface prepared to produce the desired anchoring angle[8].

In cylindrical coordinates, the director field for the ERD then writes as $\mathbf{n}(\mathbf{r}) = (\sin\chi(\mathbf{r}), 0, \cos\chi(\mathbf{r}))$, where

$$\chi(\mathbf{r}) = 2\arctan\left(\frac{r}{R(z)}\tan\frac{\alpha}{2}\right) \tag{4.41}$$

Here, $\alpha = \chi(r = R(z))$ is the anchoring angle adapted to maintain the ERD configuration. α depends on the surface geometry (radius), on the liquid crystal (elastic constant K, saddle-play constant K_{24}) and the surface treatment generating interactions between them. We considered acoustic waves in a frequency range between 20 Hz and 20 kHz (the average human audible range)

[8] Whereas homeotropic anchoring of nematics on flat surfaces is well mastered [203], anchoring nematics with an arbitrary angle on a curved surface is generally not trivial and it is particularly sensitive to the saddle-splay constant K_{24} [315].

propagating in 5CB for the ERD configuration. The Helmholtz equation was solved with finite elements.

The rectification parameter used to estimate the acoustic device's efficiency is the percent standard deviation of the lowest variation on the acoustic intensity

$$\text{Acoustic rectification}(\%) = \left| \frac{\Delta I_{bt} - \Delta I_{tb}}{\min\left(\Delta I_{bt}, \Delta I_{tb}\right)} \right| \times 100 \tag{4.42}$$

where $\Delta I_{bt} = I_t - I_b$ is the acoustic intensity variation if the wave comes from the bottom to the top of the conical frustum and $\Delta I_{tb} = I_b - I_t$ is the analogous variation for the counterpropagating case. Numerical simulations show a rectification effect for a longitudinal plane wave propagating along the conical frustum axis (see Figure 4.6). The optimization of the device parameters (geometry of the conical frustum, anchoring conditions the rectification effects...) allows to reach rectification levels up to 1300% for a continuous frequency bandwidth.

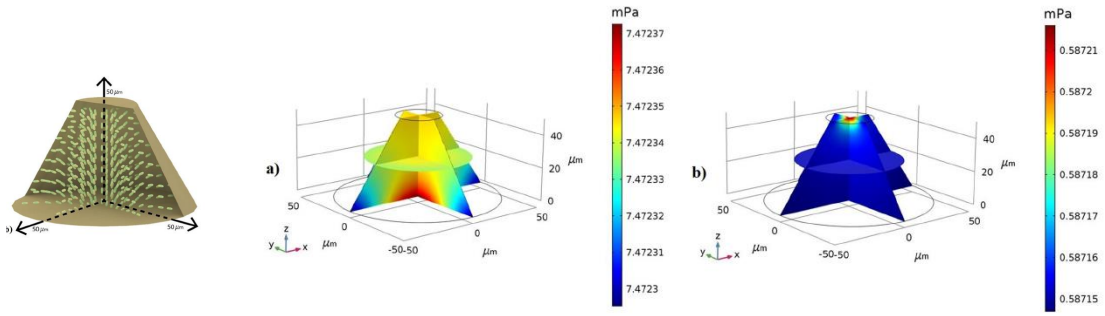

Figure 4.6: *Left*: Conical frustum with an ERD. *Middle*: Pressure field for the incoming waves from bottom to top. *Right*:Pressure field for the incoming waves from top to bottom.

4.1.3 Heat conduction

Principles of thermal design [316]-[318] Manipulation of heat flux raises intensive research efforts because of the abundant wealth of potential applications including thermal shielding or stealth of objects, concentrated photovoltaics or thermal information processing (heat-flux modulators, thermal diodes, thermal transistors and thermal memories). These prospects come from the possibility of designing energy paths in a fashion similar to that of light in transformation optics.

To do so, the first step is to determine the main peculiarities of heat transfer in the presence of a non-euclidean geometry. Generally speaking, diffusion of a passive scalar (for instance the temperature field) can be seen as a collection of Markov processes obeying the stochastic Fokker-Planck equation. In the case of Brownian motion, the Fokker-Planck equation reduces to the well-known parabolic heat equation [319]. When considering diffusion processes in the presence of a non-euclidean space, the problem is addressed by replacing the Laplace operator with the Laplace-Betrami operator Δ_{LB} [320]:

$$\frac{\partial T}{\partial t} = D\Delta_{LB}T \tag{4.43}$$

Here, D is the diffusivity and its value depends on the material, where the Laplace-Betrami operator writes as

$$\Delta_{LB} = \frac{1}{\sqrt{g}}\frac{\partial}{\partial x^i}\left(\sqrt{g}g^{ij}\frac{\partial}{\partial x^j}\right) \tag{4.44}$$

for a background geometry described by the static metric g_{ij}. Equation (4.43) is a particular case of the Eckart equation, first introduced in 1940 to study the irreversible thermodynamics of relativistic fluids and later refined by Landau and Lifshitz in 1959 [321].

For the screw dislocation, the effective metric is given by (2.23) and therefore, the generalized diffusion equation writes as:

$$\begin{aligned}\frac{\partial T}{\partial t} &= D\left[\frac{\partial^2 T}{\partial r^2}+\frac{1}{r}\frac{\partial T}{\partial r}+\frac{1}{r^2}\frac{\partial^2 T}{\partial \theta^2}+\left(\frac{\beta^2}{r^2}+1\right)\frac{\partial^2 T}{\partial z^2}\right]\\ &- \frac{2D\beta}{r^2}\frac{\partial^2 T}{\partial\theta\partial z}\end{aligned} \tag{4.45}$$

We considered an asymmetrical boundary condition, where the heat is injected through a portion only of the bottom disk (half of it in the figures below, $T(t,r,\theta,0)=T_1$ for $0<\theta<\pi$, but other portions were also studied and essentially lead to similar results). The numerical results are shown in Fig. 4.7, where the time evolution of the diffusion process is presented at eight different instants from $t=1$ to $t=70$ for dislocation parameter $\beta=5$. As exepeted, the geometry of defect happens to guide heat flux along its pitch.

Let us now move to an isotropic phase of thermal conductivity λ, in steady-state regime and having no inner heat source. Rearranging terms enables us to write the Fourier-Laplace heat conduction equations as

$$q^i = -\lambda^{ij}\partial_j T \tag{4.46}$$

$$\nabla.\mathbf{q} = p \tag{4.47}$$

where

$$\lambda^{ij} = \lambda g^{ij} \tag{4.48}$$

$$p = \frac{\lambda}{2}\, g^{ij}\,\partial_i \ln\, g\,\partial_j T \tag{4.49}$$

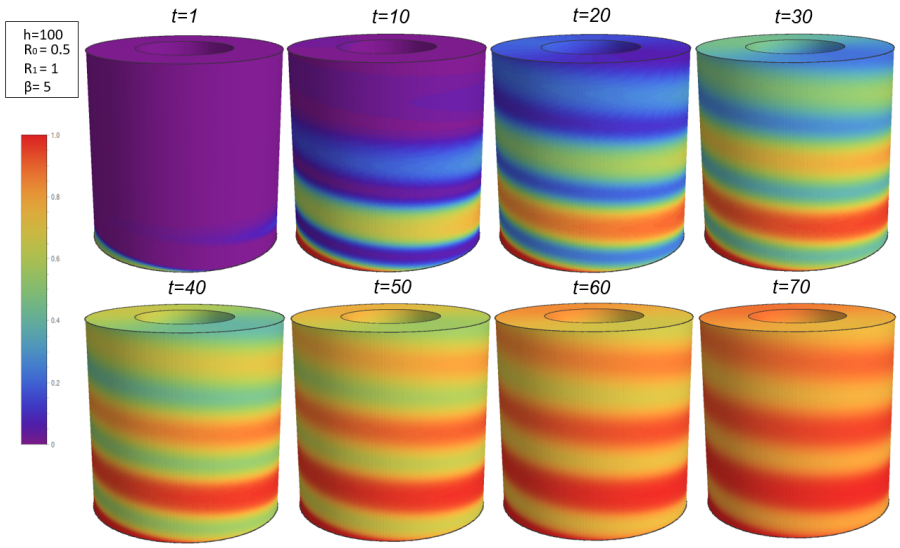

Figure 4.7: Time evolution of the diffusion process for $\beta = 5$. From top to bottom, left to right, time evolves between $t = 1$ and $t = 70$. The screw shape of the temperature profile appears clearly.

The non-flat metric modifies the thermal conductivity tensor (in a way consistent with Onsager's reciprocal relations), but it also introduces an effective internal heat source ($p \geq 0$) or sink ($p \leq 0$) that is directly coupled to the temperature field.

For a single screw dislocation, $g = 1$ and therefore the screw dislocation does not introduce any effective internal source. Moreover, (4.48) shows that heat conduction occurs exactly in the same way as in an anisotropic crystal given by

$$\lambda^{ij} = \lambda \begin{pmatrix} 1 & 0 & \beta y/r^2 \\ 0 & 1 & -\beta x/r^2 \\ \beta y/r^2 & -\beta x/r^2 & 1+\beta^2/r^2 \end{pmatrix} \tag{4.50}$$

Similarly, in the vicinity of a single disclination (or wedge dislocation), one has $g = \alpha^2$ and it can be shown that heat conduction locally occurs as in a monoclinic-like crystal with no internal source

$$\lambda^{ij} = \lambda \begin{pmatrix} \frac{\alpha^2x^2+y^2}{\alpha^2r^2} & \frac{(\alpha^2-1)xy}{\alpha^2r^2} & 0 \\ \frac{(\alpha^2-1)xy}{\alpha^2r^2} & \frac{x^2+\alpha^2y^2}{\alpha^2r^2} & 0 \\ 0 & 0 & 1 \end{pmatrix} \tag{4.51}$$

The heat flux vectors are no longer perpendicular to the isothermal surfaces, which are bent depending on the value of the Frank angle.

Once the basic effects of single line defects are understood, the next step is to taylor them to guide heat. To do so, we considered a hollow cylinder, inside which there is the core region where one aims at controlling the conductive heat flux. The cylinder is inserted inside a conducting

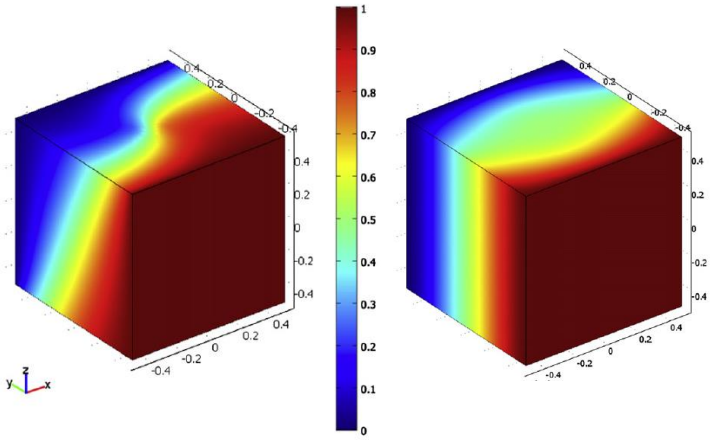

Figure 4.8: *Left:* Example of temperature field near a screw dislocation (lying on the z-axis) with $b = -0.5$ and an imposed gradient of temperature along the y-axis. *Right:* Example of temperature field, in unitary cube with the faces $y = -0.5$ and $y = 0.5$ set at fixed temperatures and the others being insulating ones, around a wedge dislocation lying on the z-direction with $\alpha = 0.5$

solid sandwiched between two heated vertical plates. The host material consists of a homogenous isotropic medium, whereas the intermediate thick cylinder consists of a nematic liquid crystal in a disclination-like configuration (no disclination core). It must be underlined that the metric-changed thermal conduction (4.48) is compatible with the usual models for heat conduction in nematics (in cartesian coordinates) [151]:

$$\lambda_{ij} = \frac{\lambda_{\parallel} + 2\lambda_{\perp}}{3}\delta_{ij} + \left(\lambda_{\parallel} - \lambda_{\perp}\right)\left(n_i n_j - \frac{\delta_{ij}}{3}\right) \tag{4.52}$$

where $\lambda_{\parallel}$ is the thermal conductivity along the director field and $\lambda_{\perp}$ in a direction orthogonal to it. The thermal conductivity of the isotropic fluid phase is taken equal to that of the host medium, to avoid additional thermal effects (such as Kapitza resistance). For thermal management, mesophases with low melting and high clearing temperatures are required: a range of about 100 K can be reached by using eutectic liquid crystal mixtures (or "guest-host systems").

Numerical results shown in figure 4.9 confirm the possibility of the heat guiding phenomena: depending on the value of elastic constants C_{33} (along the director) and C_{11} (along any direction perpendicular to the director), the device can either cloak the core region from the heat flux or concentrate heat in it. Switching from the concentrator to the cloaking device is be achieved by electric-field-driven bistable anchoring with dye-doped mematics (sufficiently high values of the electrical potential difference between the two sides of the hollow cylinder were indeed shown to induce stable anchoring transitions between homeotropic and parallel states [322]). To avoid thermoconvective instabilities in the annulus domain, the device must be thin enough and the heat flux and temperature levels must be moderate. For instance, using 5CB and MBBA, if the tempera-

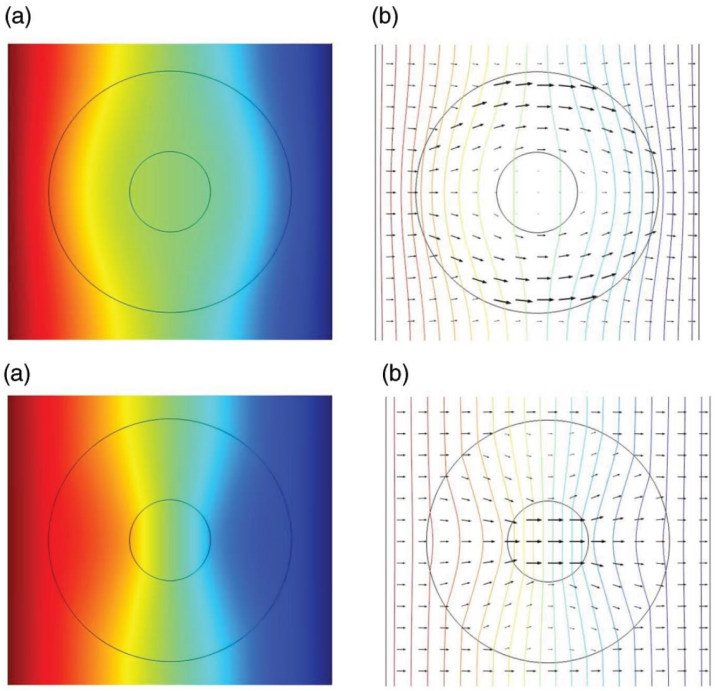

Figure 4.9: *Top*: Temperature field (a) and heat flux field (b) for a radial director field (homeotropic anchoring) and $\alpha = \sqrt{C_{33}/C_{11}} = 0.5$ *Bottom:* Temperature field (a) and heat flux field (b) for an orthoradial director field (parallel anchoring) such that $\alpha = \sqrt{C_{11}/C_{33}} = 2$

ture is about a few tens of degrees (thermoelectric applications) and the external radius of a few centimeters, the device handles heat flux that typically varies from $5W/m^2$ (repeller) to $103W/m^2$ (concentrator).

Thermal diodes [336]-[337] The previous study is now refined in order to investigate thermal rectification. Thermal rectification is a very active subject, as testified by the abundant litterature dealing with this subject (extensive reviews treating thermal rectification can be found in [338]-[339]). Thermal rectification has indeed been investigated in hard matter devices for heat conduction (including non-linear lattices [340], phase-change materials [341], thermal metamaterials [342]...), for far-field radiative transfer (phase-change materials [344], superconductors [345], dielectrics supporting phonon-polariton [346]...) and for near-field radiative transfer (phase-change media [347]-[348]...). More seldomly is heat conduction rectification considered from fluid-based devices [349] and for our concern, soft-matter-based devices.

In liquid crystals, the scalar order parameter S (Tsvetkov, 1942) depends on temperature according to Haller's approximation and so are the macroscopic physical properties of the nematic

phase. where

$$\lambda_{\parallel}(T) = \lambda_0 + \lambda_1 \times (T - T_{NI}) + \lambda_{1\parallel} \times (T - T_{NI})^{\alpha_{\parallel}} \quad (4.53)$$
$$\lambda_{\perp}(T) = \lambda_0 + \lambda_1 \times (T - T_{NI}) + \lambda_{1\perp} \times (T - T_{NI})^{\alpha_{\perp}} \quad (4.54)$$

where λ_0, λ_1, $\lambda_{1\parallel}$, $\lambda_{1\perp}$, $\alpha_{\parallel}$ and $\alpha_{\perp}$ are material-depending constants, whereas T_{NI} and T_C are, respectively, the nematic-to-isotropic temperature and the clearing-point temperature of the liquid crystal.

In a first approach, thermal rectification arises because of an asymmetry of the system along the direction of heat propagation: this is generally achieved by relying on gradients of physical properties (e.g. pore density [353], distribution of compositional defects [354]...), asymmetric geometries [350]-[351]... As we saw before, liquid crystals naturally provide a stable and flexible configuration corresponding to such asymmetry, the ERD, which already turns out to provide high levels of acoustic rectification. To achieve high rectification levels, one also considers the conical frustum of varying radius $R(z)$ with anchoring conditions adapted to maintain the ERD configuration. The rectification parameter used to estimate the thermal diode efficiency is defined as

$$\text{Thermal rectification}(\%) = \left| \frac{\Delta T_i - \Delta T_d}{\Delta T_d} \right| \times 100 \quad (4.55)$$

$\Delta T_d = T_{d,h} - T_0$ is the difference between $T_{d,h}$, the high temperature on one base produced by the heat pumped in the cylinder when working in the direct setup (i.e. when the heat is flowing from the narrow region to the wider one $= -z$ direction), and T_0, the temperature at the other base, which is also the initial temperature. Similarly, we have $\Delta T_i = T_{i,h} - T_0$ when working in the inverse setup.

Numerical simulations show a thermal rectification around 1266%. On the shape parameters, alterations on the ratio $R_r \in [0,28; 0,75]$ produced a percentage variation on the thermal rectification around 1273%, while modifications of the height $h \in [50; 75]$ μm and on the larger radius $R_l \in [50; 70]$ μm produced percentage changes lower than 5%. This indicates that the anisotropy of the conical frustum tube has a strong influence on the rectification. Other non-geometrical parameters such as the anchoring angle (in the range $[0; 90°]$) and the inward pumped heat flux (in the range $[5; 10]$ kW$/m^2$) give percentage variations on the rectification around, respectively, $3,8$ and $1,7$%. Such characteristics enable this improved thermal diode to be miniaturized, applied on well-determined areas, while robust against variations of the inward pumped heat flux. We patented the nematic-based thermal diode in 2017 (*Patent Number: BR1020170067092*).

4.2 Low-dimensional systems

4.2.1 Thermotronics

Channel of disclination dipoles [355] Real two-dimensional systems, such as graphene, boron nitride or silicene, are never perfect lattices. Most of the time, they have point and line defects which strongly impact phonon transport properties (see for instance [357] in the case of vacancies). Disclinations generally occur in the form of multipoles (such as Stone-Wales defects), as they lead to stable self-screened configurations. On a graphene lattice, the Frank angles are $\Omega_p = \pi/3$

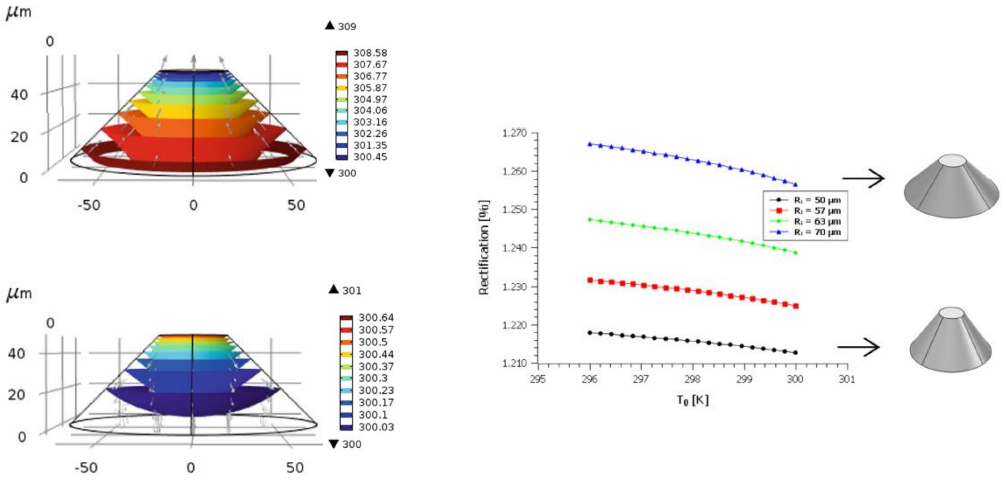

Figure 4.10: *Left*: Isothermal surfaces of a liquid crystalline thermal diode in (up) inverse thermal setup and (bottom) direct thermal setup. The frustum diode has larger radius $R_l = 70$ μm, ratio between the radii is $R_r = R_{sm}/R_l = 0,28$, the height is $h = 50$ μm, anchoring is 60° and the inward heat flux is $Q = 5\,\mathrm{kW}/m^2$ on the base with the higher temperature and T_0=296 K. *Right:* Rectification rate versus temperature T_0 of the base for different larger radii R_l.

($\alpha = 5/6$) for a pentagon disclination and $\Omega_h = -\pi/3$ for a heptagon disclination ($\alpha = 7/6$)[9]. Disclinations being line sources of curvature, they influence the geodesics followed by phonons and one can legitimately wonder if generally speaking, an array of such defects be used to taylor the thermal properties of two-dimensional systems[10].

Therefore, one considers a channel of disclination dipoles, consisting in two infinite rows made of alternate disclinations separated by distance $2a$, the distance between the rows being $2b$. The positive disclinations are at points located at $(na, (-1)^n b), n \in \mathbb{Z}$, while negative disclinations have coordinates $(na, (-1)^{(n+1)} b), n \in \mathbb{Z}$. As always done in analog gravity models, the bulk medium is considered in the continuum limit (i.e. limit of a vanishing lattice spacing). The corresponding background geometry is generally described by the spacetime line element [358]

$$ds^2 = -c^2 dt^2 + e^{-4V(x,y)} \left(dx^2 + dy^2\right) + dz^2 = g_{\mu\nu} dx^\mu dx^\nu \tag{4.56}$$

where c is the local speed of wave packet and V can be understood as a potential term experienced by particles.

[9] We recall that the Franck angle is positive when removed, negative otherwise.

[10] In principle, the question can be also raised for liquid crystals, as laser tweezers can be used to trap and manipulate disclinations in thermotropic nematics [356].

In the case of a single row of alternate defects at $y = b$ (positive disclinations at $..-4a, -2a, 0, 2a, 4a...$ and negative disclinations at $.. - 3a, -a, a, 3a...$), this function writes

$$V(x,y) = \frac{|\Omega|}{2} \sum_{p=-\infty}^{+\infty} \left\{ \ln \left[(x-2pa)^2 + (y-b)^2 \right] - \ln \left[(x-[2p-1]a)^2 + (y-b)^2 \right] \right\}$$

$$= \frac{|\Omega|}{2} \sum_{n=-\infty}^{+\infty} (-1)^n \ln \left[(x-na)^2 + (y-b)^2 \right] \tag{4.57}$$

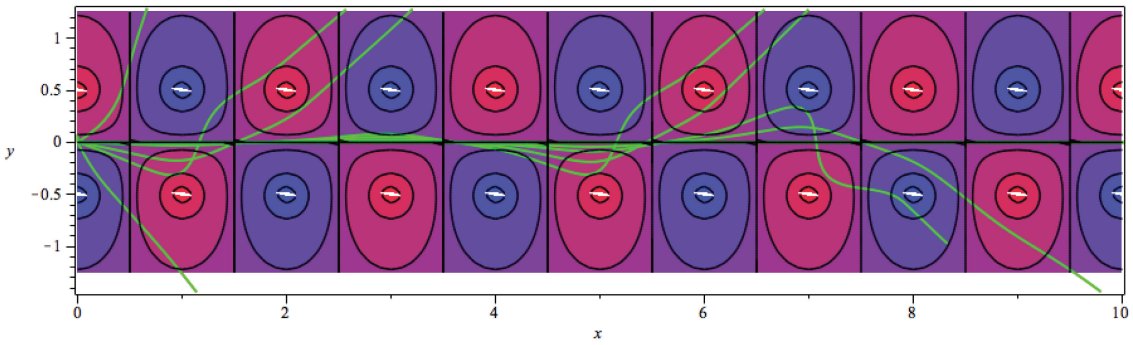

Figure 4.11: Different geodesics, shot from the origin, in the channel of disclinations geometry. The positive disclinations correspond to red contours while negative disclinations correspond to blue contours. Depending on the shooting angle, the propagation of phonons may be guided by the street of topological defects.

Tricky calculations show that the series expansion converges to (for more technical details see [355])

$$V(x,y) = \frac{|\Omega|}{4\pi} \ln \left[\left(\frac{\cosh^2\left(\frac{\pi}{2a}(y-b)\right) - \cos^2\left(\frac{\pi x}{2a}\right)}{\cosh^2\left(\frac{\pi}{2a}(y-b)\right) - \sin^2\left(\frac{\pi x}{2a}\right)} \right) \left(\frac{\cosh^2\left(\frac{\pi}{2a}(y+b)\right) - \sin^2\left(\frac{\pi x}{2a}\right)}{\cosh^2\left(\frac{\pi}{2a}(y+b)\right) - \cos^2\left(\frac{\pi x}{2a}\right)} \right) \right] \tag{4.58}$$

In the small wavelength approximation, the paths followed by phonons are no longer straight lines, but they are the geodesics of the channel of disclinations geometry, that is the trajectories

of shortest lengths in the background geometry. After some calculations, the geodesic equations reduce to:

$$\begin{aligned} \ddot{x} - 2\left(\dot{x}^2 - \dot{y}^2\right)\partial_x V - 4\dot{x}\dot{y}\partial_y V = 0, \\ \ddot{y} - 2\left(\dot{x}^2 - \dot{y}^2\right)\partial_y V - 4\dot{x}\dot{y}\partial_x V = 0. \end{aligned} \tag{4.59}$$

Without loss of generality, we chose geodesics starting at the origin, $(x_0(0) = 0, y_0(0) = 0)$, with unitary initial "speed", $x'(0) = \cos(\theta_0), y'(0) = \sin(\theta_0)$, which defines the shooting angle. In Fig. 4.11 and 4.12 some geodesics are depicted in the channel of defects for a few shooting angles. The phononic paths are attracted by the positive defects while repelled by the negative ones. This is quite natural, since the former have the geometry of a cone (with less space than the plane) and the latter of an anticone (with more space than the plane). If designing robust thermal guides seems sound, paths are yet very sensitive to the shooting angle[11]: hence, a thorough optimization of the distribution of defects deserves an additional treatment of chaos involving the statistical tools of dynamic hamiltonian systems.

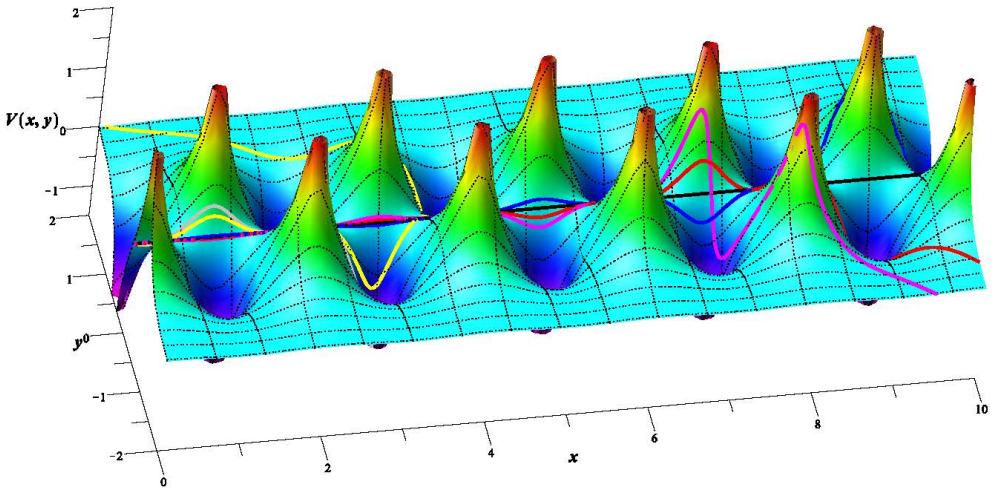

Figure 4.12: Geodesics of the channel of defects in the potential landscape.

Networks of defects [360] A step ahead in defect engineering is to consider lattices of parallel string-like defects in 3D or, equivalently, point-like defects in 2D, interacting logarithmically. Let us therefore consider a rectangular Bravais lattice in $\mathbb{R}^2$ generated by the basis vectors $\vec{a}_1 = a\hat{x}$ and $\vec{a}_2 = b\hat{y}$ such that a point of the lattice located at $\vec{R}_{mn} = m\vec{a}_1 + n\vec{a}_2$ is associated to the pair $(m, n) \in \mathbb{Z}^2$. To each point of the lattice we associate a defect. The purpose is now to find the geometric potential due to this array of defects, assuming the superposition principle. That is, we

[11] The motion of fast electrons in a silicon crystal endowed with periodically distributed atomic strings is also known to be chaotic [359].

want to perform the sum

$$V(\vec{r}) = \lambda \sum_{(m,n)\in\mathbb{Z}^2} \ln|\vec{r} - \vec{R}_{mn}|^2, \tag{4.60}$$

where $\vec{r} = x\hat{x} + y\hat{y}$ is the position of a test defect and λ is the "charge"of the logarithmic interaction. The function defined by Eq. (4.60) is a solution of the 2D Poisson equation

$$(\partial_{xx}^2 + \partial_{yy}^2)V = 2\pi\lambda \sum_{(m,n)\in\mathbb{Z}^2} \delta(x - ma)\,\delta(y - nb) \tag{4.61}$$

and therefore we will not be concerned with additive constants appearing in the logarithmic sum. This is the essence of the regularization process that we need to use since the "raw" sum in Eq. (4.60) naturally diverges. Now, defining

$$\varphi = x + iy, \qquad \bar{\varphi} = x - iy \tag{4.62}$$

$$\sigma = ma + inb, \qquad \bar{\sigma} = ma - inb \tag{4.63}$$

we write Eq. (4.60) as

$$V(x,y) = \lambda \sum_{(m,n)\in\mathbb{Z}^2} \ln\left[(\varphi - \sigma)(\bar{\varphi} - \bar{\sigma})\right] \tag{4.64}$$

Using the three identities

$$\prod_{n=1}^{\infty}\left(1 + \frac{z}{n^2A + B}\right) = \sqrt{\frac{B}{B+z}}\,\frac{\sinh(\pi\sqrt{B+z}/\sqrt{A})}{\sinh(\pi\sqrt{B/A})} \tag{4.65}$$

$$\prod_{m=1}^{\infty}\left[\cos^2 z + \sin^2 z\coth^2(m\pi\chi)\right] = \csc z\,\frac{\vartheta_1(z, e^{-\pi\chi})}{\vartheta_1'(0, e^{-\pi\chi})} \tag{4.66}$$

$$\vartheta_1(z, e^{-\pi\chi}) = 2\sum_{n=0}^{\infty}(-1)^n e^{-\pi\chi(n+1/2)^2}\sin\left[(2n+1)z\right] \tag{4.67}$$

where ϑ_1 is the Jacobi theta function, z, χ are complex numbers, one obtains after tedious calculations a compact and regularized form for the potential[12]:

$$V(x,y) = \lambda\ln\left[\frac{x^2+y^2}{\cosh^2(\pi x/b) - \cos^2(\pi y/b)}\right] + \lambda\ln\left|\frac{\vartheta_1(\frac{\pi}{b}(ix - y), e^{-\pi a/b})}{\vartheta_1'(0, e^{-\pi a/b})}\right|^2 \tag{4.68}$$

For the triangular lattice we consider $\vec{a}_1 = a\hat{x}$ and $\vec{a}_2 = a\cos(\pi/3)\hat{x} + a\sin(\pi/3)\hat{y}$ such that a point of the lattice located at $\vec{R}_{mn} = m\vec{a}_1 + n\vec{a}_2$ will lead to

$$|\vec{r} - \vec{R}_{mn}|^2 = (\varphi - \eta)(\bar{\varphi} - \bar{\eta}) \tag{4.69}$$

where φ is given by Eq. (4.62) and

$$\eta = \left(m + e^{i\pi/3}n\right)a \tag{4.70}$$

[12]Technical details are found in [360].

Following the steps of the previous section,

$$\begin{aligned} V(x,y) &= \lambda \sum_{(m,n)\in\mathbb{Z}^2} \ln\left[(\varphi-\eta)(\bar{\varphi}-\bar{\eta})\right] \qquad (4.71)\\ &= \lambda \sum_{m=-\infty}^{\infty} \ln\left[(\varphi-ma)(\bar{\varphi}-ma)\right] \\ &+ \lambda \sum_{m=-\infty}^{\infty}\sum_{n=1}^{\infty} \ln\{[\varphi^2-2ma\varphi+m^2a^2+e^{-i\pi/3}n^2a^2]\cdot \\ &\quad [\bar{\varphi}^2-2ma\bar{\varphi}+m^2a^2+e^{i\pi/3}n^2a^2]\} \qquad (4.72) \end{aligned}$$

In terms of the coordinates x and y, the final expression for the regularized potential is then

$$V(x,y) = \lambda \ln\left[\frac{\vartheta_1\left(i\frac{\pi}{a}(x+iy)\,e^{i\pi/6}, -ie^{-\frac{\sqrt{3}\pi}{2}}\right)\cdot\vartheta_1\left(i\frac{\pi}{a}(x-iy)\,e^{-i\pi/6}, ie^{-\frac{\sqrt{3}\pi}{2}}\right)}{\cosh^2\left(\frac{\pi}{2a}\left(y-\sqrt{3}x\right)\right)-\cos^2\left(\frac{\pi}{2a}\left(x+\sqrt{3}y\right)\right)}\right] \qquad (4.73)$$

The metric tensor is then deduced from (4.56). Adjusting the defect strengths λ, κ and σ along with parameters governing the geometry of a cell (namely a,b) opens the possibility to taylor material properties of the sheets, but this will only be achieved numerically considering the complexity of analytical expressions. This work may also have deep connections with Regge calculus in quantum gravity, where the smooth curved spacetime is replaced by a piecewise-flat simplicial manifold. The effect of gluing the edges of the simplexes generate a network of cone-like singularities (Regge cones) which are analogs to wedge disclinations [361].

4.2.2 Nanoelectronics

Da Costa formalism In a seminal paper published in 1981, RCT da Costa adressed the dynamics of a massive free quantum particle on a curved surface [323]: the basic idea is to add the Hamiltonian a geometric potential that accounts for the confinement the particle on the surface. Eversince, this approach has been applied successfully to a wide range of two-dimensional systems, especially carbon-based systems like nanotubes and other curved forms of graphene [324]. The experimental verification of the geometric effects predicted by da Costa in a real physical system was done in [325] by measuring the high-resolution ultraviolet photoemission spectra of a C_{60} peanut-shaped polymer.

Considering a finite thickness d for the "surface" and a confining potential given by an infinite square well in the normal direction, da Costa found that the Schrödinger operator for a free particle in this confined geometry, in the limit $d \to 0$, is [323]

$$H = -\frac{\hbar^2}{2m}\triangle_{LB} + V_{\text{geo}}, \qquad (4.74)$$

where m is the effective mass of the electron in the CNT $m = 0.173m_e$ and $\triangle_{LB}$ is the Laplace-Beltrami operator obtained from the curvilinear coordinates x^i intrinsic to the surface and the

metric tensor g_{ij} (g its determinant)

$$\triangle_{LB} = \sum_{i,j} \frac{1}{\sqrt{g}} \frac{\partial}{\partial x^i} \left(\sqrt{|g|} g^{ij} \frac{\partial}{\partial x^j} \right) \tag{4.75}$$

and the geometric potential is given by

$$V_{\text{geo}} = -\frac{\hbar^2}{2m} \left(M^2 - K \right). \tag{4.76}$$

Here, M and K refer to the mean and Gaussian curvatures, respectively. The geometric potential is a direct consequence of the quantization of the motion normal to the surface.

Let us now focus on surfaces of revolution since our interest is to study corrugated nanotubes. A surface of revolution is obtained by rotation of a plane curve around an axis. The parametric equations for the surface of revolution writes as $\mathbf{r}(q, \phi) = (\rho(q) \cos \phi,\ y = q,\ z = \rho(q) \sin \phi)$, where $q \in \mathbb{R}^1$ and $\phi \in \mathbb{S}^1$. With such parametrization, the first fundamental form (or metric tensor) is obtained as:

$$g_{ij} = \partial_i \mathbf{r}.\partial_j \mathbf{r} = \begin{pmatrix} \rho(q)^2 & 0 \\ 0 & 1 + \rho'(q)^2 \end{pmatrix} \tag{4.77}$$

and the second fundamental form (or shape tensor) is given by

$$h_{ij} = \mathbf{N}.\partial_{ij} \mathbf{r} = \frac{1}{\sqrt{1 + \rho'(q)^2}} \begin{pmatrix} \rho(q) & 0 \\ 0 & -\rho''(q) \end{pmatrix} \tag{4.78}$$

The mean and Gaussian curvatures are given respectively by $M = \frac{1}{2g}(g_{11}h_{22} + g_{22}h_{11} - 2g_{12}h_{12})$ and $K = \frac{1}{g}(h_{11}h_{22} - h_{12}h_{21})$, so that the geometric potential is analytically obtained in terms the nanotube parametrization $\rho(q)$:

$$V_{\text{geo}} = -\frac{\hbar^2}{8m} \frac{[1 + \rho'(q)^2 + \rho(q)\rho''(q)]^2}{\rho(q)^2[1 + \rho'(q)^2]^3} \tag{4.79}$$

As the potential V_{geo} depends only on the q coordinate, we can separate the Schrödinger equation into two 1D equations $\Phi'' + \ell^2 \Phi = 0$, with $\ell \in \mathbb{Z}$ in order to satisfy angular periodicity and

$$\Psi'' + \left(\frac{\rho'}{\rho} \left[1 - \frac{\rho\rho''}{1 + \rho'^2} \right] \right) \Psi' + \left(1 + \rho'^2 \right) \left[\frac{2m}{\hbar^2} (E - V_{\text{geo}})] - \frac{\ell^2}{\rho^2} \right] \Psi = 0 \tag{4.80}$$

Here, E is the total energy, $\Phi = Ae^{i\ell\phi}$ are the eigenfunctions of the angular momentum $\ell\hbar$ along the y-axis and $\Psi(q)$, the longitudinal eigenfunction.

We model the corrugated nanotube as two semi-infinite cylinders of radius R, joined by a surface of revolution generated by a curve $\rho(y)$ in the range $0 < y < L$, such that $\rho(0) = \rho(L) = R_1$. Eq. (4.80) was solved numerically with open (Robin) boundary conditions using the quantum transmitting boundary method. Then, the transmittance wre be obtained from the ratio of probability current density

$$j = \frac{\hbar}{2mi} \left(\Psi^* \Psi' - \Psi \Psi^{*'} \right) \tag{4.81}$$

Electronic notch-filter [326]-[328] We look at three generic situations: a nanotube with a single bump, one with a pinch and a wavy structure. These are shown in Figs. 4.13, 4.14 and 4.15, respectively. We create the corrugations by using the curve

$$\rho(y) = R \pm \frac{\epsilon}{2}\left[1 - \cos\left(2\,\frac{n\pi\,y}{L}\right)\right] \tag{4.82}$$

to generate the surface of revolution. In Eq. (4.82) the parameter ϵ regulates the strength of the deformation while R gives the radius of the undistorted nanotube. The $+$ sign was used to generate the single bump and wavy structures and the $-$ sign for the pinched tube. We used $n = 1$ for the pinched and bumped nanotubes and $n = 2\,,3\,,4\,,5\,,6$ for the wavy structures.

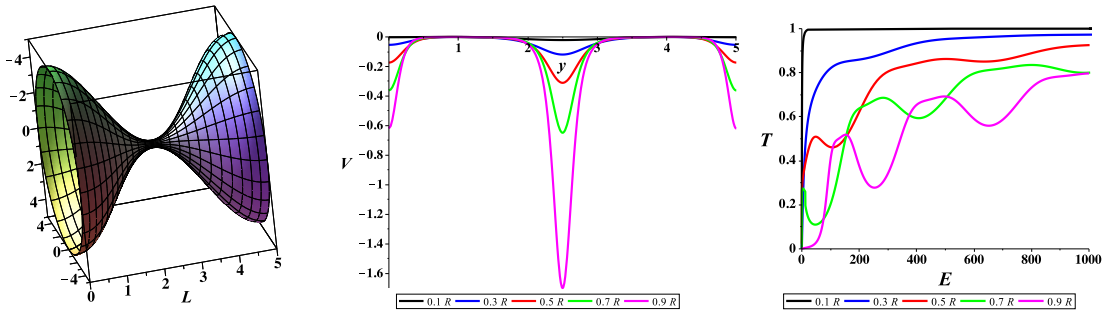

Figure 4.13: (a) Pinched nanotube. (b) Geometric potential due to the deformation shown in (a) and (c) transmittance as function of incident energy (in meV) for different waist sizes (ϵR).

The resonance peaks in the transmittance correspond to quasibound states. These are states associated to a quantum well where a particle is primarily confined but has a finite probability of tunnelling out and escaping. In the nanotube, the geometric potential, if deep enough, may have such states[13]. Although most of the incident electrons are reflected back by the geometric potential, if the energy of the electron coincides with that of a quasibound state this makes it easier for it to tunnel to the inner region of the potential and thus tunnel out of it on the opposite side. If the potential becomes deeper, the energy levels of the quasibound states shift downward implying a shift of the resonant peaks to lower energies.

The most interesting case is depicted on Fig. 4.15. As the number of bumps increases, a 1D lattice on the tube starts to take form and the geometric potential starts to look like the Dirac comb. The periodicity of the potential minima opens a gap in the energy spectrum which becomes better defined with the increasing number of oscillations. The effect on the transmittance is seen in Fig. 4.15. As expected, the energy gap sensibly reduces the transmittance and the effect becomes sharper with the number of bumps. For the curves displayed we fixed the tube length in 5 nm and changed the number of bumps. Therefore the wavelength of the wavy perturbation changes

[13]Looking at Eq. (4.80) we see that for angular momentum $\ell \neq 0$ a repulsive term $\frac{\ell^2}{\rho^2}$ is added to the geometric potential (4.79). So, the effect of the centrifugal term is to make the potential well shallower and consequently reducing the number of quasibound states, therefore of the resonances in the transmittance. For this reason, in what follows we consider only the cases of zero angular momentum ($\ell = 0$) which gives the general physical picture of the system.

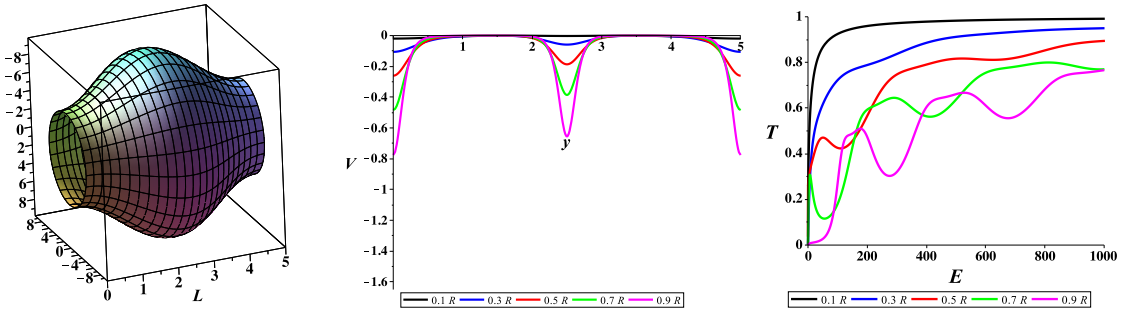

Figure 4.14: (a) Nanotube with a single bump. (b) Geometric potential due to the deformation shown in (a) and (c) transmittance as function of incident energy (in meV) for different bump sizes (ϵR).

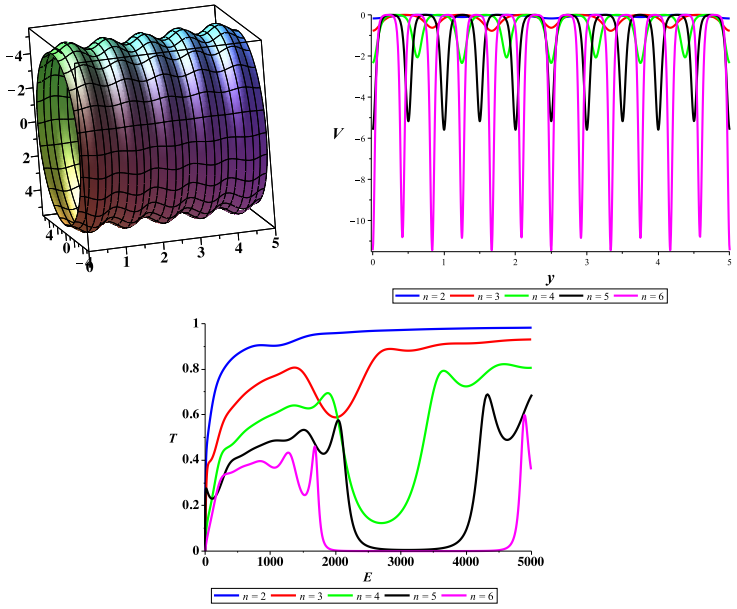

Figure 4.15: (a) Wavy nanotube. (b) Geometric potential due to the deformation shown in (a) for different numbers of bumps. (c) Transmittance as function of incident energy (in meV).

with the number of bumps. Thus the width of the gap changes accordingly[14]. The periodic array of potential wells defines a Kroning-Penney look-alike resulting in the opening of bandgaps in the electronic structure. As the number of wells increase the band gap becomes better defined.

Following a pioneering work by Ferrari and Cuoghi [329], we also considered the gauge invariant Schrödinger equation for a spinless charged particle bound to a cylindrical surface in the presence of a magnetic field:

$$i\hbar\partial_t\psi = \frac{1}{2m}\left[-\frac{\hbar^2}{\sqrt{g}}\partial_i(\sqrt{g}g^{ij}\partial_j\psi) + \frac{iq\hbar}{\sqrt{g}}\partial_i(\sqrt{g}g^{ij}A_j)\psi\right. \tag{4.83}$$

$$\left.+2iq\hbar g^{ij}A_j\partial_i\psi + q^2G^{ij}A_iA_j\psi\right] \tag{4.84}$$

where the $g = \det(g^{ij})$ is the determinant of the first fundamental form.

Numerical simulations were run to compute the longitudinal transmittance of the nanotube in the presence of bumps and depressions. They reveal that the device acts as a high-pass filter which inhibits the flow of low-energy electrons. Moreover, the effective potential also favours the transmission of electrons endowed with a tunable value of their orbital angular momentum l. Comparing the cases of bumps and depressions, the shift induced in the transmittance when l changes is more significant for the case of depressions. It reveals that deformations with negative values of ϵ are more suitable to filter low energy charge carriers. However, the magnetic field can be used to select which angular momentum will cross the deformations more easily. The deformations with positive values of ϵ are more sensitive to a change of B_0. In fact, the shift induced by a change in the magnetic field ΔB_0 is given by $\Delta l = -e\rho^2\Delta B_0/(2\hbar)$. Since the radius ρ of the nanotubes is reduced in case of depressions, more significant shifts of the transmittance contour are expected in comparison with the case of bumps.

Spin-current filter [330] Electrons also posses a spin degree of freedom, and it is now recognized that spin-orbit interactions can be significantly high on curved carbon nanotubes [331]. Can the fine-tuning of electronic transport across a nanotube be extended to spin properties ? To answer this question, we consider ballistic electrons propagating along a rotating nanotube[15] under an applied magnetic field. The point is to show that combined inertial and electromagnetic effects can allow for control of the balance between the charge and spin currents.

At sufficiently low temperatures, electrons in most metals and alloys (provided they have no magnetic order) exhibit a Fermi liquid behaviour with renormalized parameters such as the effective mass [333]. In the presence of an external magnetic field, the Hamiltonian dynamics will involve a Zeeman term and spin-orbit interactions: indeed, a nanotube rotating at angular velocity ω along its axis induces a radial electric field which switches on the spin-orbit coupling on the electrons. Following the approach described in [334], one consider the Pauli-Schrödinger equation prescribed in [334]

$$H\Psi = i\hbar\frac{\partial\Psi}{\partial t} \tag{4.85}$$

where Ψ is the two-component spinor living in the Hilbert space $\mathcal{L}^2(\mathbb{R}^3)\otimes\mathbb{C}^2$ where $\mathcal{L}^2(\mathbb{R}^3)$ is the set of square-integrable complex functions over $\mathbb{R}^3$. The Hamiltonian H contains four main

[14] It may look surprising that with only a few bumps the gap is already so well defined, but it turns out that the deepness of the potential minima grows with n^4.

[15] The great difficulty of injecting a ballistic current into a rotating nanotube via physically contacted electrodes can be overcome by photocurrent injection at optical frequencies [332]. Although our results were obtained for DC currents they can be extended to the AC domain.

contributions:

$$H = H_K + H_I + H_Z + H_{SO} \tag{4.86}$$

The term H_K corresponds to the kinetic energy, electrostatic energy $-|e|A_0$ and the da Costa potential

$$H_K = \left(\frac{1}{2m} |\Pi|^2 - |e|A_0 - \frac{\hbar^2}{8ma^2} \right) \sigma_0 \tag{4.87}$$

where $\mathbf{\Pi} = \mathbf{p} + |e|\mathbf{A}$, $\mathbf{A}$ is the vector potential, A_0 is the scalar potential and σ_0 the 2×2 identity matrix in spin space. The second term, H_I, contains inertial effects, i.e., the coupling between both the orbital degrees of freedom and the spin with rotation. In the case of a nanotube rotating around its symmetry axis, $\boldsymbol{\omega} = \omega \mathbf{e}_z$, this terms writes as

$$H_I = -\boldsymbol{\omega} \cdot [(\mathbf{r} \times \mathbf{\Pi}) + \mathbf{s}] \tag{4.88}$$

The term H_Z corresponds to the Zeeman interaction which couples the electron spin to the magnetic field:

$$H_Z = \mu_B \boldsymbol{\sigma} \cdot \mathbf{B} \tag{4.89}$$

where the Bohr magneton is $\mu_B = \frac{|e|\hbar}{2m}$ and $\boldsymbol{\sigma} = (\sigma_x, \sigma_y, \sigma_z)$ the vector of Pauli matrices. Finally, the spin-orbit term can be obtained as[16]

$$H_{SO} = -\kappa \boldsymbol{\sigma} \cdot [(\mathbf{p} + |e|\mathbf{A}) \times (\omega a \mathbf{e}_\varphi \times \mathbf{B})] \tag{4.90}$$

To diagonalize (4.85), we use the symmetric gauge $\mathbf{A} = \frac{1}{2}\mathbf{B} \times \mathbf{r} = \frac{1}{2} Ba \mathbf{e}_\varphi$ and we assume a two-component spinor of the form

$$\Psi(\varphi, z) = \begin{pmatrix} \alpha e^{-i\varphi/2} \\ \beta e^{i\varphi/2} \end{pmatrix} e^{i\ell\varphi} e^{ikz} \tag{4.91}$$

with α and β constants and with $\ell \in \mathbb{Z}$ to preserve the symmetry $\Psi(\varphi + 2\pi, z) = -\Psi(\varphi, z)$. Some thorough algebra gives for the eigenvalues

$$E_{\ell k \sigma} = \frac{1}{2}\hbar(\Omega^+ + \Omega^-) + \frac{1}{2}\sigma\hbar\sqrt{(\Omega^+ - \Omega^-)^2 + 4\gamma^2\omega^2 k^2 a^2} \tag{4.92}$$

where

$$\hbar k_\varphi^\sigma = \frac{\hbar}{a}(\ell + \sigma/2) + \frac{1}{2}|e|Ba = \frac{\hbar}{a}\left(\ell + \sigma/2 + \Phi/\Phi_0\right) \tag{4.93}$$

$$\hbar\Omega^\pm = \frac{\hbar^2 k^2}{2m} - \frac{\hbar^2}{8ma^2} + \frac{\hbar^2 (k_\varphi^\sigma)^2}{2m} - \hbar\omega k_\varphi^\sigma a \pm \frac{1}{2}\hbar(\omega - \omega_c) \mp \gamma\hbar\omega k_\varphi^\sigma a \tag{4.94}$$

and $\Phi_0 = h/|e|$ is the flux quantum. For the normalized eigenstates, one gets

$$\Psi_{\ell k +} = \begin{pmatrix} \cos\frac{\theta}{2} e^{-i\varphi/2} \\ -i\sin\frac{\theta}{2} e^{i\varphi/2} \end{pmatrix} e^{i(\ell\varphi + kz)} \quad \Psi_{\ell k -} = \begin{pmatrix} i\sin\frac{\theta}{2} e^{-i\varphi/2} \\ -\cos\frac{\theta}{2} e^{i\varphi/2} \end{pmatrix} e^{i(\ell\varphi + kz)}. \tag{4.95}$$

with

$$\tan\theta = \frac{2\gamma\omega k a}{\Omega^- - \Omega^+} \tag{4.96}$$

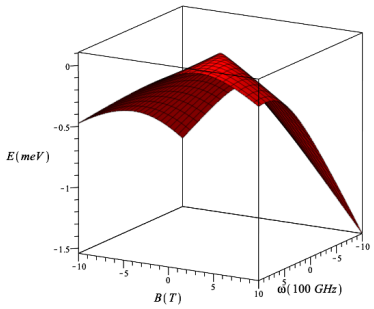

(a) $\ell = 0$, $\sigma = -1$

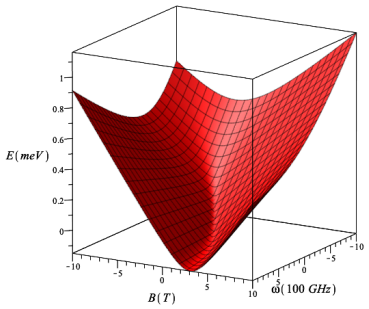

(b) $\ell = 0$, $\sigma = +1$

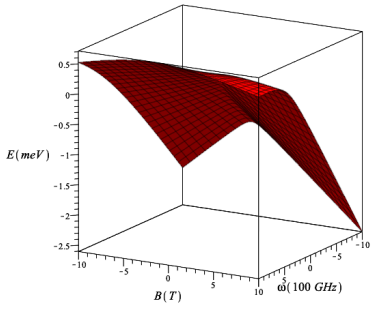

(c) $\ell = -1$, $\sigma = -1$

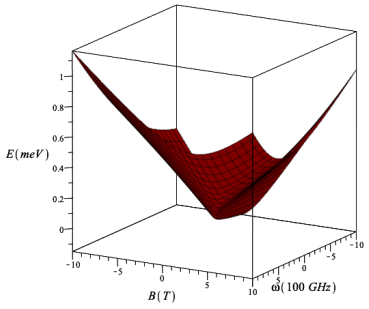

(d) $\ell = -1$, $\sigma = +1$

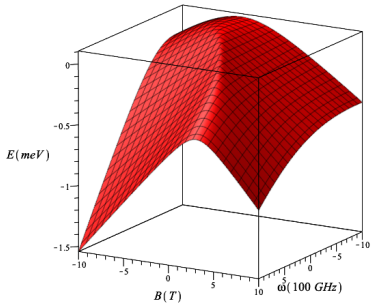

(e) $\ell = +1$, $\sigma = -1$

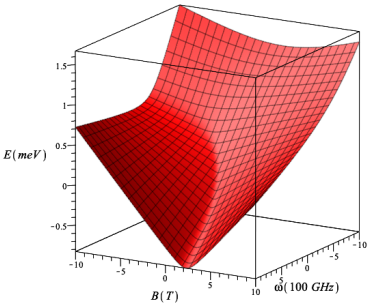

(f) $\ell = +1$, $\sigma = +1$

Figure 4.16: Energy (in meV) of a few $|\ell k\sigma\rangle$ states, in the axial magnetic field case, for $k = 1/a$, a= 50 nm, as a function of magnetic field and rotation speed.

The charge and spin current densities can be calculated respectively from [335]

$$\mathbf{J}_{\ell k\sigma} = -|e|\Psi^{\dagger}_{\ell k\sigma}\mathbf{v}\Psi_{\ell k\sigma} \quad \text{with} \quad \mathbf{v} = \frac{i}{\hbar}[H,\mathbf{r}\,] \tag{4.97}$$

$$\mathbf{S}^{a}_{\ell k\sigma} = \frac{1}{2}\Psi^{\dagger}_{\ell k\sigma}\{\mathbf{v},\mathbf{s}_a\}\Psi_{\ell k\sigma} \quad \text{with} \quad s_a = \frac{1}{2}\hbar\sigma_a \tag{4.98}$$

Here, the tensorial character of the spin current density is encoded in the upperscript a which refers to the spin polarization considered and the anticommutator is required for symmetrization. Since the motion is constrained onto the nanotube, only two spatial components $\mathbf{v}_\varphi = \frac{ia}{\hbar}\,[H,\varphi]$ and $\mathbf{v}_z = z = \frac{i}{\hbar}[H,z]$ are needed. The calculation gives for the charge current densities, respectively in the azimuthal direction and along the nanotube axis direction:

$$J_{\varphi,\ell k\sigma} = -|e|\Big[\frac{\hbar\ell}{ma} + \frac{|e|Ba}{2m} - \omega a + \sigma\big(\gamma\omega a - \frac{\hbar}{2ma}\big)\cos\theta\Big] \tag{4.99}$$

$$J_{z,\ell k\sigma} = -|e|\Big[\frac{\hbar k}{m} + \sigma\gamma\omega a\sin\theta\Big] \tag{4.100}$$

In (4.99), the first term (in $\propto \hbar\ell$) corresponds to the paramagnetic current density while the second term, linear in B, is the diamagnetic contribution. The next term is its rotation counterpart and the last term, depending on γ, is due to the spin-orbit interaction. The structure of (4.100) is similar, except it does not involve diamagnetic contributions.

In the azimuthal (φ) direction, we have, for the two spin labels

$$S^{z}_{\varphi,\ell k\sigma} = \frac{\hbar}{2}\left[\sigma\left(\frac{\hbar\ell}{ma} + \frac{|e|Ba}{2m} - \omega a\right)\cos\theta + \gamma\omega a - \frac{\hbar}{2ma}\right]. \tag{4.101}$$

whereas in the z direction, we have

$$S^{z}_{z,\ell k\sigma} = \frac{\hbar}{2}\left[\sigma\frac{\hbar k}{m}\cos\theta\right]. \tag{4.102}$$

Differently from the charge current, the SO term contributes only to the φ component. Moreover, a comparison between (4.99) and (4.101) and between (4.100) and (4.102) shows that, for a given eigenstate, it is possible to tune either the magnetic field and/or the rotation velocity in order to cancel the charge currents while keeping non-vanishing spin currents. For instance, for the z-component of the charge current this happens provided that

$$\gamma\omega\sin\theta = -\sigma\frac{\hbar k}{ma}. \tag{4.103}$$

On the other hand, the cancellation of the z-component of spin current happens at combinations of ω and B such that

$$\cos\theta = 0. \tag{4.104}$$

In this case, the z-component of the spin current vanishes, leaving a charge only current that depends both on the magnetic field and rotation speed and, amazingly, on the spin polarization state, as

[16] The spin-orbit term follows from the fact that, due to rotation, the electron experiences an associated electric field although only a magnetic field is applied in the rest frame. We omit other contributions coming from the non-relativistic limit of Dirac equation like the Darwin term or the corrections to kinetic energy.

can be seen in Eq. (4.100). This is due to the SO term that couples spin polarization, magnetic field and rotation. Inspection of Eq. (4.96) shows that this case corresponds to having $\Omega^+ = \Omega^-$, which gives a simpler relation between B and ω, that is $2\kappa(\ell + \frac{\sigma}{2})B\omega + |e|a^2B^2\omega + \frac{|e|}{m}B - \omega = 0$. Furthermore, the currents can have their direction inverted by choice of the appropriate sector of parameter space (B, ω).

5

Foundations and didactics of electrodynamics

The majority of the courses I gave these past years have been dealing with classical electrodynamics and optics. During that experience, the students turned out to be a permanent source of (self-)questioning: not that much on technical calculations, but on the deep structures hidden in Maxwell's theory and mostly on how to clarify and convey the key-concepts of fields and waves. To me, the most convincing answer lies in the formulation of electrodynamics in terms of differential forms (exterior algebra), to which this chapter is dedicated. Its content is mostly taken from a series of lectures and a published paper entitled *Improving student understanding of electrodynamics: the case for differential forms* [363].

Section 5.3, not included in [363], was added in order to clarify some of the research perspectives discussed in the general conclusion. It is a brief account of premetric electrodynamics, a revolutionary standpoint based on seminal works by Yuri Obukhov and Friedrich Hehl. The point here is to show that besides pedagogical purpose, exterior algebra is also a powerful tool to investigate how the topological structure of electromagnetism and this latter itself may underlie the Minkowski spacetime.

5.1 Introduction

Why is undergraduate electromagnetism so commonly considered difficult? In an essay entitled *Why is Maxwell's theory so hard to understand?* [364], Freeman Dyson suggests the answer lies in the concept of field, introduced firstly by M. Faraday. Actually, understanding what is the electromagnetic field requires to give up the familiar concepts of Newtonian mechanics (acceleration, mass, force...) in favor of intangible objects remote from directly accessible experience.

Yet mechanical models and classical electromagnetism (EM) still keep something in common: an extensive use of the concept of three-dimensional vector. Although J.C. Maxwell originally used quaternions algebra in his *Treatise on electricity and magnetism* (1873), J.W. Gibbs, O. Heaviside and H. Hertz developed vector calculus to rewrite Maxwell's equations into the more compact form

familiar to every student. In free space, these equations are given in SI units by: [365, 366]

$$\mathbf{curl}\,\mathbf{E} + \frac{\partial \mathbf{B}}{\partial t} = 0 \tag{5.1}$$

$$\mathrm{div}\,\mathbf{D} = \rho \tag{5.2}$$

$$\mathbf{curl}\,\mathbf{H} - \frac{\partial \mathbf{D}}{\partial t} = \mathbf{j} \tag{5.3}$$

$$\mathrm{div}\,\mathbf{B} = 0 \tag{5.4}$$

$$\mathbf{D} = \varepsilon_0 \mathbf{E} \tag{5.5}$$

$$\mathbf{B} = \mu_0 \mathbf{H} \tag{5.6}$$

Here, the source-terms in the nonhomogeneous equations (5.2) and (5.3) are ρ, the electric free charge density, and $\mathbf{j}$, the electric free current density. $\mathbf{E}$ is the electric field, $\mathbf{D}$ is the electric flux density, $\mathbf{H}$ is the magnetic field and $\mathbf{B}$ is the magnetic flux density.

The first four equations are desirable because of Helmholtz decomposition theorem, which states that any vector field (vanishing at infinity) is unique and well-defined provided its curl and its divergence are specified (note that these latter are supplied not only from the free charges and currents, but also from the partial time derivatives of the fields). The last two equations, known as the constitutive relations, are required in order to close the system of equations.

A foretaste of the misconceptions encountered in EM is obtained by paying attention to the terminology. On the one hand, depending on the context, $\mathbf{H}$ is called 'magnetic field' (our choice here), but also 'magnetic field intensity', 'magnetic field strength' or even 'magnetising force' (electrical engineering): the latter three suggest that $\mathbf{H}$ is not the fundamental magnetic quantity (see for example [367]). On the other hand, $\mathbf{B}$ is known as 'magnetic induction field' (ought to Faraday's law), 'magnetic flux density' (our choice here) but EM textbooks sometimes refer to it as the 'magnetic field'. [368, 369] The electric part of the field has a less disparate terminology: $\mathbf{E}$ is always called 'electric field' and only $\mathbf{D}$ is known as 'electric flux density', 'electric displacement field' or 'electric induction'. There again, the latter two underline the idea of $\mathbf{D}$ being an auxiliary quantity and therefore, we opted for the less-used term of 'electric flux density' (an important asset of such choice is that it emphasizes the parallel between $\mathbf{E}$ and $\mathbf{H}$ on the one hand, between $\mathbf{D}$ and $\mathbf{B}$ on the other hand).

All this may come from a widespread way for building Maxwell's equations in matter (see for example the review [370]): as suggested by Lorentz, electrons and nuclei in a medium produce rapidly varying microscopic fields $\mathbf{e}(\mathbf{x}, t)$ and $\mathbf{b}(\mathbf{x}, t)$, that obey Maxwell's equations in free space. Performing a Lorentz-Rosenfeld averaging procedure allows to retrieve macroscopic quantities and in particular, the smoothing of source-terms gives rise to new macroscopic effective fields, namely $\mathbf{D}$ and $\mathbf{H}$, which thus appear as auxiliary quantities (or excitations) relevant primarily in matter. Therefore, in vacuum constitutive relations, $\mathbf{B}$ and $\mathbf{H}$ (resp. $\mathbf{D}$ and $\mathbf{E}$) seem to be redundant fields as they are simply equal up to a multiplicative physical constant.

A particularly insightful exercise is then to examine how the fields transform under a coordinate transformation $\{x, y, z\} \to \{u(x, y, z), v(x, y, z), w(x, y, z)\}$. Denoting by J the Jacobian matrix, Pendry and Ward [371] showed that Maxwell's equations remain invariant provided the old and the new fields (primed quantities) are related by:

$$\mathbf{E}' = J^{-T}\mathbf{E} \quad \mathbf{H}' = J^{-T}\mathbf{H} \tag{5.7}$$

$$\mathbf{D}' = \frac{J}{\det J}\mathbf{D} \quad \mathbf{B}' = \frac{J}{\det J}\mathbf{B} \tag{5.8}$$

D and **E** (resp. **B** and **H**) do not transform in the same way and hence, they are not redundant although mathematically, they are described by the same kind of object: vectors.

Another intriguing point is that **E** and **H** obey a similar transformation law (as **D** and **B** do), suggesting the pair share a common mathematical nature. Sometimes, an additional clarification is introduced based on mirror symmetries, dividing the fields into polar (or true) vectors such as **E** and **D**, and axial vectors (or pseudovectors) such as **B** and **H**.[366]

However, it is obviously not enough to enlighten the form of all (5.7)-(5.8) and as remarked by Kitano, [372] "*in spite of the simple appearance, the constitutive relations, even for the case of vacuum, are the non-trivial part of the EM theory.*".

The fact that **D** and **E** (resp. **B** and **H**) are not redundant in free space is largely unknown and it raises at least two questions: 1) What is the true nature of their connection? 2) Are there pedagogical examples that could help illustrate their different physical contents? In this paper, we use exterior calculus to answer these two questions and in doing so, all the points raised in the previous paragraphs.

Exterior calculus originates from the pioneering works of Grassmann and Cartan and it is concerned with the properties of mathematical objects called differential forms. These latter have raised considerable attention because of their many applications in physics, as testified by the number of articles [372, 373, 374, 375, 376, 377, 378, 379, 380] and books [116, 381, 382, 383, 384, 385, 386, 387, 388, 389] dedicated to differential forms, but they are usually not introduced at an undergraduate level and as far as we know, only more advanced textbooks make abundant use of this formalism (see e.g. [381, 387, 390, 391]).

In the first section of this work, the basic ideas of exterior calculus are introduced in an intuitive way. Only a very basic knowledge of linear algebra will be used to define differential forms along with the different operations which they allow to perform. A particular emphasis will be put on the assets of this formalism from the standpoint of teaching EM in introductory university courses. Then, we illustrate and discuss some key differences between **D** and **E** by working out two examples.

5.2 A primer on exterior calculus

5.2.1 What are differential forms?

Introducing differential forms in a handy but yet accurate way is probably the most challenging part of an exterior-calculus-based electrodynamics course. [374] Undergraduate students are generally familiar with exact (or total) differentials, as those abound in thermodynamics courses. Given a Cartesian coordinate system on the Euclidean space $\mathbb{R}^3$, the total differential of any scalar function F writes as (Einstein's summation convention on repeated indices is used)

$$dF = \frac{\partial F}{\partial x}dx + \frac{\partial F}{\partial y}dy + \frac{\partial F}{\partial z}dz = \frac{\partial F}{\partial x^a}dx^a. \tag{5.9}$$

When changing the function, only the partial derivatives will change: this means that anytime an exact differential is computed, one is working in a vector space whose basis elements are the $\{dx^a, a = 1..3\} = \{dx, dy, dz\}$.

More generally, any object (not necessarily a total differential) that is written as a linear combination of dx^j is called a 1-form and it belongs to the 1-form vector space (or cotangent space)

denoted by $\Lambda^1\left(\mathbb{R}^3\right)$. Once given the 1-form vector space, more general objects can be built in a natural way: this is the idea underlying the more general concept of tensors (technically, a (m,p)-tensor is simply a multilinear map acting on a collection of m 1-forms and p vectors to produce a real number - for more details, see for example [392]). Taking the antisymmetrized tensor product (denoted for short by $\wedge$) for each pair of 1-form basis elements gives

$$dx^a \otimes dx^b - dx^b \otimes dx^a = dx^a \wedge dx^b. \tag{5.10}$$

Here, the regular tensor product $\otimes$ is defined as the ordered product of pairs of 1-forms (and of vectors) and it is associative.

Now, it appears that one can generate only a finite number of non-zero terms, which are a linearly independent and spanning subset of a new vector space: $\Lambda^2\left(\mathbb{R}^3\right)$, the space of 2-forms. For example, in Cartesian coordinates, the 2-form basis written in the right cyclic order is the set: $dy \wedge dz, dz \wedge dx, dx \wedge dy$ (no element dx^a is repeated as (5.10) would return 0). That process can be iterated for p-uples basis elements $\{dx^{a_1} \wedge .. \wedge dx^{a_p}, a_1 \neq .. \neq a_p\}$ and generates forms of degree p (or p-forms) that belong to a vector space $\Lambda^p\left(\mathbb{R}^3\right)$ of dimension $C_3^p = 3\,!/(p\,!(3-p)\,!)$. By construction, a p-form is a completely antisymmetric (0,p) tensor. Concretely, for Cartesian coordinates in $\mathbb{R}^3$, the general expression for a form of degree

$$\begin{array}{lll} 0 & \text{is} & f(x,y,z) \\ 1 & \text{is} & f_1(x,y,z)dx + f_2(x,y,z)dy + f_3(x,y,z)dz \\ 2 & \text{is} & g_1(x,y,z)dy \wedge dz + g_2(x,y,z)dz \wedge dx \\ & & +g_3(x,y,z)dx \wedge dy \\ 3 & \text{is} & g(x,y,z)dx \wedge dy \wedge dz \end{array}$$

As seen above, the cotangent space is a vector space associated to 1-forms. In a similar fashion one associates ordinary vectors to a 'tangent space' as follows. A vector can be seen as an operator which, when acting on a function, gives its directional derivative along the vector direction. That is, taking the directional derivative of a function F along the vector $\mathbf{v}$ at the point x one gets

$$D_{\mathbf{v}}F(x) = \mathbf{v} \cdot \nabla F(x) = v^a \partial_a F(x). \tag{5.11}$$

We see that there is a one-to-one correspondence between vectors and derivations such that the vector $\mathbf{v}$ may be represented by its components in the basis $\{\partial_a\}$. It follows that the linear space spanned by this basis is a vector space called the tangent space at the point $x \in \mathbb{R}^3$. Like in the case of the p-forms, the wedge product between vectors can be used to generate higher order vectors, or p-vectors.

The spaces of p-forms and of p-vectors can be defined on base spaces that are more general than $\mathbb{R}^3$. For any manifold $\mathcal{M}$ of dimension n (that is a smooth hypersurface that locally looks like $\mathbb{R}^n$), once given a coordinate system $\{x^a, a = 1..n\}$, one gets the vector coordinate basis $\{\mathbf{e}_a = \partial/\partial x^a = \partial_a\}$ and a 1-form basis $\{dx^a\}$. These two sets are said dual, in the sense that when they act upon each other, it returns a real number as prescribed by

$$dx^a\left(\partial_b\right) = \partial_b\left(dx^a\right) = \delta_b^a. \tag{5.12}$$

In other words, a 1-form is a linear map from a vector space onto $\mathbb{R}$ and more generally, a p-form is a multilinear map acting on a collection of p-vectors onto $\mathbb{R}$. Note that in mathematics, there are other notions of duality, such as Hodge duality which will be introduced in section 5.2.

Next to that algebraic standpoint on forms, another way to grasp forms is from integral calculus. Indeed, differential forms "*are the things which occur under integral signs*":[384] a form of degree p is simply an object that one integrates p-times to get a scalar. Stated otherwise, "*a differential form is simply this: an integrand*" .[388] A particular care must be taken when introducing forms that way.

First, exterior calculus relies strictly speaking on Lebesgue integrals, not on Riemann integrals.

Second, it is customary in calculus to drop the wedge sign when computing double (multiple) integrals such as $\iint_R f(x,y)dxdy$, where the domain of integration is defined as $R = [x_1, x_2] \times [y_1, y_2]$. But then, the Fubini's exchange-of-integration-order formula may look contradictory with the antisymmetry property of the 2-form $dx \wedge dy$. Although subtle, the disagreement is nothing but apparent: indeed, switching dx with dy also involves a reparametrization of the integration domain $p : R \to R' = [y_1, y_2] \times [x_1, x_2]$. As for any p-form u $\iint_R u = -\iint_{p(R)} u$ if the map p reverses the orientation of the integration domain (conversely, there is a plus sign if the map preserves orientation), then the antisymmetry feature of forms is retained in the customary calculus formulas.

Third, introductory calculus courses define integrals as the limits of Riemann sums when the partition becomes infinitely fine, $\int_a^b f(x)dx = \lim_{\Delta x \to 0} \sum_k f(x_k)\Delta x$, where the x_k are points evenly spaced in the interval $[a, b]$. This suggests that "dx" is in practice a shorthand notation for an infinitely thin width, which it is not. As explained by Spivak,[393] "*Classical differential geometers (and classical analysts) did not hesitate to talk about 'infinitely small' changes dx^i of the coordinates x^i, just as Leibnitz had. No one wanted to admit that this was nonsense, because true results were obtained when these infinitely small quantities were divided into each other*". A rigorous connection between infinitesimal elements and 1-forms belongs to the realm of non-standard analysis, a branch of mathematics developed in the 1960s by Abraham Robinson.[394]

To sum up, the differential form dx is rightly understood as a basis element of the cotangent space, but not as a tiny change: this is why one favors the introduction of differential forms from the algebraic standpoint instead of the more widespread analysis standpoint.

A popular way to gain insight on 1, 2 and 3-forms in $\mathbb{R}^3$ is to use graphical representations known as Schouten pictograms.[395] The main idea is to plot a p-form field ω as a foliation built from its kernel $\mathrm{Ker}\,\omega$. Recalling that differential forms act on vectors returning real numbers (see Eq. (5.12)), the kernel of a form α is the set of all vectors $\mathbf{v}$ such that $\alpha(\mathbf{v}) = 0$. A foliation is a family of hypersurfaces of dimension $3 - p$, filling $\mathbb{R}^3$ with no overlap. One can define it from the kernel if and only if $\mathrm{Ker}\,\omega$ is an integrable plane field (this is known as Pfaff's problem and a general criterion involving the exterior derivative d introduced in the next paragraph is $\omega \wedge d\omega = 0$). For 1-forms, integrability means that there is always a 2-surface that is locally tangent to the plane field defined by $\mathrm{Ker}\,\omega$. To be more concrete, let us focus on the 1-form $\omega = dr$ in cylindrical coordinates $\{r, \theta, z\}$: its kernel is simply obtained at each point from (5.12) $dr(\partial_\theta) = 0, dr(\partial_z) = 0$. Hence, the plane field generated by vectors $\{\partial_\theta, \partial_z\}$ is the family of planes, tangent to 2-surfaces $r = C^{st}$.

Although it might look appealing, this visual interpretation may help for a first initiation to the language of forms, but this rarely goes beyond an introductory level: as discussed in Ref. [388], there are many simple forms whose kernels are not integrable and present "contact structures" (for example $xdy + dz$). Hence, we will not rely on that point of view in the reminder of this work.

5.2.2 Wedge product, exterior derivative and vector calculus identities

Relation (5.10) introduces an algebraic operation between 1-forms: the wedge (or exterior) product, denoted by the symbol $\wedge$. More generally, given two forms u, v (of degree m), w (of degree p) and z (of degree q), it can be shown easily that the wedge product obeys the three following properties:

$$u \wedge w = (-1)^{mp} w \wedge u \qquad \text{(supercommutativity)} \tag{5.13}$$

$$u \wedge (w \wedge z) = (u \wedge w) \wedge z \qquad \text{(associativity)} \tag{5.14}$$

$$(\alpha u + \beta v) \wedge w = \alpha u \wedge w + \beta v \wedge w \qquad \text{(linearity)} \tag{5.15}$$

$u \wedge w$ is a form of degree $m+p$. As remarked previously, supercommutativity implies that $dx^a \wedge dx^a = 0$: hence, for a base space of dimension n, no form of degree $p > n$ can exist. The set of all $\{\Lambda^p(\mathcal{M}), p = 0..n\}$ equipped with the exterior product defines an algebra known as the Grassmann algebra.

Although the meaning of the wedge product may be obscure, it is still a familiar object to students in the usual Euclidean space.

When u is a 0-form (a scalar) and w is a p-form, the wedge is simply the scalar multiplication and it will be omitted.

When computing the wedge product of two 1-forms $u = u_a dx^a$ and $v = v_a dx^a$, it comes

$$\begin{aligned} u \wedge v = \quad & (u_y v_z - u_z v_y)\, dy \wedge dz + (u_z v_x - u_x v_z)\, dz \wedge dx \\ & + (u_x v_y - u_y v_x)\, dx \wedge dy. \end{aligned} \tag{5.16}$$

The components of $u \wedge v$ look like the components obtained from the usual cross product between vectors $(u_x \mathbf{e}_x + u_y \mathbf{e}_y + u_z \mathbf{e}_z) \times (v_x \mathbf{e}_x + v_y \mathbf{e}_y + v_z \mathbf{e}_z)$ (the exact forms-vectors connection and its inferences will be refined later, see also Ref. [375]). Roughly speaking, when applied to 1-forms in $\mathbb{R}^3$, $\wedge$ has the meaning of a cross-product.

What about the wedge product between a 1-form and a 2-form? A straightforward calculation shows that for a 1-form u and a 2-form $w = w_x dy \wedge dz + w_y dz \wedge dx + w_z dx \wedge dy$, the wedge product yields

$$u \wedge w = (u_x w_x + u_y w_y + u_z w_z)\, dx \wedge dy \wedge dz. \tag{5.17}$$

This time, $\wedge$ behaves like the ordinary dot product between the components of u and w.

The wedge product concatenates two forms to produce a new form of higher degree. Another possibility to increase the degree of a form is to take the exterior derivative of a form. The exterior derivative of a p-form is a linear mapping from $\Lambda^p(\mathcal{M})$ to $\Lambda^{p+1}(\mathcal{M})$ defined formally in n dimensions as

$$d\omega \equiv \left(\frac{\partial}{\partial x^a} dx^a \right) \wedge \omega \qquad a = 1..n \tag{5.18}$$

It generalizes the notion of total differential of a scalar function (5.9). Unlike the ordinary derivative, it is a dimensionless operator. Besides, it obeys the two following properties

$$d(u \wedge v) = (du) \wedge v + (-1)^p u \wedge dv \text{ (Leibniz)} \tag{5.19}$$

$$d(du) = 0 \qquad \text{(Nilpotence)} \tag{5.20}$$

with p the degree of u.

From the nilpotence property, if a p-form ω is exact (i.e. there is a $(p-1)$-form u such that $\omega = du$), then it is necessarily closed (its exterior derivative vanishes). Conversely, Poincaré's

lemma states that a closed p-form is always locally exact but generally not globally, depending on the topology of the base space $\mathcal{M}$ (this is the object of the de Rham cohomology).

The exterior derivative of terms such as $g\left(x^1, x^2...\right) dx^{a_1} \wedge .. \wedge dx^{a_p}$ is obtained using both the Leibniz formula and the nilpotence property in (5.18)

$$d\left(g\left(x^1, x^2...\right) dx^{a_1} \wedge .. \wedge dx^{a_p}\right) = (dg) \wedge dx^{a_1} \wedge .. \wedge dx^{a_p} \tag{5.21}$$

In practice, the exterior derivative of a p-form simply consists in computing the sum of the partial derivatives of its components and then in discarding terms within which a same dx^a is repeated.

It is interesting to point out the coherence of the notations employed heretofore: for the 0-form $u = x^1$, (5.21) leads to $du = d(x^1) = dx^1$.

The exterior derivative must not be confused with either the Lie derivative (which computes variations with respect to a vector field and is connected to d via the Cartan formula) or with the covariant derivative (which is dedicated to parallel transport and requires a connection on the manifold).

Similarly to the wedge product, some insight on d can be gained by expressing (5.19)-(5.20) with forms in $\mathbb{R}^3$. For example in Cartesian coordinates, the exterior derivative of a 0-form $F(x, y, z)$ gives (5.9), but now with a clarified meaning for the dx^a. Hence, the exterior derivative of a 0-form returns a 1-form with components similar to the ordinary gradient operator. Likewise, the exterior derivative of a 1-form u gives after straightforward algebra

$$\begin{aligned} du = \quad & (\partial_x u_y - \partial_y u_x)\, dx \wedge dy + (\partial_y u_z - \partial_z u_y)\, dy \wedge dz \\ & + (\partial_z u_x - \partial_x u_z)\, dz \wedge dx. \end{aligned} \tag{5.22}$$

One recognizes a 2-form whose components correspond to the ordinary curl operator of a vector field with appropriate components (discussed later). Finally, applying the exterior derivative to a 2-form w leads to a 3-form with components analogous to the ordinary divergence operator

$$dw = (\partial_x w_x + \partial_y w_y + \partial_z w_z)\, dx \wedge dy \wedge dz. \tag{5.23}$$

To sum up, grad, curl and div are just a unique operator in disguise, d, applied to forms of different degrees. But there is more: the exterior derivative not only unifies grad, curl and div, but it also generalizes them to arbitrary dimensions (this is responsible for Burke's thought-provoking statement "Div, Grad, Curl are Dead".[396])

As a sidenote, it is worth noting that the inverse operation to derivation, integration, also exists in exterior calculus, but there are some subtleties compared to ordinary integration familiar to students. There is indeed a natural way to integrate a p-form over a p-dimensional submanifold (note that the degree of the form has to be the same as the dimension of the domain of integration), which does not rely on lengths, angles or scalar products and is hence purely topological. Such integral is not defined in the sense of Riemann but it is properly performed with respect to Lebesgue measure.[397] In practice, this means that integration of a 1-form u on a path $\mathcal{C}$

$$\int_{\mathcal{C}} u = \int_{\mathcal{C}} u_x dx + u_y dy + u_z dz$$

can not be interpreted as the usual circulation of a vector field $\mathbf{u}$ along the curve $\mathcal{C}$

$$\int_{\mathcal{C}} \mathbf{u}.\mathbf{ds}$$

as the scalar product requires the knowledge of the geometry of $\mathcal{M}$ (technically, the metric). But there is worse: there is no consistent way to define the flux of u, as that would involve integration of a 1-form on a domain of dimension 2. As can be guessed, the degree of u must be increased beforehand, as expressed by the generalized Stokes theorem:[376]

$$\int_{\partial\mathcal{D}} u = \int_{\mathcal{D}} du. \tag{5.24}$$

5.2.3 Hodge star operator

Another ingredient is necessary to reformulate EM with differential forms. To apprehend this, consider the example of a vector field whose counterpart is a 1-form field. As we just saw, the exterior derivation only allows us to build a curl-like equation, leaving the divergence part undefined. This violates Helmholtz theorem (whatever its time-dependent form may be [398]), meaning that the field is not defined unambiguously. Another variation on the same theme: in virtue of the nilpotence property (5.20), having only $\wedge$ and d at our disposal leaves no room for equations involving a Laplacian. As we shall see, these two problems are solved by the Hodge duality, which consists in a mapping between p-forms and $(n-p)$-forms (remember that n is the dimension of the manifold). Beforehand, one must introduce two objects: the metric tensor and the inner product.

So far, all mathematical objects that have been introduced are purely topological, i.e. they are relying neither on angles nor on distances. These latter can be computed only when the base space is equipped with a metric structure ($\mathcal{M}$ is then called a pseudo-Riemannian manifold). The metric consists in a symmetric $(0,2)$ tensor denoted by g, which defines the scalar product between two vectors:

$$g(\mathbf{u},\mathbf{v}) = g_{ab}\, dx^a(\mathbf{u}) \otimes dx^b(\mathbf{v}). \tag{5.25}$$

From (5.12), its appears that the components of g are simply the scalar products between the coordinate basis elements $g_{ab} = g(\partial_a, \partial_b)$. What is the physical content of these components? In the flat Eulidean plane, the displacement vector $\mathbf{\Delta s} = (\Delta x, \Delta y)$ has a length squared given by Pythagoras theorem $\Delta s^2 = \Delta x^2 + \Delta y^2$, so that $g_{11} = 1, g_{22} = 1, g_{12} = g_{21} = 0$. However, on the surface of a sphere (of radius R), an arc of length squared is given by $\Delta s^2 = R^2\Delta\theta^2 + R^2\sin^2\theta\Delta\phi^2$ so that $g_{11} = R^2, g_{22} = R^2\sin^2\theta, g_{12} = g_{21} = 0$. From these examples, one understands that the components of g are related in particular to the curvature of the manifold, a property which remains true in higher dimensions. The metric is real and symmetric, hence the inverse metric exists and obeys $g_{ac}g^{cb} = \delta_a{}^b$. This provides a one-to-one correspondence between the components of a 1-form v and those of a vector $\mathbf{v}$:

$$v_a = g_{ab}v^b. \tag{5.26}$$

Locally, there is always an orthonormal coordinate basis such that g_{ab} reduces to a diagonal matrix having only $+1$'s or -1's on its diagonal: the signature of the metric is the couple $(s, n-s)$ where s is the number of -1's. From the standpoint of general relativity, the metric tensor is Lorentzian (e.g. with signature=(1,3)) and it is obtained as a solution of Einstein's field equations.[116, 392, 399, 400]

The inverse metric g^{ab} defines the inner product $\langle , \rangle$ between two p-forms according to:

$$p = 1: \quad \left\langle dx^a, dx^b \right\rangle = g^{ab} \tag{5.27}$$

$$p > 1: \quad \left\langle dx^{a_1} \wedge .. \wedge dx^{a_p}, dx^{b_1} \wedge .. \wedge dx^{b_p} \right\rangle = \begin{vmatrix} g^{a_1 b_1} & \cdots & g^{a_1 b_p} \\ \vdots & \ddots & \vdots \\ g^{a_p b_1} & \cdots & g^{a_p b_p} \end{vmatrix}. \tag{5.28}$$

The inner product between 1-forms is the equivalent of the dot product for vectors.

Finally, having at our disposal the metric and the inner product, the Hodge dual operator (or star operator $\star$) is an invertible linear map between $v \in \Lambda^p(\mathcal{M})$ and $\star\, v \in \Lambda^{n-p}(\mathcal{M})$ such that [383]

$$u \wedge (\star\, v) = \langle u, v \rangle \sqrt{|\det g_{ab}|}\, dx^1 \wedge .. \wedge dx^n \tag{5.29}$$

(here u is of the same degree as v).

An equivalent and more explicit definition is given by [401]

$$\star v = \frac{1}{(n-p)!} v^{\mu_1 \ldots \mu_p} \sqrt{|\det g_{ab}|} \epsilon_{\mu_1 \ldots \mu_n} dx^{\mu_{p+1}} \wedge ... \wedge dx^{\mu_n}, \tag{5.30}$$

where

$$v = v_{\mu_1 \ldots \mu_p} dx^{\mu_1} \wedge ... \wedge dx^{\mu_p}. \tag{5.31}$$

and the totally anti-symmetric Levi-Civita symbol is defined as

$$\begin{aligned} \epsilon_{\mu_1 \ldots \mu_n} &= +1 \text{ if } \mu_1, ..\mu_n \text{ is an even permutation of 1,..n} \\ &= -1 \text{ if } \mu_1, ..\mu_n \text{ is an odd permutation of 1,..n} \\ &= 0 \text{ otherwise} \end{aligned} \tag{5.32}$$

Contrary to $\wedge$ and d, the Hodge dual is a metric-dependent operator and it obeys the properties:

$$\star\,(\star\, v) = (-1)^{s+p(n-p)}\, v \tag{5.33}$$

$$u \wedge (\star\, v) = v \wedge (\star\, u) \tag{5.34}$$

$$u \wedge (\star\, u) = 0 \Rightarrow u = 0. \tag{5.35}$$

To understand what (5.29) really does, let us illustrate its action on the p-form basis for the flat Euclidean space in spherical coordinates $\{r, \theta, \phi\}$:

$$\star\,(d\theta \wedge d\phi) = \frac{1}{r^2 \sin\theta} dr, \tag{5.36}$$

$$\star\,(dr \wedge d\theta) = \sin\theta d\phi \tag{5.37}$$

$$\star\,(d\phi \wedge dr) = \frac{1}{\sin\theta} d\theta, \tag{5.38}$$

$$\star\,(dr \wedge d\theta \wedge d\phi) = \frac{1}{r^2 \sin\theta}. \tag{5.39}$$

These relations are of course completed by means of (5.33). When the metric is diagonal, they are obtained for any curvilinear coordinates by following the simple recipe: respecting the right

cyclic order, the action of the Hodge dual on a p-uple returns the missing $(n-p)$-uple, each dx^a being multiplied by its corresponding Lamé coefficient (the square root of the metric $\sqrt{g_{aa}}$ (no index summation)). Although $\star\, v$ appears as some kind of orthogonal complement of the p-form v, we will see later that in EM it can be pictured more accurately as a rotation between the electric and magnetic parts of the field.

Having the Hodge operator at our disposal, one is now in position to address the questions asked at the beginning of this section. Symmetrically to the exterior derivative which increases the degree of forms, one can now define a derivation operation that lowers the degree of the forms: this is the coderivative δ defined as

$$\delta v = (-1)^{s+p(n-p)} \star d \star v. \tag{5.40}$$

The coderivative maps $\Lambda^p(\mathcal{M}) \to \Lambda^{p-1}(\mathcal{M})$, in a similar fashion as a divergence operator which returns a scalar from a higher-degree object, vector or pseudovector. It obeys the two following properties:[402]

$$\delta(\delta u) = 0 \qquad \text{(Nilpotence)} \tag{5.41}$$

$$du \wedge (\star\, v) = u \wedge \star(\delta v) + d\,(u \wedge \star v\,) \tag{5.42}$$

That is the missing piece required to construct second derivatives that do not identically vanish. Indeed, the anticommutator between d and δ, known as the Laplace-de Rham operator, generalizes the usual Laplace operator for vectors in $\mathbb{R}^3$ to p-forms on an arbitrary base space $\mathcal{M}$:

$$\Delta v = (\delta d + d\delta)\, v. \tag{5.43}$$

It also provides a way to close the set of equations required to define the field: instead of the curl and divergence required for vector fields, form fields are unambiguously defined by their derivative and their coderivative.

This is the main result of the Hodge decomposition theorem, that generalizes the Helmholtz theorem.[403] Moreover, the Hodge operator connects in a precise manner $\wedge$, d and their counterparts in vector analysis. The case of 1-forms has already been settled: they are translated unambiguously into vectors as prescribed by (5.26). Now, looking back at (5.17), we remarked that when dealing with a 1-form u and a 2-form v, $u \wedge v$ behaves like the ordinary dot product: but as the right hand side is a 3-form and not a 0-form (a scalar), it is in fact $\star(u \wedge v)$ (and not simply $u \wedge v$) that actually returns a 0-form and corresponds to the ordinary dot product. A similar statement holds for divergence which corresponds to $\star d$ of a 2-form (and not simply d) as appears from (5.23). More generally, taking the Hodge dual translates unambiguously 3-forms into scalars. The case of 2-forms may look trickier at first glance, as they can be translated either as bivectors (using the metric two times to raise each index) or as vectors (taking the Hodge star and then using the metric on the 1-form obtained). However, it can be shown after some algebra that, for a diagonal metric in 3 dimensions, these two procedures lead to the same components (this is no longer true in 4 dimensions). Hence, as summarized in Ref. [374], for $u, v \in \Lambda^1\mathcal{M}$, $\mathbf{u} \times \mathbf{v}$ identifies with $\star(u \wedge v)$ and **curl u** with $\star\, du$.

5.3 Outcomes

5.3.1 Unification of vector analysis

As seen previously, depending on the degree of the forms between which it is applied, and up to a Hodge dual, the wedge product unifies scalar multiplication, cross product and scalar product whereas exterior derivative unifies grad, curl and div operators. Bearing that in mind, let us investigate on a few examples how (5.19)-(5.20) are translated for forms of different degrees in $\mathbb{R}^3$. Beginning with the nilpotence property applied to a 0-form F, dF stands for the gradient and as it is a 1-form, its exterior derivative gives the curl, so that in the end one retrieves the well-known formula

$$\star\, d\,(dF) = 0 \;\rightarrow\; \mathbf{curl}\,(\mathbf{grad}\, F) = 0. \tag{5.44}$$

For a 1-form u, the same approach leads to

$$\star\, d\,(du) = 0 \;\rightarrow\; \mathrm{div}\,(\mathbf{curl}\,\mathbf{u}) = 0. \tag{5.45}$$

Considering the Leibniz formula, in the case of two 0-forms F and G, it comes that

$$\begin{aligned} &d\,(F \wedge G) = (dF) \wedge G + (-1)^0\, F \wedge dG \\ &\rightarrow\; \mathbf{grad}\,(F\,G) = G\,\mathbf{grad}\, F + F\,\mathbf{grad}\, G. \end{aligned} \tag{5.46}$$

For F a 0-form and u a 1-form, one obtains

$$\begin{aligned} &\star\, d\,(F \wedge u) = \star\,(dF \wedge u) + (-1)^0\, F\,(\star\, du) \\ &\rightarrow\; \mathbf{curl}\,(F\,\mathbf{u}) = \mathbf{grad}\, F \times \mathbf{u} + F\mathbf{curl}\,\mathbf{u}. \end{aligned} \tag{5.47}$$

For two 1-forms, this now gives

$$\begin{aligned} &\star\, d\,(u \wedge v) = \star\,(du \wedge v) + (-1)^1 \star\,(u \wedge dv) \\ &\rightarrow\; \mathrm{div}\,(\mathbf{u} \times \mathbf{v}) = (\mathbf{rot}\,\mathbf{u})\,.\mathbf{v} - \mathbf{u}.\,(\mathbf{rot}\,\mathbf{v})\,. \end{aligned} \tag{5.48}$$

As can be understood from these examples, the various identities of vector analysis simply come down to two short formulas, (5.19) and (5.20). Other identities involving the mixed product and triple vector product can also be derived from the antisymmetry properties of the wedge product.[374] Finally, all formulas involving integration of scalar and vector fields can also be retrieved from (5.24). Indeed, when applied to a 0-form $F(x)$, it simply gives the fundamental theorem of calculus

$$\int_{[a,b]} dF = \int_{\partial[a,b]} F \;\rightarrow\; \int_{[a,b]} \frac{\partial F}{dx^i} dx^i = F\,(b) - F\,(a)\,.$$

Once a metric is given, one can draw connections between the usual integral identities and the generalized Stokes theorem: the Stokes formula is obtained from (5.24) applied to a 1-form, whereas the Gauss formula comes from (5.24) applied to a 2-form. The Green identities are obtained by integrating (5.42) and then using the Stokes theorem [402]

$$\int_{\mathcal{D}} dF \wedge (\star dG) + \int_{\mathcal{D}} F \wedge (\star \Delta G) = \int_{\partial\mathcal{D}} F \wedge \star dG \tag{5.49}$$

$$\int_{\mathcal{D}} F(\star \Delta G) - G(\star \Delta F) = \int_{\partial\mathcal{D}} F(\star dG) - G(\star dF) \tag{5.50}$$

for F and G two 0-forms. Integration of the Leibniz formula also provides an interesting result:

$$\int_{\mathcal{D}} (du) \wedge v = \int_{\partial\mathcal{D}} u \wedge v - (-1)^p \int_{\mathcal{D}} u \wedge dv \tag{5.51}$$

where (5.24) was used to simplify the second integral: this expression generalizes integration by parts at arbitrary dimensions.

5.3.2 "Forms illuminate EM..."

In this section, we reformulate electromagnetic theory in the language of differential forms and in so doing we discuss its axiomatics. Indeed, there are some redundancies within the set of equations, as can be seen from the Maxwell-Thomson equation (5.4). In virtue of Schwarz's theorem, $\text{div}\,\mathbf{B} = 0 \;\Rightarrow\; \text{div}\,\partial_t\mathbf{B} = 0$, so that $\partial_t\mathbf{B}$ is a purely solenoidal field. Hence, it expresses as the curl of a "potential", which is nothing else than Maxwell-Faraday equation (5.1). In order to clarify the foundations and the structure of EM, we therefore proceed by trying to use the minimal set of mathematical and physical objects at each step: in particular, following the prescription of Obukhov and Hehl, [395] we will try to postpone the use of the metric (which originates from another interaction, gravitation) to as late as possible. Let us begin with a very general statement: electric charge is a quantifiable physical property. In practice, given a 3-dimensional compact domain $\mathcal{V}$, it means that one can always count (at least classically) the number of elementary charges localized within $\mathcal{V}$ and then obtain the total charge Q. This defines a 3-form electric charge density ρ such that

$$Q = \int_{\mathcal{V}} \rho \tag{5.52}$$

This relation is purely topological, as it does not rely on lengths or angles. As ρ is a 3-form in $\mathbb{R}^3$, then necessarily

$$d\rho = 0. \tag{5.53}$$

This equation has no analog in the usual Maxwell-Heaviside formulation of EM and comes from the fact that electric charge is quantifiable. A first outcome arises in virtue of the Poincaré lemma: as ρ is a closed form, it is locally exact so that there exist a potential 2-form D such that

$$\rho = dD. \tag{5.54}$$

One recognizes here the exterior calculus version of the Maxwell-Gauss equation (5.2). Hence, electric flux density translates into a 2-form D.

A second outcome appears when taking the time derivative of ρ and using Schwarz's theorem: as $d(\partial_t\rho) = 0$, in virtue of the Poincaré lemma again, $\partial_t\rho$ is exact so that there exists in any contractible domain a 2-form potential j such that

$$\partial_t\rho = d(-j). \tag{5.55}$$

One recognizes here the continuity equation for the electric charge, which is usually built as a spin-off of (5.2) and (5.3). Note that as suggested by the usual continuity equation, the term in $\text{div}\,\mathbf{j}$ confirms that the electric current density is indeed a 2-form. But there is more: combining (5.54) and (5.55), it comes that $d\,(j + \partial_t D) = 0$, so that once again from the Poincaré lemma, there exists a 1-form potential H such that

$$j + \partial_t D = dH. \tag{5.56}$$

This is the Maxwell-Ampère equation (5.3).

To summarize, D and H are potentials associated to sources ρ and $\mathbf{j}$ and they are introduced from topological equations, which result from the fact that electric charges are quantifiable. Hence, they are relevant not only in matter, but also in free space and they «*are microphysical quantities of the same type likewise - in contrast to what is stated is most textbooks*»[404].

The last set of equations is based on the absence of magnetic monopoles, which can also be expressed from a counting procedure on the 3D compact domain $\mathcal{V}$ (also coming from the idea that charges are quantifiable):

$$Q_M = 0 = \int_{\mathcal{V}} \rho_M, \tag{5.57}$$

so that the 3-form magnetic charge density identically vanishes, $\rho_M = 0$. This is the physical content of the Maxwell-Thomson equation (5.4)

$$dB = 0, \tag{5.58}$$

where B is the 2-form magnetic flux density. Hence, from the Poincaré lemma, once again deriving (5.58) with respect to time and using the Schwarz's theorem, there exists a 1-form potential E, the electric field, such that

$$\partial_t B = d(-E). \tag{5.59}$$

This is the exterior algebra version of the Maxwell-Faraday equation (5.1) and its similarity with (5.55) highlights its status of continuity equation for the magnetic flux. As suggested by the usual form of the Maxwell-Faraday equation, the term in $\mathbf{curl}\,\mathbf{E}$ confirms that the electric field is indeed a 1-form.

Moreover, forms and their associated vector fields do not share the same dimension. Combining (5.52) with (5.54) and using the Stokes theorem gives the Gauss theorem

$$Q = \int_{\partial \mathcal{V}} D. \tag{5.60}$$

A quick dimensional analysis reveals that the dimension of D is that of a charge $[D] = \mathtt{C}$ (but its components recover the regular dimension $\mathtt{C/m}^2$), $[j] = \mathtt{C/s}$ $[H] = \mathtt{C/s}$, $[B] = flux = \mathtt{J.s/C}$ and $[E] = \mathtt{J/C}$. We are now in position to address the problem of the transformation laws (5.7)-(5.8) mentioned in the introduction. Indeed, consider a general coordinate change $\{x, y, z\} \to \{u(x, y, z), v(x, y, z), w(x, y, z)\}$, one is looking for the components of E in the new coordinate system. Straightforward algebra gives

$$\begin{aligned} E &= E_a dx^a = E_x \left(\frac{\partial x}{\partial u} du + \frac{\partial x}{\partial v} dv + \frac{\partial x}{\partial w} dw \right) + ... \\ &= \left(\frac{\partial x}{\partial u} E_x + \frac{\partial y}{\partial u} E_y + \frac{\partial z}{\partial u} E_z \right) du + ... \\ &= \left[\left(J^{-T} \right)_{11} E_x + \left(J^{-T} \right)_{12} E_y + \left(J^{-T} \right)_{13} E_z \right] du + ..., \end{aligned}$$

which agrees with (5.7). On the other hand, for the 2-form D, it comes that

$$\begin{aligned} D \quad &= D_x dy \wedge dz + D_y dz \wedge dx + D_z dx \wedge dy \\ &= D_x \left(\frac{\partial y}{\partial u^a} du^a \right) \wedge \left(\frac{\partial z}{\partial u^b} du^b \right) + ... \\ &= D_x \left[\left(\frac{\partial y}{\partial v} \frac{\partial z}{\partial w} - \frac{\partial z}{\partial v} \frac{\partial y}{\partial w} \right) dv \wedge dw + ... \right] + ... \\ &= D_x \left[\left(\text{Com } J^{-1} \right)_{11} dv \wedge dw + \left(\text{Com } J^{-1} \right)_{12} dw \wedge du \right. \\ &\quad \left. + \left(\text{Com } J^{-1} \right)_{13} du \wedge dv ... \right] + ... \\ &= \left[D_x \left(\frac{J}{\det \text{ J}} \right)_{11} + D_y \left(\frac{J}{\det \text{ J}} \right)_{21} + D_z \left(\frac{J}{\det \text{ J}} \right)_{31} \right] \\ &\quad dv \wedge dw + ..., \end{aligned}$$

which agrees with (5.8). The notation Com M refers to the matrix of cofactors of M. The transformation laws for $\mathbf{E}$ and $\mathbf{D}$ are different because, fundamentally, these correspond to two different mathematical objects: forms of different degrees.

Now, considering (5.54), (5.56), (5.58) and (5.59), it appears that the number of unknowns exceeds the number of equations. The role devoted to the constitutive relationships is precisely to fill this gap by providing additional connections between the different parts of the electromagnetic field (as the purpose of the present work is mainly pedagogical, we will not discuss the more technical cases of non-linear media and magneto-electric effects). As in 3D 1-forms and 2-forms are naturally mapped into each other by the Hodge dual operator, the only admissible translation of (5.5)-(5.6) is:

$$D = \varepsilon_0 \star E, \tag{5.61}$$

$$B = \mu_0 \star H. \tag{5.62}$$

The constitutive relations are metric-coupled dual relations needed to close Maxwell's equations. This highlights one extremely important point: as the four Maxwell's equations can be built without the metric, it is the main purpose of constitutive relations to reveal how the EM field couples to geometry. Moreover, in free space, it is customary from the standpoint of vector analysis to proceed to Gauss field identification $\mathbf{E} = \mathbf{D}$, $\mathbf{H} = \mathbf{B}$ (up to dimensional multiplicative constants). As mentioned in section II.C, when the metric is diagonal, this identity applies but anytime the metric has off-diagonal terms, this identification fails (see for instance the mixing of EM components in the Sagnac effect.[405]) Writing constitutive relations from exterior algebra clarifies why Gauss identification may not apply: the action of Hodge operator - and consequently the constitutive properties of vacuum - results from the geometric properties of space, so that anytime these latter are non-trivial, the links between the different fields are non-trivial as well (in 4D, vacuum constitutive properties are only related to the conformal part of the metric [406]).

In other words, vacuum has to be considered as a full-fledged medium with its own optical properties, as testified by the terminology of ε_0, i.e. the permittivity of free space. Like in any material medium, the electric part of the field is determined by both $\mathbf{E}$ and $\mathbf{D}$ (resp. by $\mathbf{H}$ and $\mathbf{B}$ for the magnetic part) that encompass information of different kinds and are not redundant quantities even in free space. This is in fact very close to Maxwell's original view on the field, as expressed explicitly in his *Treatise*: "*We are thus led to consider two different quantities, the magnetic force*

and the magnetic induction, both of which are supposed to be observed in a space from which the magnetic matter is removed.".[407]

5.3.3 "... and EM illuminates forms."

The formula defining the Hodge dual makes its meaning rather abstruse. Although $\star\, u$ might appear as some kind of orthogonal complement of the p-form u, a deeper way to understand Hodge star is related to an internal symmetry of Maxwell's equations, known as S-duality.

In the absence of sources, these latter are left invariant when performing "cross-rotations" between the electric and magnetic parts of the field: [366, 369]

$$\mathbf{E}' = \mathbf{E}\cos\alpha - \mathbf{B}\sin\alpha \tag{5.63}$$

$$\mathbf{B}' = \mathbf{E}\sin\alpha + \mathbf{B}\cos\alpha \tag{5.64}$$

where for simplicity we use units for which $c = 1$. Following a remark by Weber,[408] this duality rotation can be expressed in a more compact form from the Weber vector $\mathbf{F} = \mathbf{E} + i\mathbf{B}$ (cf. Ref. [409]):

$$\mathbf{F}' = e^{i\alpha}\,\mathbf{F} = (\cos\alpha + i\sin\alpha)\,(\mathbf{E} + i\mathbf{B}) \tag{5.65}$$

$$= (\mathbf{E}\cos\alpha - \mathbf{B}\sin\alpha) + i\,(\mathbf{E}\sin\alpha + \mathbf{B}\cos\alpha)\,. \tag{5.66}$$

α is a mixing angle related to the relative proportions of electric and magnetic fields.

A direct connection with the Hodge operator can be made but at the cost of working in four dimensions. In this case, the electric 1-form E and the magnetic 2-form B are gathered within the Faraday 2-form

$$F = E \wedge dt + B \tag{5.67}$$

Taking the 4D-exterior derivative and using (5.59) gives:

$$\begin{aligned} d_4 F &= dE \wedge dt + dB + \partial_t B \wedge dt \\ &= (-\partial_t B) \wedge dt + \partial_t B \wedge dt = 0 \end{aligned} \tag{5.68}$$

Similarly, one defines the Maxwell 2-form as

$$G = \star_4 F = D - H \wedge dt \tag{5.69}$$

and this latter obeys the source equation:

$$\begin{aligned} d_4 G &= dD + \partial_t D \wedge dt - dH \wedge dt \\ &= \rho + \partial_t D \wedge dt - (j + dD) \wedge dt \\ &= \rho - j \wedge dt = J \end{aligned} \tag{5.70}$$

When applied on a 2-form in a 4D Lorentzian metric, (5.33) becomes $\star_4^2 = -1$, in a similar fashion to the imaginary unit $i^2 = -1$. Hence, one constructs the following operator on a 2-form as

$$\exp(\star_4\,\alpha) = \cos\alpha + \star_4\,\sin\alpha. \tag{5.71}$$

Like the complex number $\exp(i\theta)$, it obeys

$$e^{\star_4\,\alpha} e^{\star_4\,\beta} = e^{\star_4\,(\alpha+\beta)} = e^{\star_4\,\beta} e^{\star_4\,\alpha} \tag{5.72}$$

$$e^{\star_4 \frac{\pi}{2}} = \star_4. \tag{5.73}$$

In Cartesian coordinates, applying the dual rotation operator (5.71) to the Faraday 2-form leads to

$$\begin{aligned} e^{\star_4\,\alpha}F &= \cos\alpha\, F + \sin\alpha\, \star_4 F \\ &= \cos\alpha\,(E_x dx\wedge dt + .. + B_x dy\wedge dz + ..) \\ &+ \sin\alpha\, \star_4 (E_x dx\wedge dt + .. + B_x dy\wedge dz + ..) \\ &= (E_x\cos\alpha - B_x\sin\alpha)\, dx\wedge dt + .. \\ &+ (E_x\sin\alpha + B_x\cos\alpha)\, dy\wedge dz + .. \end{aligned} \tag{5.74}$$

A comparison with (5.66) shows that the Hodge operator acts as a dual rotation between electric 2-forms and magnetic 2-forms. In the section 5.4, we will explore how the Hodge dual applies on the EM field in the presence of non trivial vacuua.

5.3.4 Separating the wheat from the chaff: premetric electrodynamics

Back to axiomatics The foundations of classical electrodynamics look different when using differential forms. Only two axioms, the locality of electric charge (5.52) and the absence of magnetic charge (5.57), are needed to recover Maxwell's equations. Charge conservation is simply an outcome of the first axiom. The status of D and B is not the same as in Lorentz-Rosenfeld approach: they do not come from averaging processes but they are microscopic fields instead, coming from 1) a charge counting procedure, 2) a way to delimit an arbitrary 3-volume V by a boundary ∂V and 3) a way to know what is inside and what is outside.

That latter point is in accordance with an old but subtle criticism made by Kottler [410] and Van Dantzig [411]: the "contamination" of all known theories of the electromagnetic interaction by gravity. Indeed, as soon as the dual constitutive relations are involved, the use of Hodge star operator implies a metric, that is an object shaped by the gravitational interaction (a detailed account on the historical developments of these ideas can be found in [412]). As explained by Whittaker [413] «*the notion of metric is a very complicated one: it requires measurements with clocks and scales, generally with rigid bodies, which are themselves things of extreme complexity. Hence it seems undesirable to take the notion of a metric as a fundament, also of phenomena which are much simpler and independent of it. I might state as a principle, or rather as a program: to formulate the fundamental laws of physics in a form independent of metrical geometry* ».

As connections with gravity are discussed, we will now work in 4 dimensions. This constrains the form of possible topological electromagnetic equations as, for instance, any 4-form always has a vanishing exterior derivative. Considering three non-compact dimensions of space is crucial here and several justifications have been given, including arguments borrowed from the stability of planetary orbits (the first classical treatment [414] was made by Ehrenfest in 1920[1] and the relativistic one is due to Tangherlini [415]), thermodynamics [416] and knot theory [417]. What can be taken for granted are Maxwell's equations (5.68) and (5.70), with no dual relation connecting between the Faraday tensor (5.67) and the Maxwell tensor (5.69).

[1]The problem was also discussed in Immanuel Kant's 1747 paper *Thoughts on the True Estimation of Living Forces*. The German philosopher somehow foreshadowed Ehrenfest's paper as he related the three dimensions of space to Coulomb's inverse-square law: « *Substances in our universe interact with each other so that the acting force is inversely proportional to the square of the distance... If the number of dimensions were different, the forces of attraction would have different properties and dimensions* ».

Topological constitutive relation Let us make a quick count: topological equations rely on 2 fundamental fields F and G, so there are 12 independent unknowns but only 8 independent equations. This means that premetric equations are an underdetermined system. As F and G are of the same degree, the simplest guess is to assume a linear and local relation between strengths and excitations in order to close this system. The third axiom of premetric electrodynamics hence writes

$$G_{\mu\nu} = \frac{1}{4}\varepsilon_{\mu\nu\alpha\beta}\,\chi^{\alpha\beta\delta\gamma}F_{\delta\gamma} \tag{5.75}$$

where $\varepsilon_{\mu\nu\alpha\beta}$ is the Levi-Civita symbol (5.32) and $\chi^{\alpha\beta\delta\gamma}$ is the constitutive tensor density (36 independent components). Following [418], this latter can be decomposed into its three irreducible pieces:

$$\chi^{\alpha\beta\delta\gamma} = {}^{(a)}\chi^{\alpha\beta\delta\gamma} + {}^{(s)}\chi^{\alpha\beta\delta\gamma} + {}^{(p)}\chi^{\alpha\beta\delta\gamma} \tag{5.76}$$

where

- The first term is defined as
$$ {}^{(a)}\chi^{\alpha\beta\delta\gamma} = \chi^{[\alpha\beta\delta\gamma]} \tag{5.77}$$
It has only one component and corresponds to an axion field (a possible candidate for cold dark matter).

- The second term is defined as
$$ {}^{(s)}\chi^{\alpha\beta\delta\gamma} = \frac{1}{2}\left(\chi^{\delta\gamma\alpha\beta} - \chi^{\alpha\beta\delta\gamma}\right) \tag{5.78}$$
It has fifteen independent components and corresponds to a skewon field (assumed to be involved in hypothetical vacuum polarization effects).

- The third term is the principal (or metric-dilaton) part and it writes as
$$ {}^{(p)}\chi^{\alpha\beta\delta\gamma} = \chi^{\alpha\beta\delta\gamma} - {}^{(a)}\chi^{\alpha\beta\delta\gamma} - {}^{(s)}\chi^{\alpha\beta\delta\gamma} \tag{5.79}$$
It has twenty independent components.

In the eikonal aproximation, the propagation of a wave in a spacetime with the closure relation (5.75) obeys the generalized Fresnel equation [419]:

$$\mathcal{G}^{\alpha\beta\delta\gamma}k_\alpha k_\beta k_\delta k_\gamma = 0 \tag{5.80}$$

where k^α is the 4-wavevector and $\mathcal{G}$ is the Tamm-Rubilar tensor density:

$$\mathcal{G}^{\alpha\beta\delta\gamma} = \frac{1}{4!}\varepsilon_{\eta\lambda\nu\theta}\varepsilon_{\tau\omega\sigma\xi}\,\chi^{\eta\lambda\tau(\alpha}\,\chi^{\beta|\omega\nu|\delta}\,\chi^{\gamma)\theta\sigma\xi} = \mathcal{G}^{\alpha\beta\delta\gamma}\left({}^{(s)}\chi + {}^{(p)}\chi\right) \tag{5.81}$$

In the geometrical optics limit, the axion part does not influence the propagation of light. Developping (5.80) leads to the quartic dispersion relation in vacuum

$$0 = M_0\omega^4 + M_1\omega^3 + M_2\omega^2 + M_3\omega + M_4 = M_0\left(\omega^2 + a\omega + b\right)\left(\omega^2 + c\omega + d\right) \tag{5.82}$$

where $M_0 = \mathcal{G}^{0000}$, $M_1 = 4\mathcal{G}^{000i}k_i$, $M_2 = 6\mathcal{G}^{00ij}k_ik_j$, $M_3 = 4\mathcal{G}^{0ijm}k_ik_jk_m$ and $M_4 = \mathcal{G}^{ijmn}k_ik_jk_mk_n$.

Emergence of a flat metric structure In agreement with experimental data [420], a reasonable requirement is that there is no vacuum birefringence (no skewon contribution): this implies that the vacuum light-cone condition is unique. Two additional constraints are the time-reversal symmetry of the light-cone [2] and the real-valuedness of the solution. Following [421], uniqueness is fulfilled provided that $a = c = M_1/2M_0$ and $b = d = (4M_0M_2 - M_1^2)/8M_0^2$. An important simplification stems from the time-reversal symmetry, which means that $M_1 = M_3 = 0$: hence, $a = c = 0$ and $b = d = M_2/2M_0$. The real-valuedness then implies that $4M_0M_2 \leq 0$, which means that $b = d < 0$. Plugging all these conditions into (5.82) gives that

$$0 = \omega^2 + a\omega + b = \omega^2 + \frac{3\mathcal{G}^{00ij}}{\mathcal{G}^{0000}} k_i k_j \tag{5.83}$$

where the second term is negative, ought to the real-valuedness constraint. It must be emphasized that the derivation of this dispersion relation is totally metric-free.

Now, grouping terms as done in (2.31), it turns out that (5.83) can be rewritten as

$$0 = \tilde{\eta}^{\alpha\beta} k^\alpha k^\beta \tag{5.84}$$

with $\tilde{\eta}^{00} = 1$ and $\tilde{\eta}^{ij} = 3\mathcal{G}^{00ij}/\mathcal{G}^{0000}$. The absence of vacuum birefringence combined to the topological Maxwell's equations naturally gives rise to an emerging background metric. Bearing in mind the discussions of Chapter 2, one may wonder if this is a physical spacetime or an effective/analogue geometry. Obukhov and Hehl clearly make the call in favour of the first possibility: «*the light cone (and the spacetime metric) is an electromagnetic construct* »[14]. This can only make sense if $\tilde{\eta}$ is the Minkowski's flat spacetime metric η. Two points advocate for such conclusion:

1. As expected, the signature of of the emerging metric structure is Lorentzian and $\tilde{\eta}^{00} = 1 = \eta^{00}$.
2. Going backwards and plugging the emerging metric $\tilde{\eta}$ into the constitutive tensor density (5.75), all this construction is compatible with the 4-dimensional definition of Hodge star operator (see section 5 in [422]).

One last question: how do spacetime distortions - degrees of freedom associated to gravity - fit in the picture? Maybe the most natural answer lies in the tetrad field (2.1) and in teleparallelism [423]: it is formally equivalent to general relativity (for a detailed discussion, see [424]), the role played by curvature being replaced by torsion. For $g_{\mu\nu} = \eta_{\alpha\beta}\, e_\mu{}^\alpha e_\nu{}^\beta$, the metric tensor g is then understood as the product two contributions: one, the tetrad part $\eta_{\alpha\beta}$, is ruled by the gravitational interaction, and the other one, the flat metric $\eta_{\alpha\beta}$, emerges from electromagnetic interaction.

5.4 Vacuum as a polarizable medium

5.4.1 Classical vacuum: electrostatics in a uniform gravitational field

As it is well known, Newton's law of gravitation as given by the potential $\Phi(\boldsymbol{r})$, may be obtained from any metric theory of gravitation which, in the weak field limit, turns into

$$ds^2 = -\,(1 + 2\Phi)\, dt^2 + d\ell^2, \tag{5.85}$$

[2] The future part of the light-cone has the same angle as the past part of the light-cone.

where $d\ell$ represents the space part of the metric.

Whittaker [425] took the limit of Schwarzschild's metric,

$$ds^2 = -\left(1 - \frac{2M}{r}\right) dt^2 + \frac{1}{1 - \frac{2M}{r}} dr^2 + r^2 \left(d\theta^2 + \sin^2\theta d\varphi^2\right), \tag{5.86}$$

at a large distance from the gravitating centre such that the Newtonian potential $-gz$ appears in the time part of the metric. The result is

$$ds^2 = -\left(1 + 2gz\right) dt^2 + \left(dx^2 + dy^2 + \frac{dz^2}{1 + 2gz}\right), \tag{5.87}$$

which thus corresponds to an attractive uniform Newtonian gravitational field parallel to the z-axis.

Considering an electric field weak enough such that its contribution to the gravitational field of this spacetime is negligible, Whittaker derived Laplace's equation for the scalar electrostatic potential in the absence of sources:

$$\frac{\partial^2 V}{\partial x^2} + \frac{\partial^2 V}{\partial y^2} + (1 + 2gz) \frac{\partial^2 V}{\partial z^2} = 0. \tag{5.88}$$

Now, one considers a uniformly charged infinite x-y plane. Denoting by σ the uniform areal charge density, the corresponding volume charge density 3-form is $\rho = \sigma\delta(z)\, dx \wedge dy \wedge dz$. It can be easily seen that the displacement field 2-form

$$D = \frac{1}{2}[\Theta(z) - \Theta(-z)]\sigma\, dx \wedge dy \tag{5.89}$$

obeys the Maxwell-Gauss law $dD = \rho$ and the expected planar symmetry $D(-z) = -D(z)$. Here $\Theta(z)$ is the Heaviside step function.

Now, the 2-form D is related to E via $D = \varepsilon_0 \star_4 (E \wedge dt)$ and symmetry tells us that the electric field 1-form writes $E = \tilde{E}\, dz$. We use (5.30) to compute $\star_4(dz \wedge dt) = dx \wedge dy$. Note that $|\det g_{ab}| = 1$ for the metric (5.87). We then have

$$D = \epsilon_0 \tilde{E} dx \wedge dy \tag{5.90}$$

and finally that

$$E = \frac{1}{2\varepsilon_0}[\Theta(z) - \Theta(-z)]\sigma\, dz. \tag{5.91}$$

On the other hand, Eq. (5.88) becomes $(1 + 2gz)\, \frac{\partial^2 V}{\partial z^2} = 0$, or $\frac{\partial^2 V}{\partial z^2} = 0$, which gives the usual g-independent 0-form potential

$$V(x, y, z) = -\frac{\sigma}{2\epsilon_0}|z|. \tag{5.92}$$

With $E = -dV$ one confirms the electric field 1-form given by Eq. (5.91).

Comparing the expressions (5.89) and (5.91) reveals that $D_{xy} = \varepsilon_0 E_z$, similarly to what happens in flat spacetime: hence, there is no vacuum polarization due to the uniform gravitational field.

5.4.2 Quantum vacuum: wave propagation in a Casimir vacuum

The Casimir effect was first discovered by Hendrik Casimir in 1948 and it corresponds to a macroscopic force due the quantum vacuum fluctuations. That force appears when two parallel plates are separated from one another by a vacuum layer of thickness a and it is generally attractive. Propagation of an electromagnetic field in the so-called Casimir vacuum can be adequately described as experiencing the following geometry: [426]

$$g_{\mu\nu} = \eta_{\mu\nu} - \frac{d_2(z)}{d_1(z)+d_2(z)} n_\mu n_\nu \tag{5.93}$$

where $\eta_{\mu\nu} = (-1,+1,+1,+1)$ is the flat Minkowski metric and $n_\mu = (0,0,0,1)$ is the unit vector orthogonal to the plates. The variable z is the coordinate x^3, which is measured in the direction perpendicular to the plates. Functions $d_1(z)$ and $d_2(z)$ are determined from quantum electrodynamics and a perturbative expansion up to order α^2 gives:[426]

$$d_1(z) = -\frac{1}{16\pi} + O(\alpha^2) \tag{5.94}$$

$$d_2(z) = -\frac{11\pi\alpha^2}{64800\, a^4 m_e^4} \tag{5.95}$$

with m_e the electron mass. In Cartesian coordinates, the Casimir vacuum metric can thus be approximated by

$$g_{\mu\nu} = \begin{bmatrix} -1 & 0 & 0 & 0 \\ 0 & 1 & 0 & 0 \\ 0 & 0 & 1 & 0 \\ 0 & 0 & 0 & 1 - C\alpha^2 \end{bmatrix} \tag{5.96}$$

where $C = 11\pi^2/4050\, a^4 m_e^4$. In the absence of magnetic sources, Eq. (5.69) becomes $D = \star_4 F$. Now, using (5.30) we have for the components of D

$$D_{\rho\sigma} = \frac{1}{2} F^{\mu\nu} \sqrt{|g|}\epsilon_{\mu\nu\rho\sigma} = \frac{1}{2} g^{\mu\alpha} g^{\nu\beta} F_{\alpha\beta} \sqrt{|g|}\epsilon_{\mu\nu\rho\sigma}. \tag{5.97}$$

This leads to

$$D^j = \sqrt{-g}|g^{00}|g^{jj}E_j \tag{5.98}$$

with no summation on the j index. Ought to the symmetries of the problem, only the z-component of the field is relevant and therefore using (5.96) leads to

$$\varepsilon = 1 - \frac{11\pi^2}{8100\, a^4 m_e^4}\alpha^2 + O(\alpha^2) \tag{5.99}$$

Although the second term is probably far too small to be detectable, quantum vacuum behaves in principle as a polarized medium, as is well-known in quantum electrodynamics. As there are no gradient of the dielectric constant, the refractive index of the Casimir vacuum is a constant given by the square root of (5.99). Note that as emphasized in Ref. [426], the dielectric constant being the same along the three axes, no birefringence is expected.

5.5 Concluding remarks

In the wake of Ref. [427], we hold exterior calculus to be a precious pedagogical tool for teaching electrodynamics. Although students are more comfortable with vector analysis, picturing the EM

field as three-dimensional vectors turns out to be misleading in some cases. Conversely, picturing the EM field as differential forms is probably less intuitive at first sight, but it leads to a deeper understanding of EM.

The main concepts of exterior calculus were introduced from undergraduate linear algebra and calculus. Contrary to a widespread misconception, differential forms are not tiny quantities, they are dual vectors. The many formulas used in vector analysis can be concisely written in terms of the wedge product and the exterior derivative. Exterior calculus also helps clarifying the axiomatics of EM. From two postulates on electric charge (Eq. (5.52)) and magnetic charge (Eq. (5.57)) or equivalently (5.58), the whole set of Maxwell's equations can be recovered without relying on the background geometry: in other words, their foundation is purely topological and does not require any metric structure. Metric properties of the manifold appear on the other hand in the constitutive relations. **D** and **E** (resp. **H** and **B**) must indeed be understood as forms of different degrees that carry different information. They are connected by a duality relation that requires the knowledge of the background geometry, as the Hodge star operator is explicitly depending on the metric.

According to Sir W.L. Bragg, «*the important thing about science is not so much to obtain new facts as to discover new ways of thinking about them* »(cited in Ref. [428]). For such a purpose, the relevance of exterior calculus goes far beyond the realm of electrodynamics. As a matter of fact, this formalism is likely to enlighten conceptual issues arising in thermodynamics, fluid mechanics...[384] Forthcoming developments may also involve the Yang-Mills theories: these are generalizations of Maxwell's equations but built from larger symmetry groups ($SU(N)$ instead of $U(1)$) and they require additional ingredients taken from exterior calculus.

6 Conclusion

6.1 Some research perspectives

6.1.1 Extension of electrodynamics for cosmology

Several authors endeavor to generalize Maxwell's theory in order to get of rid of singularities, to relax certain symmetries or to include corrections likely to solve open issues in the standard model (for instance the dark sector). Among the most remarkable attempts, one can mention

- non-linear extensions such: Born-Infeld theory (1934).
- extensions to massive fields: Proca (1936), vector galileon (2014)...
- extensions to higher-order derivatives: Bopp-Podolski theory (1940).
- extensions to non-abelian gauge groups: Yang-Mills theory (1954)
- extensions to fields of higher degrees: Kalb-Ramond theory (1974).
- extensions to supplementary bosons: axions (1978), dark photons (2009)...
- Non-Lorentzian extensions: Maxwell-Carroll-Field-Jackiw (1990).
- ...

In the previous chapter, we discussed the assets of the exterior algebra to formulate a topological theory of electrodynamics. This turns out to be crucial to understand how fundamental interactions are related one another. Eventually, Maxwell's theory mingles the electromagnetic and the gravitational interaction: it is expressed from the metric tensor, which is a dynamical object shaped by Einstein's equations. This statement can be extended to the weak and strong forces, which are also burdened by gravity. Obukhov and Hehl's premetric electrodynamics showed that from the axiomatic point of view, spacetime can be seen as an emergent property of a purely topological

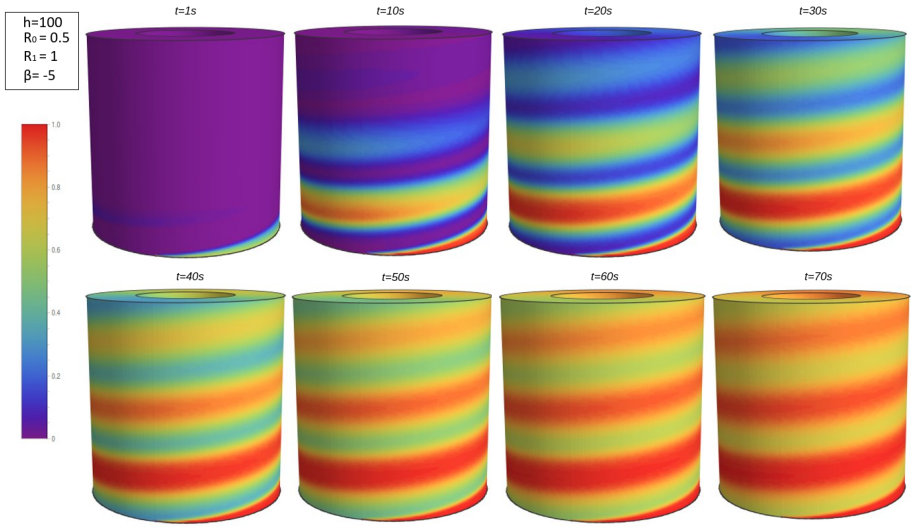

Figure 6.1: Diffusion of a passive scalar in the vicinity of a screw dislocation (upcoming paper).

theory of the electromagnetic field and most of all, that some of the aforementioned extensions (such as axions) naturally arise in such framework.

A first line of action for future researches is to determine possible topological formulations for the extensions listed hereinabove, and afterwards to seek their connections with metric structures. An exploratory work is in progress with Bertrand Berche and Fernando Moraes on formulating Kalb-Ramond electrodynamics from differential forms. The upcoming steps consist in relaxing the geometric constituents in the spirit of Obukhov and Hehl's works and to look for a sufficient set of axioms to build a premetric formulation.

A second line of action is to explore extended electrodynamics theories in the context of non-standard cosmologies, for which the relevance of a correction to Maxwell's theory seems likely. A first step to understand the coupling of these fields to the geometry (curvature and/or torsion) will be to deal with the case of cosmic strings (chiral or not). Then, in the extension of my previous works, the main idea will consist in studying the electromagnetic field in Kleinian universes, in Milne's universes ... and to propose, if possible, analog models allowing to test the results in the laboratory.

6.1.2 Functionalization of materials

The use of geometric properties to design transport in materials will be explored along two main axes. The first of these axes concerns the engineering of defects in condensed matter. Heat transfers in the presence of an integer charge disclination (source of curvature) have shown that nematic liquid crystals are robust candidates for making thermal diodes. The next step will be to study disclinations of non-integer charge and the distributions of such defects. It is an analytically difficult job because of the complexity of the equivalent metric (non-diagonal terms) and numerical processing will be essential. In solids and in smectics, screw dislocations (sources of torsion)

have multiple effects on transport phenomena: at the macroscopic scale, they imprint their helical structure to the wave fronts (angular orbital moment) and on a microscopic scale, they couple with electronic spins. I am currently working with Bertrand Berche and two students (A Manapany and L Moueddene) on the diffusion processes of passive scalars in the vicinity of dislocations. The results obtained seem to indicate that the defect produces a guiding effect on the transport of the scalar field, as depicted on Fig. 6.1. This work will be continued to the case of defects comprising both curvature and torsion (dispiration), and afterwards to distributions of such objects.

A second line of research concerns the functionalization of low dimensional systems. The existence of Stone-Wales type dipoles (pentagonal and heptagonal disclinations) in graphene modifies the local curvature of the sheet, which strongly impacts its physical properties (electrical, mechanical, thermal [283]). From the work carried out on the periodic distributions of disclinations, I would like to develop the control of electronic transport in graphene by optimizing the defect network (shape of unit cells, size parameters...). In the case of nanotubes, the work carried out in collaboration with Fernando Santos (VUmc, Netherlands) is in progress for objects presenting a non-trivial curvature and/or topology (pseudospheres, Gabriel's trumpets, toric knots, etc.) .

6.1.3 Active matter as geometry

A very large number of living systems (cell membranes, cytoskeletons, bacteria colonies, shoal of fish, etc.) present a local orientation order of the same type as that existing in nematics (see Fig 6.2). But unlike usual liquid crystals, these self-organized systems are coupled in a non-trivial way to their environment. They draw from it, on an individual scale, the energy inputs necessary for the accomplishment of elementary functions (homeostasis, locomotion, reproduction. ..): this is called the active matter (for comprehensive introductions, see [429]-[431]).

The orientation singularities corresponding to topological defects obviously exist in the active matter: a distinction is mainly made between $+1/2$ charge defects ("comets") and $-1/2$ charge defects ("trefoils"). In passive liquid crystals, the defect patterns have a marked tendency to relax: either by the combination of a defect with another defect of opposite topological charge, or by migration to the boundaries. Conversely, the Berris-Edwards equations governing the active material show a proliferation of comet-trefoil dipoles correlated with low Reynolds number turbulence.

My research project is to use the tools of differential geometry and the knowledge acquired regarding the effects of defects on fields in order to understand the mechanisms of cancerization. Indeed, the images of malignant breast tumors have shown the existence of a transition of orientation of the collagen fibers [432]: this is the signature of a tumor evolving from a type II cancer (non-invasive) to a type III cancer (invasive). This transition is likely to leave relics in the form of defects. As the distribution of stresses around a comet-type defect greatly favors its mobility in comparison with trefoil-type defects, it should promote the invasion of healthy cells. I wish to develop a detailed modeling of this process from internal collaborations at the laboratory and external collaborations: Erms Pereira from the University of Leeds, who has a solid expertise in solving Beris-Edwards equations and studying defects, Antonio Monari from Université de Paris, who is a biochemist with a renowned expertise in the modeling of cancers... Moreover, the proliferation of these defects should be detected from the signatures they leave on a radiation field and thus allow the early diagnosis of aggressive tumors. This point will constitute my second line of research in the field of active matter. Several external contacts are possible on this topic, including for example Fatmir Asllanaj (CNRS, Nancy) with whom I have already collaborated and who is developing numerical tools for the diagnosis of tumors in the infrared range (photoacoustic imaging, based on light-hemoglobin

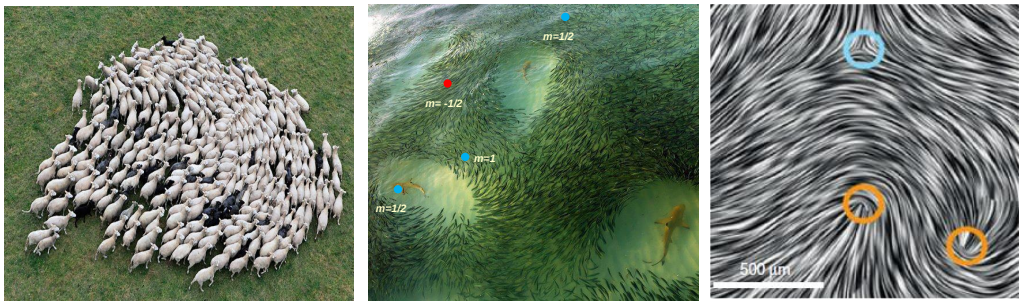

Figure 6.2: Three examples of active matter. *Left*: A self-organized system with nematic order: the flock of sheep. *Middle*: Shoal of fish threatened by sharks and the corresponding topological defects. *Right*: Mouse fibroblast cells and trefoil/comet defects.

interactions).

6.2 Teaching activities, supervisory work and administrative charges

My teaching activities began in the form of casual teaching and a position of teaching fellow during my PhD years at Université de Poitiers. After my postdoctoral fellowship in Canada, I was hired as a teaching fellow at Université de Nantes. The following chart provides a detailed account of my teaching duties:

School	**Description**	**Level**	**Annual hourly volume per group (eq. tut. class.)**
ISAE-ENSMA	Quantum and statistical physics (tutorial classes)	L3	21h15
ISAE-ENSMA	Radiative transfer (tutorial classes)	M2	8h45
ISAE-ENSMA	Heat transfer (practicum)	M2	35h
Polytech'Nantes	Mechanics of deformable solids (practicum)	L3	24h
Polytech'Nantes	Complex analysis (tutorial classes)	M1	10.5h
Polytech'Nantes	Heat transfer (practicum)	M1	28h

I was then recruited at the Université de Lorraine as an associate professor (section 30 - Optics) in

2006. As part of my current functions, I work in three structures: 1) Polytech'Nancy (engineering school) which is my main component of affiliation 2) Mines Nancy (engineering school) and 3) the Faculty of Science and Technology. The details of my activities in each of these components are shown in the table below:

School	**Description**	**Level**	**Annual hourly volume per group (eq. tut. class.)**
Polytech'Nancy	General physics (practicum)	L1	52h
Polytech'Nancy	Electromagnetism (tutorial classes)	L2	14h
Polytech'Nancy	Electromagnetic waves and geometrical optics (lectures/tutorial classes/practicum)	L2	16h/16h/12h
Polytech'Nancy	Wave optics and lasers (tutorial classes)	L3	16h
Polytech'Nancy	Quantum mechanics (tutorial classes)	L3	12h
Ecole des Mines	Quantum physics (tutorial classes)	L3	22h
Ecole des Mines	Statistical physics (tutorial classes)	L3	22h
FST Nancy	Topology and condensed matter physics (lectures)	M2	6h

I am responsible for the course unit *Electromagnetic waves and geometrical optics* at Polytech'Nancy and in this context, I take on various teaching functions (design of original test papers, facilitation of the web page of the courses, PeiP passing juries, internship defenses, supervision of students during company visits, renovation of practicum...). I am also involved at various levels in the life of the Polytech network (jury for admission based on application file followed by an interview, correction of copies of the GEIPI-Polytech competitive exam, participation to open house days ...) and I chaired for several years french baccalaureate juries.

The experience acquired during these fifteen years of teaching electrodynamics led me to deepen the axiomatic and didactic aspects (first article published on the subject in 2020 in the American Journal of Physics [363]). The use of the external calculus due to Cartan and Grassmann makes it possible to reformulate Maxwell's equations in a more coherent, more compact and richer form than the usual formulation proposed by Gibbs and Heaviside: 1) it clarifies the physical content of the constitutive relations , 2) it offers a unifying framework for vector analysis (for example, gradient, rotational and divergence correspond to a single operator, the outer derivative) and 3) it reveals the topological structures of the electromagnetic field (premetric electrodynamics). This activity was the subject of two seminars at the Jean Lamour Institute (2019). I am currently writing a book covering electrodynamics and optics (fundamental aspects, technological applications, corrected exercises).

I supervised two PhD students (Valentin Jean, 2011-2014, joint supervision with D Lacroix; Frankbelson Azevedo, 2015-2018, joint supervision with B Berche) and seven M2 students. From an administrative point of view, I was part of the selection committee for the recruitment of associate

professors (section 30 - Optics) and nowadays, I have been elected to the National Committee of the CNRS (section 13) and I belong to the editorial board of Lorraine University Editions (EDUL). I regularly review for several journals (American Journal of physics, Physical Review, Scientific Report ...) and I am currently a member of 2 PhD monitoring committees (Claude Dimo, Valentin Anfray).

Bibliography

[1] JC Maxwell. On physical Lines of force. Philosophical Magazine 10(1) pp 27-83 (1856).

[2] O Darrigol. The quantum electrodynamocs analogy in early nuclear theory or the roots of Yukawa's theory. Revue d'histoire des sciences 41 (3-4), pp. 225-297 (1988).

[3] See pp. 559-574 in Enrico Fermi Collected Papers. Accademia Nazionale dei Lincei and the University of Chicago Press, Vol 1: Italia 1921-1938, (1962).

[4] R Oppenheimer. Analogy in science. American Psychologist, 11(3), pp. 127–135 (1956).

[5] Y Nambu and G Jona-Lasinio. Dynamical Model of Elementary Particles Based on an Analogy with Superconductivity I. Phys. Rev. 122(1), pp. 345-358 (1961). Y Nambu and G Jona-Lasinio. Dynamical Model of Elementary Particles Based on an Analogy with Superconductivity II. Phys. Rev. 124(1), pp. 246-254 (1961).

[6] KG Wilson. The Renormalization Group and Strong Interactions. Phys. Rev. D 3 1818 (1971).

[7] PG De Gennes. An analogy between superconductors and smectics A. Solid State Communications 10(9), pp. 753-756 (1972).

[8] E Elizalde. Bernhard Riemann, a(rche)typical mathematical-physicist ? Front. Phys. (2013).

[9] WK Clifford. On the space-theory of matter. Proceedings of the Cambridge Philosophical Society, 2 pp. 157-158 (1870).

[10] In 1895, HA Rowland stated that «electricity no longer exists, for the name electricity as used to the present time signifies at once that a sustance is meant, and there is nothing more certain than that electricity is not a substance.»Quoted in KK Darrow. Physics Today 9 (8), P 24 (1956).

[11] H Weyl. Ann. Phys. (Lpz.) 59, 101 (1919).

[12] J.A. Wheeler. *Geometrodynamics*, Academic Press New-York (1962).

[13] CW Misner and JA Wheeler. Classical physics as geometry: Gravitation, electromagnetism, unquantized charge and mass as properties of curved empty spacetime. Annals of Physics 2(6), pp. 525-603 (1957).

[14] FW Hehl, YN Obukhov. To Consider the Electromagnetic Field as Fundamental, and the Metric Only as a Subsidiary Field. Foundations of Physics 35 (12) (2005).

[15] G Unger and NJ Popławski. Big Bounce and Closed Universe from Spin and Torsion. The Astrophysical Journal, 870 (78) (2019).

[16] V Fock and D Iwanenko D. Géometrie quantique linéaire et déplacement parallèle. Compt. Rend. Acad Sci. Paris 188, 1470 (1929).

[17] A Trautman A. Spin and torsion may avert gravitational singularities-dominated inflation, Nature Phys. Sci. 242 7 (1973).

[18] SD Brechet, MP Hobson and AN Lasenby. Classical big-bounce cosmology: dynamical analysis of a homogeneous and irrotational Weyssenhoff fluid, Class. Quantum Grav. 25, 245016 (2008).

[19] TWB Kibble. Lorentz invariance and the gravitational field. J. Math. Phys. 2, 212 (1961).

[20] DW Sciama. The Physical Structure of General Relativity. Rev. Mod. Phys. 36, pp. 463–469 (1964).

[21] FW Hehl, P von der Heyde, D Kerlick and J Nester. General relativity with spin and torsion: Foundations and prospects. Rev. Mod. Phys. 48, 393 (1976).

[22] T Clifton, PG Ferreira, A Padilla and C Skordis. Modified gravity and cosmology. Physics Reports, 513 (1–3), pp. 1-189 (2012).

[23] FW Hehl. Gauge Theory of Gravity and Spacetime, in *Einstein Studies*. Birkhäuser, Boston, MA (2015).

[24] M Blagojevic and FW Hehl. Gauge Theories of Gravitation, a reader with commentaries. Imperial College Press, London (2013).

[25] RT Hammond. Torsion gravity. Rep. Prog. Phys. 65, pp. 599-649 (2002).

[26] M Mathisson. Neue Mechanik materieller Systeme. Acta Physica Polonica. 6. pp. 163–209 (1937).

[27] A Papapetrou. Spinning Test-Particles in General Relativity. I. Proc. R. Soc. Lond. A. 209 (1097), pp. 248–258 (1951).

[28] PB Yasskin and WR Stoeger. Propagation equations for test bodies with spin and rotation in theories of gravity with torsion. Phys. Rev. D 21 pp. 2081–2094 (1980).

[29] Y Ne'eman and FW Hehl. Test matter in a spacetime with nonmetricity. Class. Quant. Grav. 14 A251–A260 (1997).

[30] D Puetzfeld and YN Obukhov. Propagation equations for deformable test bodies with microstructure in extended theories of gravity. Phys. Rev. D 76 084025 (2007).

[31] G Bertone and D Hooper. History of dark matter. Rev. Mod. Phys. 90, 045002 (2018).

[32] AV Minkevich. Accelerating Universe with spacetime torsion but without dark matter and dark energy. Physics Letters B, 678(5), pp. 423-426 (2009).

[33] A Tilquin and T Schücker. Torsion, an alternative to dark matter? General Relativity and Gravitation, 43(11), 2965 (2011).

[34] NJ Popławski. Matter-antimatter asymmetry and dark matter from torsion. Physical Review D, 83(8), 084033 (2011).

[35] AS Belyaev, MC Thomas and IL Shapiro. Torsion as a dark matter candidate from the Higgs portal. Phys. Rev. D 95, 095033 (2017).

[36] PJE Peebles and B Ratra. The cosmological constant and dark energy. Rev. Mod. Phys. 75, 559 (2007).

[37] V de Sabbata and C Sivaram. Torsion and the cosmological constant problem. Astrophysics and Space Science 165 (1), pp. 51-55 (1990).

[38] SL Cacciatori, MM Caldarelli, A Giacomini, D Klemm and DS Mansi. Chern-Simons formulation of three-dimensional gravity with torsion and nonmetricity. J. Geom. Phys. 56 2523 (2006).

[39] NJ Popławski. Cosmological constant from quarks and torsion. Ann. Phys. (Berlin) 523, 291 (2011).

[40] NJ Popławski. Cosmological consequences of gravity with spin and torsion. Astr. Rev. 8(3), pp. 108-115 (2013).

[41] AN Ivanov and M. Wellenzohn. Einstein-Cartan Gravity with Torsion Field Serving as an Origin for the Cosmological Constant or Dark Energy Density. The Astrophysical Journal 829 (47), pp. 1-9 (2016).

[42] S Weinberg. The cosmological constant problem. Review of Modern Physics 61 pp. 1-23 (1989).

[43] J Weyssenhoff and A Raabe. Relativistic dynamics of spin-fluids and spin-particles Acta Phys. Pol. 9 7 (1947).

[44] M. Gasperini. Spin-dominated inflation in the Einstein-Cartan theory. Phys. Rev. Lett. 56, 2873 (1986).

[45] MO Ribas, and GM Kremer. Fermion fields in Einstein-Cartan theory and the accelerated-decelerated transition in a primordial universe. Gravitation and Cosmology, 16(2), pp. 173-177 (2010).

[46] NJ Popławski. Cosmology with Torsion: An Alternative to Cosmic Inflation. Phys Lett B 694(3), pp. 181-185 (2010).

[47] J Magueijo, TG Zlosnik and TWB Kibble. Cosmology with a spin. Phys Rev D, 87(6), 063504 (2013).

[48] S Akhshabi, E Qorani and F Khajenabi. Inflation by spin and torsion in the Poincaré gauge theory of gravity. EPL 119 29002 (2017).

[49] D Kranas, CG Tsagas, JD Barrow and D Iosifidis. Friedmann-like universes with torsion. The European Physical Journal C, 79(4), 1-12.(2019).

[50] GD Kerlick. "Bouncing" of simple cosmological models with torsion. Annals of Physics 99(1), pp. 127-141 (1976).

[51] NJ Popławski. Nonsingular, Big-bounce cosmology from spinor-torsion coupling. Phys Rev D 85(10) 107502 (2012).

[52] Q Huang, P Wu and H Yu. Emergent scenario in the Einstein-Cartan theory. Phys Rev D, 91(10), 103502 (2015).

[53] S Lucat and T Prokopec. Cosmological singularities and bounce in Cartan-Einstein theory. Journal of Cosmology and Astroparticle Physics 2017 (2017).

[54] B Vakili and S Jalalzadeh. Signature transition in Einstein–Cartan cosmology. Physics Letters B, 726(1-3), pp. 28-32 (2013).

[55] D Battefeld and P Peter. A critical review of classical bouncing cosmologies. Physics Reports, 571, pp. 1-66 (2015).

[56] R Brandenberger and P Peter. Bouncing cosmologies: progress and problems. Foundations of Physics, 47(6), pp. 797-850 (2017).

[57] J Ipser and P Sikivie. Gravitationally repulsive domain wall. Phys. Rev. D 30, pp. 712-719 (1984).

[58] P Jones, G Muñoz, M Ragsdale and D Singleton. The general relativistic infinite plane. Am. J. Phys. 76(1), pp. 73-78 (2008).

[59] J Spinelly, U De Freitas and EB de Mello. Gravitating magnetic monopole in the global monopole spacetime. Physical Review D, 66(2), 024018 (2002).

[60] P Langacker and S-Y Pi. Magnetic Monopoles in Grand Unified Theories. Phys. Rev. Lett. 45, 1 (1980).

[61] R Holman, TWB Kibble, Soo-Jong Rey. How Efficient Is The Langacker-Pi Mechanism of Monopole Annihilation ? Phys.Rev.Lett. 69, pp. 241-244 (1992).

[62] R Jeannerot, J Rocher and M Sakellariadou. How generic is cosmic string formation in supersymmetric grand unified theories. Phys Rev D 68, 103514 (2003).

[63] B Carter, P Peter and A Gangui. Avoidance of collapse by circular current-carrying cosmic string loops. Phys. Rev. D 55, 4647 (1997).

[64] P Peter. Structure of cosmic strings: a survey. New Astronomy Reviews 45, pp. 277–281 (2001).

[65] P Auclair, P Peter, C Ringeval D Steer. Irreducible cosmic production of relic vortons. Journal of Cosmology and Astroparticle Physics, 2021(03), 098 (2021).

[66] VB Bezerra. Gravitational analogue of the Aharonov-Bohm effect in four and three dimensions. Phys. Rev. D 35, 2031 (1987).

[67] PA Ade et al. Planck 2013 results. XXV. Searches for cosmic strings and other topological defects. Astronomy & Astrophysics, 571, A25 (2014).

[68] W Buchmuller, V Domcke and K Schmitz. From NANOGrav to LIGO with metastable cosmic strings. Physics Letters B, 135914 (2020). See also S Blasi, V Brdar and K Schmitz. Has NANOGrav found first evidence for cosmic strings? ArXiv preprint arXiv:2009.06607 (2020). J Ellis and M Lewicki. Cosmic string interpretation of NANOGrav pulsar timing data. arXiv preprint arXiv:2009.06555 (2020).

[69] A Vilenkin and EPS Shellard. *Cosmic strings and other topological defects*. Cambridge University Press (1994).

[70] MB Hindmarsh and TWB Kibble. Cosmic strings. Rep Prog Phys 58, pp. 477-562 (1995).

[71] JAG Vickers. Generalised cosmic strings. Class. Quantum Grav. 4 pp. 1-9 (1987).

[72] R Geroch and J Traschen. Strings and other distributional sources in general relativity. Phys Rev D 36, 1017 (1987).

[73] RA Puntigam and HH Soleng. Volterra distortions, spinning strings, and cosmic defects. Classical and Quantum Gravity, 14(5), 1129 (1997).

[74] DV Gal'tsov and PS Letelier. Spinning strings and cosmic dislocations. Phys. Rev. D 47, 4273 (1993).

[75] KP Tod. Conical singularities and torsion. Class. Quantum Grav. 11, 1331 (1994).

[76] M. Hindmarsh, A. Wray. Gravitational effects on line sources and the zero-width limit, Phys. Lett. B **251**(4) (1990).

[77] WA Hiscock. Exact gravitational field of a string. Phys. Rev. D 31, 3288 (1985).

[78] JR Gott. Gravitational lensing effects of vacuum strings-Exact solutions. Astrophys. J. 288, 422 (1985).

[79] B Allen and AC Ottewill. Effects of curvature couplings for quantum fields on cosmic-string space-times. Phys. Rev. D 42(8), pp. 2669-2677 (1990).

[80] BA Bilby, R Bullough and E Smith. Proc. Roy. Soc. London, A231 263 (1955)

[81] E Kröner. Kontinums Theories der Versetzungen und Eigenspanungen. Springer–Verlag, Berlin – Heidelberg (1958).

[82] M Kleman and J Friedel. Disclinations, dislocations, and continuous defects: A reappraisal, Rev. Mod. Phys. 80, 61 (2008).

[83] M Kleman. The general theory of dislocations. In FRN Nabarro, *Dislocations In Solids* 5, pp. 243–297, Amsterdam North-Holland Publishing Company (1980).

[84] IE Dzyaloshinskii. Gauge Theories and Densities of Topological Singularities (North-Holland, Amsterdam, The Netherlands), chapter 4, in *Physics of Defects*, Les Houches Session XXXV, edited by R Balian, M Kleman and JP Poirier (1981).

[85] E Kröner. Continuum theory of defects. In R. Balian et al., editor, Les Houches, Session XXXV (1980) – *Physics of Defects*, pages 282–315. North-Holland Publishing Company (1981).

[86] A Kadic and DGB Edelen. A gauge theory of dislocations and disclinations. Springer–Verlag, Berlin – Heidelberg (1983).

[87] IA Kunin and BI Kunin. Gauge theories in mechanics. In *Trends in Application of Pure Mathematics to Mechanics*. Lecture Notes in Physics 249 pp. 246–249, Berlin-Heidelberg, Springer-Verlag (1986).

[88] MC Valsakumar and D Sahoo. Gauge theory of defects in the elastic continuum. Bulletin of Materials Science, 10(1-2), pp. 3-44 (1988).

[89] M Lazar and C Anastassiadis. The gauge theory of dislocations: static solutions of screw and edge dislocations. Philosophical Magazine, 89(3), pp. 199-231 (2009).

[90] M Lazar and FW Hehl. Cartan's Spiral Staircase in Physics and, in Particular, in the Gauge Theory of Dislocations. Found Phys 40, pp. 1298–1325 (2010).

[91] DG Edelen and DC Lagoudas. Gauge theory and defects in solids. Elsevier (2012).

[92] MO Katanaev and IV Volovich. Theory of defects in solids and three-dimensional gravity. Annals of Physics, 216(1), pp. 1-28 (1992).

[93] MO Katanaev and IV Volovich. Scattering on dislocations and cosmic strings in the geometric theory of defects. Annals of Physics, 271(2), pp. 203-232 (1999).

[94] MO Katanaev. Geometric theory https://www.overleaf.com/project/5f647d4c5478a80001fb2d7bof defects. Physics-Uspekhi, 48(7), 675 (2005).

[95] L Landau et E Lifchitz. *Theory of elasticity*, Pergamon Press (1989).

[96] M Baggioli, I Kriuchevskyi, TW Sirk and A Zaccone. Plasticity in Amorphous Solids Is Mediated by Topological Defects in the Displacement Field. Phys. Rev. Lett. 127, 015501 (2021).

[97] F Vogel. Dislocations in low-angle boundaries in germanium. Acta Metallurgica 3, pp. 245-248 (1955).

[98] S Ellis. Dislocations in germanium. J. Appl. Phys. 26 pp. 1140-1146 (1955).

[99] R DeWit. Theory of Disclinations: IV. Straight Disclinations. Journal of research of the Notional Bureau of Standards-A. Physics and Chemistry 77A (5) (1973).

[100] M Charlotte, L Truskinovsky. Lattice dynamics from a continuum viewpoint. Journal of the Mechanics and Physics of Solids 60(8), pp. 1508-1544 (2012).

[101] C Davini. A proposal for a continuum theory of defective crystals. Archive for Rational Mechanics and Analysis 96(4), pp. 295-317 (1986).

[102] CW Oseen. The theory of liquid crystals. Trans. Faraday Soc. 29, 883 (1933).

[103] H Zöcher. The effect of a magnetic field on the nematic state. Trans. Faraday Soc. 29, 945 (1933).

[104] FC Frank. I. Liquid crystals. On the theory of liquid crystals. Discuss. Faraday Soc. 25, 19 (1958).

[105] R De Wit. A view of the relation between the continuum theory of lattice defects and non-Euclidean geometry in the linear approximation. International Journal of Engineering Science, 19(12), pp. 1475-1506 (1981).

[106] W Cai, A Arsenlis, CR Weinberger and VV Bulatov. A non-singular continuum theory of dislocations. Journal of the Mechanics and Physics of Solids, 54(3), pp. 561-587 (2006).

[107] S Zhou, SV Shiyanovskii, H-S Park and OD Lavrentovich. Fine structure of the topological defect cores studied for disclinations in lyotropic chromonic liquid crystals. Nature Comm. 8, 14974 (2017).

[108] W Gordon Zur Lichtfortpflanzung nach der Relativitätstheorie, Ann. Phys. Leipzig **72**, pp. 421-456 (1923).

[109] J Reignier. De l'éther de Fresnel à la relativité restreinte, Annales Fondation Louis de Broglie **29**, pp. 21-56 (2004). Disponible à l'url: `http://aflb.ensmp.fr/AFLB-291/aflb291p021.pdf`.

[110] L Landau et E Lifchitz. *The classical theory of fields*, Pergamon Press (1989).

[111] QM Pham, Sur les équations de l'électromagnétisme dans la matière. C. R. Hebd. Seanc. Acad. Sci., 242, pp. 465–467 (1956).

[112] J Plebanski. Electromagnetic waves in gravitational fields, Phys. Rev. **118**, 1396-1408 (1960).

[113] F De Felice. On the gravitational field acting as an optical medium. Gen. Relativ. Gravit., 2, pp. 347–357 (1971).

[114] VA De Lorenci and R Klippert. Analogue gravity from electrodynamics in nonlinear media. Phys. Rev. D, 65, 064027, pp. 1–6 (2002).

[115] SM Carroll. *Spacetime and geometry*, 1^{st} edition, Addison-Wesley (2004).

[116] C Misner, KS Thorne, JA Wheeler. *Gravitation*, Freeman (1973), p. 1108.

[117] M Born and E Wolf. *Principles of optics*, 7th edition, Cambridge University Press (1999).

[118] J Evans, KK Nandi and A Islam. The optical-mechanical analogy in general relativity: new methods for the paths of light and of the planets, Am. J. Phys. **64**, 1404-1415 (1996).

[119] PM Alsing. The optical-mechanical analogy for stationary metrics in general relativity, Am. J. Phys. **66**, 779-790 (1998).

[120] M Horz and P Haupt. On the principle of Fermat in elastodynamics. Continuum Mechanics and Thermodynamics, 7(2), pp. 219-230 (1995).

[121] IY Tamm. J. Russ. Phys.-Chem. Soc. 56, pp. 3-4, 1 (1925).

[122] C Satiro and F Moraes. Lensing effects in a nematic liquid crystal with topological defects. The European Physical Journal E, 20(2), pp. 173-178 (2006).

[123] C Satiro and F Moraes. On the deflection of light by topological defects in nematic liquid crystals. The European Physical Journal E, 25(4), pp. 425-429 (2008).

[124] E Brasselet. Singular Optics of Liquid Crystal Defects. In *Liquid Crystals: New Perspectives*, P Pieranki and MH Godinho, Wiley, p. 1-70 (2021).

[125] M Novello, VA De Lorenci, JM Salim and R Klippert. Geometrical aspects of light propagation in nonlinear electrodynamics. Phys. Rev. D, 61(4), 045001 (2000).

[126] U Leonhardt and TG Philbin. Transformation optics and the geometry of light. Progress in Optics, 53, pp. 69-152 (2009).

[127] VG Veselago. Sov. Phys. Usp. 10, pp. 509–18 (1968).

[128] JB Pendry. Negative refraction makes a perfect lens. Phys. Rev. Lett. 85 pp. 3966–9 (2000)

[129] RA Shelby, DR Smith, and S Schultz. Experimental verification of a negative index of refraction. science, 292(5514), pp. 77-79 (2001).

[130] U Leonhardt and TG Philbin. General relativity in electrical engineering. New Journal of Physics 8 247 (2006).

[131] S Dehdashti, H Wang, Y Jiang, Z Xu and H Chen. Review of black hole realization in laboratory base on transformation optics. Progress In Electromagnetics Research, 154, pp. 181-193 (2015).

[132] M McCall et al. Roadmap on transformation optics. Journal of Optics, Volume 20, Number 6 (2018).

[133] M Kadic, T Bückmann, R Schittny and M Wegener. Metamaterials beyond electromagnetism. Reports on Progress in physics, 76(12), 126501 (2013).

[134] M Wegener. Metamaterials beyond optics. Science, 342(6161), pp. 939-940 (2013).

[135] MH Lu, L Feng and YF Chen. Phononic crystals and acoustic metamaterials. Materials today, 12(12), pp. 34-42 (2009).

[136] G Ma and P Sheng. Acoustic metamaterials: From local resonances to broad horizons. Science advances, 2(2), e1501595 (2016).

[137] SA Cummer, J Christensen and A Alù. Controlling sound with acoustic metamaterials. Nature Reviews Materials, 1(3), pp. 1-13 (2016).

[138] Y Wu, Y Lai and ZQ Zhang. Elastic metamaterials with simultaneously negative effective shear modulus and mass density. Phys. Rev. Lett. 107(10), 105506 (2011).

[139] A Srivastava. Elastic metamaterials and dynamic homogenization: a review. International Journal of Smart and Nano Materials, 6(1), pp. 41-60 (2015).

[140] A Colombi, P Roux, S Guenneau, P Gueguen and RV Craster. Forests as a natural seismic metamaterial: Rayleigh wave bandgaps induced by local resonances. Scientific reports, 6(1), pp. 1-7 (2016).

[141] A Colombi, D Colquitt, P Roux, S Guenneau and RV Craster. A seismic metamaterial: The resonant metawedge. Scientific Reports volume 6, 27717 (2016).

[142] D Mu, H Shu, L Zhao and S An. A review of research on seismic metamaterials. Advanced Engineering Materials, 22(4), 1901148 (2020).

[143] M Farhat, S Enoch, S Guenneau, and AB Movchan. Broadband Cylindrical Acoustic Cloak for Linear Surface Waves in a Fluid. Phys. Rev. Lett. 101, 134501 (2008).

[144] S Zou et al. Broadband waveguide cloak for water waves. Phys. Rev. Lett. 123(7), 074501 (2019).

[145] I Peralta, VD Fachinotti and JC Alvarez Hostos. A brief review on thermal metamaterials for cloaking and heat flux manipulation. Advanced Engineering Materials, 22(2), 1901034 (2020).

[146] Y Li et al. Transforming heat transfer with thermal metamaterials and devices. Nature Reviews Materials, 6(6), pp. 488-507 (2021).

[147] S Zhang, DA Genov, C Sun and X Zhang. Cloaking of matter waves. Physical Review Letters, 100(12), 123002 (2008).

[148] C Valagiannopoulos. Perfect quantum cloaking of tilted cylindrical nanocavities. Phys. Rev. B 101(19), 195301 (2020).

[149] E Pereira and F Moraes. Flowing liquid crystal simulating the Schwarzschild metric. Central European Journal of Physics, 9(4), pp. 1100-1105 (2011).

[150] SK Roy, P Baral, R Koley and P Majumdar. Granular Matter as a Gravity Analogue (2020), unpublished. ArXiv preprint arXiv:2011.01194.

[151] WK Barros and E Pereira. Concurrent guiding of light and heat by transformation optics and transformation thermodynamics via soft matter. Scientific reports, 8(1), pp. 1-11 (2018).

[152] G Pawlik, K Tarnowski, W Walasik, A Mitus, IC Khoo, Optics Letters, Vol. 39 Issue 7, pp.1744-1747 (2014).

[153] Y Chen, B Ai and Z Wong. Soft optical metamaterials. Nano Convergence 7, pp. 1-17 (2020).

[154] E Scholz. E. Cartan's attempt at bridge-building between Einstein and the Cosserats–or how translational curvature became to be known as torsion. The European Physical Journal H, 44(1), pp. 47-75 (2019).

[155] C Barceló, S Liberati and M Visser. Analogue gravity. Living reviews in relativity, 14(1), 3 (2011).

[156] MJ Jacquet, S Weinfurtner and F König. The next generation of analogue gravity experiments. Phil. Trans. R. Soc. A.37820190239 (2020).

[157] M Visser. Essential and inessential features of Hawking radiation. International Journal of Modern Physics D, 12(04), pp. 649-661 (2003).

[158] LJ Garay, JR Anglin, JI Cirac and P Zoller. Sonic black holes in dilute Bose-Einstein condensates. Physical Review A, 63(2), 023611 (2001).

[159] M Novello, M Visser and GE Volovik. Artificial black holes. World Scientific (2002).

[160] VA De Lorenci, R Klippert and YN Obukhov. On optical black holes in moving dielectrics. Phys. Rev. D, 68, 061502, pp. 1–4 (2003).

[161] O Lahav et al. Realization of a sonic black hole analog in a Bose-Einstein condensate. Phys Rev Lett, 105(24), 240401 (2010).

[162] C Barceló. Analogue black-hole horizons. Nature Physics, 15(3), pp. 210-213 (2019).

[163] Y Kedem, EJ Bergholtz and F Wilczek. Black and white holes at material junctions. Phys Rev Research 2, 043285 (2020).

[164] WG Unruh. Experimental Black Hole Evaporation. Phys. Rev. Lett. 46 1351 (1981).

[165] C Barcelo, S Liberati and M Visser. Towards the observation of Hawking radiation in Bose–Einstein condensates. International Journal of Modern Physics A, 18(21), pp. 3735-3745 (2003).

[166] S Giovanazzi. Hawking radiation in sonic black holes. Phys Rev Lett, 94(6), 061302 (2005).

[167] G Rousseaux et al. Observation of negative-frequency waves in a water tank: a classical analogue to the Hawking effect ?. New Journal of Physics, 10(5), 053015 (2008).

[168] TG Philbin et al. Fiber-optical analog of the event horizon. Science, 319(5868), pp. 1367-1370 (2008).

[169] PD Nation, MP Blencowe, AJ Rimberg and E Buks. Analogue Hawking radiation in a dc-SQUID array transmission line. Phys Rev Lett, 103(8), 087004 (2009).

[170] A Recati, N Pavloff and I Carusotto. Bogoliubov theory of acoustic Hawking radiation in Bose-Einstein condensates. Phys Rev A, 80(4), 043603 (2009).

[171] J Macher and R Parentani. Black-hole radiation in Bose-Einstein condensates. Physical Review A, 80(4), 043601 (2009).

[172] F Belgiorno et al. Hawking radiation from ultrashort laser pulse filaments. Phys Rev Lett, 105(20), 203901 (2010).

[173] S Weinfurtner, EW Tedford, MC Penrice, WG Unruh and GA Lawrence. Measurement of stimulated Hawking emission in an analogue system. Phys. Rev. Lett., 106(2), 021302 (2011).

[174] S Weinfurtner, EW Tedford, MC Penrice, WG Unruh and GA Lawrence. Classical aspects of Hawking radiation verified in analogue gravity experiment. In *Analogue Gravity Phenomenology*, pp. 167-180, Springer, Cham. (2013).

[175] J Steinhauer. Observation of quantum Hawking radiation and its entanglement in an analogue black hole. Nature Physics, 12(10), pp. 959-965 (2016).

[176] JRM de Nova, K Golubkov, VI Kolobov and J Steinhauer. Observation of thermal Hawking radiation and its temperature in an analogue black hole. Nature, 569(7758), pp. 688-691 (2019).

[177] J Prat-Camps, C Navau and A Sanchez. A magnetic wormhole. Scientific reports, 5, 12488 (2015).

[178] C Peloquin, LP Euvé, T Philbin and G Rousseaux. Analog wormholes and black hole laser effects in hydrodynamics. Phys Rev D, 93(8), 084032 (2016).

[179] J Zhu et al. Elastic waves in curved space: mimicking a wormhole. Phys Rev Lett, 121(23), 234301 (2018).

[180] F dos S Azevedo, JD M de Lima, A de Pádua Santos and F Moraes. Optical wormhole from hollow disclinations. Phys Rev A 103, 023516 (2021).

[181] C Barcelo, S Liberati and M Visser. (2003). Analogue models for FRW cosmologies. International Journal of Modern Physics D, 12(09), 1641-1649.

[182] S Weinfurtner. Analogue model for an expanding universe. General Relativity and Gravitation, 37(9), pp. 1549-1554 (2005).

[183] P Jain, S Weinfurtner, M Visser and CW Gardiner. Analog model of a Friedmann-Robertson-Walker universe in Bose-Einstein condensates: Application of the classical field method. Physical Review A, 76(3), 033616 (2007).

[184] W Unruh and R Schützhol. (Eds.). Quantum analogues: from phase transitions to black holes and cosmology. Springer (2007).

[185] P Pedram and S Jalalzadeh. Signature change from Schutz's canonical quantum cosmology and its classical analogue. Phys Rev D, 77(12), 123529 (2008).

[186] M Simões and M Pazetti. Liquid-crystals cosmology. EPL 92(1), 14001 (2010).

[187] D Figueiredo, F Moraes, S Fumeron, and B Berche. Cosmology in the laboratory: An analogy between hyperbolic metamaterials and the Milne universe. Phys. Rev. D 96, 105012 (2017).

[188] EB Kolomeisky. Natural analog to cosmology in basic condensed matter physics. Phys Rev B, 100(14), 140301 (2019).

[189] Z Fifer et al. Analog cosmology with two-fluid systems in a strong gradient magnetic field. Phys Rev E, 99(3), 031101 (2019).

[190] T Jacobson et al. Rapidly Expanding BEC Ring: Analog Cosmology in a Lab. Bulletin of the American Physical Society (2020).

[191] E Howard. Cosmology analogues in optical systems. In EPJ Web of Conferences 238, 11008, EDP Sciences (2020).

[192] H Chen, CT Chan and P Sheng. Transformation optics and metamaterials. Nature materials, 9(5), pp. 387-396 (2010).

[193] JB Pendry, A Aubry, DR Smith and SA Maier. Transformation optics and subwavelength control of light. science, 337(6094), pp. 549-552 (2012).

[194] F Sun et al. Transformation optics: From classic theory and applications to its new branches. Laser & Photonics Reviews, 11(6), 1700034 (2017).

[195] J Zhang, JB Pendry and Y Luo. Transformation optics from macroscopic to nanoscale regimes: a review. Advanced Photonics, 1(1), 014001 (2019).

[196] H Chen and CT Chan. Acoustic cloaking and transformation acoustics. Journal of Physics D: Applied Physics, 43(11), 113001 (2010).

[197] U Iemma, M Carley and R Pellegrini. Tailoring acoustic metamaterials to aeroacoustic applications. In INTER-NOISE and NOISE-CON Congress and Conference Proceedings 249(8), pp. 274-281. Institute of Noise Control Engineering (2014).

[198] P Deymier et al. Spacetime representation of topological phononics. New J. Phys. 20 053005 (2018).

[199] GW Milton, M Briane and JR Willis. On cloaking for elasticity and physical equations with a transformation invariant form. New J. Phys. 8 248 (2006).

[200] PG de Gennes, J. Prost. *The physics of liquid crystals*, 2nd edition, Oxford University Press (1993).

[201] S Chandrasekhar. *Liquid crystals*, 2nd edition, Cambridge University Press (1992).

[202] M Kleman and OD Lavrentovich. *Soft Matter Physics.* Springer-Verlag, New York (2003).

[203] P Oswald and P Pieranski. *Liquid Crystals: Concepts and Physical Properties Illustrated by Experiments.* Taylor & Francis, 1st edition (2018)

[204] S Chandrasekhar and GS Ranganath. The structure and energetics of defects in liquid crystals. Advances in Physics, 35(6), pp. 507-596 (1986).

[205] M Kléman. Defects in liquid crystals. Reports on Progress in Physics, 52(5), 555 (1989).

[206] OD Lavrentovich, P Pasini, C Zannoni and S Zumer (Eds.). Defects in liquid crystals: Computer simulations, theory and experiments (Vol. 43). Springer Science & Business Media (2012).

[207] WH Zurek. Cosmological experiments in condensed matter systems. Physics Reports 276 pp. 177-221 (1996).

[208] HR Trebin, Defects in liquid crystals and cosmology. Liquid crystals **24**, 127-130 (1998).

[209] F Moraes. Condensed matter physics as a laboratory for gravitation and cosmology. Braz. J. Phys. 30 (2) pp. 304-308 (2000).

[210] TW Kibble. Phase-transition dynamics in the lab and the universe. Physics Today, 60(9), 47 (2007).

[211] G Toulouse and M Kléman. Principles of a classification of defects in ordered media. Journal de Physique Lettres, 37(6), pp. 149-151 (1976).

[212] MV Kurik and OD Lavrentovich. Defects in liquid crystals: homotopy theory and experimental studies. Soviet Physics Uspekhi, 31(3), 196 (1988).

[213] T Kibble. Topology of cosmic domains and strings, J. Phys. A **9**, pp. 1387-1398 (1976).

[214] C Satiro, AM De M Carvalho and F Moraes. An Asymmetric Family of Cosmic Strings. Modern Physics Letters A, 24(18), pp. 1437-1442 (2009).

[215] M Kleman. Some aspects of defect theory in spacetime. Published in The Thirteenth Marcel Grossmann Meeting, World Scientific pp. 2531-2533 (2015).

[216] I Chuang, R Durrer, N Turok and B Yurke. Cosmology in the Laboratory: Defect Dynamics in Liquid Crystals. Science 251(4999), pp. 1336-1342 (1991).

[217] MJ Bowick, L Chandar, EA Schiff and AM Srivastava. The cosmological Kibble mechanism in the laboratory: string formation in liquid crystals. Science, 263(5149), pp. 943-945 (1994).

[218] S Digal, R Ray and AM Srivastava. Observing correlated production of defects and antidefects in liquid crystals. Physical Review Letters, 83(24), 5030 (1999).

[219] H Mukai, PRG Fernandes, BF De Oliveira and GS Dias. Defect-antidefect correlations in a lyotropic liquid crystal from a cosmological point of view. Phys Rev E, 75(6), 061704 (2007).

[220] R Repnik et al. Symmetry breaking in nematic liquid crystals: analogy with cosmology and magnetism. J. Phys.: Condens. Matter 25, 404201 (2013).

[221] VMH Ruutu et al. Vortex formation in neutron-irradiated superfluid 3 He as an analogue of cosmological defect formation. Nature, 382(6589), pp. 334-336 (1996).

[222] A Vilenkin. Cosmics strings and domain walls. Phys Rep 121 (5), pp. 263-315 (1985).

[223] R.H. Brandenberger. Topological defects and structure formation, Int. J. Mod. Phys. A **9** 2117-2189 (1994).

[224] G Duclos. Topological structure and dynamics of three-dimensional active nematics. Science 367(6482), pp. 1120-1124 (2020).

[225] M Visser. Traversable wormholes: Some simple examples. Phys. Rev. D 39, 3182 (1989).

[226] JG Cramer, RL Forward, MS Morris, M Visser, G Benford and GA Landis. Natural wormholes as gravitational lenses. Physical Review D, 51(6), 3117 (1995).

[227] KR Popper. In search of a better world: lectures and essays from thirty years. Taylor and Francis (1994).

[228] P Ben-Abdallah, V Le Dez, D Lemonnier and Fumeron S. Inhomogeneous radiative model of refractive and dispersive semi-transparent stellar atmospheres. JQSRT 95, 701 (2001).

[229] K Schwarzschild. On the equilibrium of the Sun's atmosphere. Nachrichten von der Königlichen Gesellschaft der Wissenschaften zu Göttingen. Math.-phys. Klasse 195, pp. 41-53 (1906).

[230] J Bicak and P Hadrava. General-relativistic radiative transfer theory in refractive and dispersive media. Astronomy and Astrophysics 44(2), pp. 389-399 (1975).

[231] D Mihalas. Stellar atmospheres. 2nd edition, Freeman & Co, San Francisco (1978).

[232] S Fumeron. International Journal of Modern Physics D 18(2) pp. 223–236 (2009).

[233] MF Modest. Radiative heat transfer. 3rd Edition, Academic Press Inc (2013).

[234] S Knop, PH Hauschildt and E Baron. General relativistic radiative transfer. Astronomy & Astrophysics, 463(1), pp. 315-320 (2007).

[235] F Azevedo, F Moraes, F Mireles, B Berche, S Fumeron. The wiggly cosmic string as a waveguide for massless and massive fields. Phys. Rev. D 96 084047 (2017)

[236] A Vilenkin. Looking for cosmic strings. Nature 322, pp. 613-614 (1986).

[237] FB Feng. Radio jets and galaxies as cosmic string probes. Frontiers of Physics 7, 461 (2012).

[238] PF Gonzalez-Diaz and JA Jiménez Madrid. Wiggly cosmic strings accrete dark energy. International Journal of Modern Physics D 15, 603 (2006).

[239] FJ Asturias and SR Aragon. The hydrogenic atom and the periodic table of the elements in two spatial dimensions. Am. J. Phys. 893 (53) (1985).

[240] D Figueiredo, FA Gomes, S Fumeron, B Berche and F Moraes. Mimicking Kleinian cosmology with electronic metamaterials. Phys. Rev. D 94, 755 (2016).

[241] JB Hartle and SW Hawking, Phys. Rev. D 28, 2960 (1983).

[242] AD Sakharov, Sov. Phys. JETP 60, 214 (1984), [Sov. Phys. Usp.34,409(1991)].

[243] A White, S Weinfurtner and M Visser. Signature change events: A challenge for quantum gravity?. Classical and Quantum Gravity, 27(4), 045007 (2010).

[244] J Mielczarek. Signature change in loop quantum cosmology. In Relativity and Gravitation, pp. 555-562, Springer, Cham. (2014).

[245] M. Bojowald and J. Mielczarek. Journal of Cosmology and Astroparticle Physics 2015, 052 (2015).

[246] L Alty, Classical and Quantum Gravity 11, 2523 (1994).

[247] D Dragoman and M Dragoman. Metamaterials for ballistic electrons. Journal of applied physics, 101(10), 104316 (2007).

[248] S Fumeron, B Berche, F Santos, E Pereira and F Moraes. Optics near a hyperbolic defect. Phys. Rev. A 92 063806 (2015).

[249] M Gasperini and G Veneziano. String Theory and Pre-big bang Cosmology, Il Nuovo Cimento C 38, 160 (2015).

[250] J Khoury, BA Ovrut, N Seiberg, PJ Steinhardt and N Turok. From big crunch to big bang. Phys. Rev. D 65, p. 086007 (2002).

[251] PJ Steinhardt and N Turok. Cosmic evolution in a cyclic universe. Phys. Rev. D 65 (12) p. 126003 (2002).

[252] GT Horowitz and AR Steif. Singular string solutions with nonsingular initial data. Physics Letters B 258 (1), pp. 91–96 (1991).

[253] P Małkiewicz and W Piechocki. Probing the cosmological singularity with a particle. Classical and Quantum Gravity 23 (23), p. 7045 (2006).

[254] Ø Grøn and S Hervik. Einstein's general theory of relativity: with modern applications in cosmology. Springer Science & Business Media, 2007.

[255] AJ Tolley, N Turok, and PJ Steinhardt. Cosmological perturbations in a big-crunch–big-bang space-time.Phys. Rev. D 69 (10), p. 106005 (2004).

[256] P Małkiewicz and W Piechocki. A simple model of big-crunch/big-bang transition. Classical and Quantum Gravity 23 (9), p. 2963 (2006).

[257] L Baulieu, J de Boer, B Pioline and E Rabinovici. Proceedings of the NATO Advanced Institute on String Theory: From Gauge Interactions to Cosmology vol. 208. Springer Science & Business Media (2006).

[258] JD Lawrence. A catalog of special plane curves. Dover Publications (2014).

[259] K Kowalski and J Rembielinski. On the dynamics of a particle on a cone. Annals of Physics 329, pp. 146– 157 (2013).

[260] FWJ Olver, DW Lozier, RF Boisvert and CW Clark. NIST handbook of mathematical functions. Cambridge University Press (2010).

[261] E Prugovecki. Quantum mechanics in Hilbert space Academic Press 92 (1982).

[262] J Xiang, OD Lavrentovich. Mol. Cryst. Liq. Cryst. 559, p.106 (2012).

[263] AJ Tolley and N Turok. Quantum fields in a bigcrunch/big-bang spacetime. Phys. Rev. D 66, p. 106005 (2002).

[264] E Poisson. The gravitational self-force. General Relativity and Gravitation, pp. 119–141 (2012).

[265] E Poisson. The motion of point particles in curved spacetime. Living Reviews in Relativity 7, p. 6 (2004).

[266] RP Feynman. "There's plenty of room at the bottom", reprinted in Journal of Microelectromechanical Systems, 1 (1) p. 60–66 (1992).

[267] DR Smith, JB Pendry and MC Wiltshire. Metamaterials and negative refractive index. Science, 305 (5685), pp. 788-792 (2004).

[268] NI Zheludev, YS Kivshar. From metamaterials to metadevices. Nature 11 (2012).

[269] S Xiao, T Wang, T Liu, C Zhou, X Jiang and J Zhang. Active metamaterials and metadevices: a review. Journal of Physics D: Applied Physics, 53 (2020).

[270] B Li, L Wang, G Casati. Negative differential thermal resistance and thermal transistor. Appl. Phys. Lett. 88 (2006)

[271] OP Saira, M Meschke, F Giazotto, AM Savin, M Mottonen, JP Pekola. Heat transistor: demonstration of gate-controlled electronic refrigeration. PRL 99 (2007).

[272] N Li, J Ren, L Wang, G Zhang, P Hanggi, B Li. Colloquium: Phononics: manipulating heat flow with electronic analogs and beyond Rev. Mod. Phys. 84 (2012).

[273] Y Liu, Y Xu, SC Zhang and W Duan, W. Model for topological phononics and phonon diode. Physical Review B, 96 (2017).

[274] L Wang, B Li. Thermal logic gates: computation with phonons PRL 99 (2007).

[275] S Narayana, Y Sato. Heat flux manipulation with engineered thermal materials. PRL 108 (2012).

[276] S Guenneau, C Amra, D Veynante. Transformation thermodynamics: cloaking and concentrating heat flux. Opt. Express 20 (2012).

[277] M Maldovan. Narrow-low frequency spectrum and heat management by thermocrystals. PRL 110 (2013).

[278] M Maldovan. Sound and heat revolutions in phononics. Nature 503 (2013).

[279] VC Sanchez, A Jachak, RH Hurt and AB Kane. Biological Interactions of Graphene-Family Nanomaterials: An Interdisciplinary Review. Chem. Res. Toxicol 25 (1), pp. 15–34 (2012).

[280] PM Thibado, P Kumar, S Singh, M Ruiz-Garcia, A Lasanta, and LL Bonilla. Fluctuation-induced current from freestanding graphene. PRE 102 (2020).

[281] AG Olabi, MA Abdelkareem, T Wilberforce, ET Sayed. Application of graphene in energy storage device – A review. Renewable and Sustainable Energy Reviews 135 (2021).

[282] J Haskins, A Kinaci, C Sevik, H Sevincli, G Cuniberti and T Cagin, Control of Thermal and Electronic Transport in Defect-Engineered Graphene Nanoribbons. ACS Nano 5(5) (2011).

[283] B Ni, T Zhang, J Li, X Li and H Gao. Topological Design of Graphene. Handbook Graphene. Phys. Chem. Biol (2019)..

[284] A Jangizehi, F Schmid, P Besenius, K Kremer and S Seiffert. Defects and defect engineering in Soft Matter. Soft Matter 16, pp. 10809-10859 (2020).

[285] T Orlova et al. Creation and manipulation of topological states in chiral nematic microspheres. Nature communications 6.1 pp. 1-9 (2015).

[286] L Marrucci, C Manzo and D Paparo. Optical spin-to-orbital angular momentum conversion in inhomogeneous anisotropic media. Physical review letters, 96(16), 163905 (2006).

[287] B Piccirillo et al. Photon spin-to-orbital angular momentum conversion via an electrically tunable q-plate. Applied Physics Letters, 97(24), 241104 (2010).

[288] P Vaveliuk et al. Structure of the dielectric tensor in nematic liquid crystals with topological charge. JOSA A, 27(6), pp. 1466-1472 (2010).

[289] N Kravets, N Podoliak, M Kaczmarek and E Brasselet. Self-induced liquid crystal q-plate by photoelectric interface activation. Applied Physics Letters, 114(6), 061101 (2019).

[290] N Kravets and E Brasselet. Taming the swirl of self-structured liquid crystal q-plates. Journal of Optics, 22(3), 034001 (2020).

[291] J Hwang et al. Electro-tunable optical diode based on photonic bandgap liquid-crystal heterojunctions. Nature materials, 4(5), pp. 383-387 (2005).

[292] MH et al. Simple electro-tunable optical diode using photonic and anisotropic liquid crystal films. Thin Solid Films, 509(1-2), pp. 49-52 (2006).

[293] AE Miroshnichenko, E Brasselet and YS Kivshar. Reversible optical nonreciprocity in periodic structures with liquid crystals. Applied Physics Letters, 96(6), 26 (2010).

[294] S Fumeron, ER Pereira, F Moraes. Generation of optical vorticity from topological defects. Physica B 476 p. 735 (2015).

[295] Y Shen et al. Optical vortices 30 years on: OAM manipulation from topological charge to multiple singularities. Light: Science & Applications 8 (90) (2019).

[296] C Loussert, U Delabre and E Brasselet. Manipulating the orbital angular momentum of light at the micron scale with nematic disclinations in a liquid crystal film. Phys. Rev. Lett. 111(3), 037802 (2013).

[297] S Fumeron, B Berche, E Medina, FAN Santos and F Moraes. Using torsion to manipulate spin currents. EPL 117, 785 (2017).

[298] IL Shapiro. Physical aspects of the space–time torsion. Phys. Rep. 357, 113 (2002).

[299] A Zecca. Dirac Equation in Space–Time with Torsion. Int. J. Theor. Phys. 41, 421 (2002).

[300] JD McCrea. Irreducible decompositions of nonmetricity, torsion, curvature and Bianchi identities in metric-affine spacetimes. Class. Quantum Grav. 9, 553 (1992).

[301] B Berche, E Medina and A Lopez. Spin superfluidity and spin-orbit gauge symmetry fixing. EPL,97 35467007 (2012).

[302] VG Bagrov, IL Buchbinder and IL Shapiro. Izv. VUZov, Fisica (in Russian, English translation: Sov.J.Phys.) 35 (3), 5 (1992). See also hep-th/9406122.

[303] F Caruso, JA Helayel-Neto, J Martins and V Oguri. Effects on the non-relativistic dynamics of a charged particle interacting with a Chern-Simons potential. Eur. Phys. J. B 86 (2013).

[304] F Dos Santos Azevedo, D Figueiredo, F Moraes, Bertrand Berche and S Fumeron. Optical concentrator from a hyperbolic liquid-crystal metamaterial. EPL 124 (3) (2018).

[305] X Zhang, Z Liu. Superlenses to overcome the diffraction limit. Nature Materials 7, pp. 435–441 (2008).

[306] E Pereira, S Fumeron and F Moraes. Metric approach for sound propagation in nematic liquid crystals. Phys. Rev. E, 87(2), 022506 (2013).

[307] UR Fischer and M Visser. Riemannian geometry of irrotational vortex acoustics, Phys. Rev. Lett. **88**, 110201 (2002). An unpublished preprint on geometrical acoustics was written by the same author in 1993 (see M Visser. Acoustic propagation in fluids: an unexpected example of Lorentzian geometry. arXiv preprint gr-qc/9311028).

[308] S Fumeron, F Moraes and E Pereira. (2016). Retrieving the saddle-splay elastic constant K_{24} of nematic liquid crystals from an algebraic approach. The European Physical Journal E, 39(9), pp. 1-11 (2016).

[309] PE Cladis, M Kleman. Non-singular disclinations of strength $S = +1$ in nematics, J. Physique 33, 591 (1972).

[310] RB Meyer, On the existence of even indexed disclinations in nematic liquid crystals. Phil. Mag. 27, 405 (1973).

[311] I Vilfan, M Vilfan and S Zumer. Defect structures of nematic liquid crystals in cylindrical cavities. Phys. Rev. A, 43(12), 6875 (1991).

[312] MV Burylov. Equilibrium configuration of a nematic liquid crystal confined to a cylindrical cavity, JETP 85(5), pp. 873-886 (1997).

[313] R Fleury et al. Sound isolation and giant linear nonreciprocity in a compact acoustic circulator. Science, 343(6170), pp. 516-519 (2014).

[314] E Viana, F Moraes, S Fumeron, E Pereira. High rectification in a broadband subwavelength acoustic device using liquid crystals. Journal of Applied Physics 125, 959 (2019).

[315] G Crawford, DW Allender, J Doane. Surface elastic and molecular-anchoring properties of nematic liquid crystals confined to cylindrical cavities. Phys Rev A 45(12), 8693 (1992).

[316] S Fumeron, ER Pereira, F Moraes. Modeling heat conduction in the presence of a dislocation. Int. J. Therm. Sci. 67, 687 (2013).

[317] S Fumeron, ER Pereira, F Moraes. Principles of thermal design with nematic liquid crystals. Phys. Rev. E 89, 684 (2014).

[318] S Fumeron, F Moraes and ER Pereira. Thermal and shape topological robustness of heat switchers using nematic liquid crystals. The European Physical Journal E 41, 1001 (2018).

[319] GA Pavliotis. The Fokker–Planck Equation. In: Stochastic Processes and Applications. Texts in Applied Mathematics 60. Springer, New York, NY (2014).

[320] M Smerlak. Tailoring diffusion in analog spacetimes. PRE 85, 041134 (2012).

[321] J Peitz and S Appl. 3+1 formulation of non-ideal hydrodynamics. Mon. Not. R. Astron. Soc. 296, pp. 231-244 (1998).

[322] J Kim, K Le, S Dhara, F Araoka, K Ishikawa and H Takezoe. Heat-driven and electric-field-driven bistable devices using dye-doped nematic liquid crystals. J. Appl. Phys. 107, 123108 (2010).

[323] RCT da Costa. Quantum mechanics of a constrained particle. Phys. Rev. A 23, p. 1982 (1981).

[324] V Atanasov and A Saxena. Electronic properties of corrugated graphene: the Heisenberg principle and wormhole geometry in the solid state. Journal of Physics: Condensed Matter 23(17), 175301 (2011).

[325] J Onoe, T Ito, H Shima, H Yoshioka, and S Kimura. Observation of Riemannian geometric effects on electronic states. EPL 98, 27001 (2012).

[326] F Santos, S Fumeron, B Berche, F Moraes F. Geometric effects in the electronic transport of deformed nanotubes. Nanotechnology 27 135302 (2016).

[327] S Fumeron, B Berche, F Moraes, F Santos. Tayloring energy levels with curvature ? An illustration of Da Costa formalism. Journal of Physics: Conf. Series 785, 777 (2017).

[328] F Serafim, FAN Santos, JRF Lima, S Fumeron, B Berche, F Moraes. Magnetic and geometric effects on the electronic transport of metallic nanotubes. JAP 129, 1338 (2021).

[329] G Ferrari and G Cuoghi. Schrödinger Equation for a Particle on a Curved Surface in an Electric and Magnetic Field. Phys. Rev. Lett. 100, 230403 (2008).

[330] MM Cunha, JRF Lima, F Moraes, S Fumeron, B Berche. Spin current generation and control in carbon nanotubes by combining rotation and magnetic field. Journal of Physics: Condensed Matter 32, 1335 (2020).

[331] G. Steele, F. Pei, E. Laird, J. Jo, H. Meerwaldt, and L. Kouwenhoven. Large spin-orbit coupling in carbon nanotubes. Nat. Commun. 4, 1573 (2013).

[332] R Newson, A Green, MC Hersam and H Van Driel. Coherent injection and control of ballistic charge currents in single-walled carbon nanotubes and graphite. PRB 83, 115421 (2011).

[333] P Phillips, Advanced Solid State Physics. Cambridge University Press (2012).

[334] M Matsuo, J Ieda, E Saitoh, and S Maekawa. Spin-dependent inertial force and spin current in accelerating systems. PRB 84, 104410 (2011).

[335] B Berche, C Chatelain, E Medina. Mesoscopic rings with Spin-Orbit interactions. Eur. J. Phys. 31, 541 (2010).

[336] D Melo, I Fernandes, F Moraes, S Fumeron, E Pereira. Thermal diode made by nematic liquid crystal. Phys. Lett. A 380 pp. 3121-3127 (2016).

[337] JG Silva, S Fumeron, F Moraes and ER Pereira. High Thermal Rectifications Using Liquid Crystals Confined into a Conical Frustum. Brazilian Journal of Physics 48, 870 (2018).

[338] G Wehmeyer, T Yabuki, C Monachon, J Wu and C Dames. Thermal diodes, regulators, and switches: Physical mechanisms and potential applications. Applied Physics Reviews, 4(4), 041304 (2017).

[339] MY Wong, CY Tso, TC Ho and HH Lee. A review of state of the art thermal diodes and their potential applications. International Journal of Heat and Mass Transfer, 164, 120607 (2021).

[340] B Li, L Wang and G Casati. Thermal diode: Rectification of heat flux. Physical review letters, 93(18), 184301 (2004).

[341] J Ordonez-Miranda et al. Conductive thermal diode based on the thermal hysteresis of VO_2 and nitinol. Journal of Applied Physics, 123(8), 085102 (2018).

[342] Y Li et al. Transforming heat transfer with thermal metamaterials and devices. Nature Reviews Materials, 6(6), pp. 488-507 (2021).

[343] SO Kasali, J Ordonez-Miranda and K Joulain. Conductive thermal diode based on two phase-change materials. International Journal of Thermal Sciences, 153, 106393 (2020).

[344] P Ben-Abdallah and SA Biehs. Phase-change radiative thermal diode. Applied Physics Letters, 103(19), 191907 (2013).

[345] E Nefzaoui, K Joulain, J Drevillon and Y Ezzahri. Radiative thermal rectification using superconducting materials. Applied Physics Letters, 104(10), 103905 (2014).

[346] K Joulain, Y Ezzahri, J Drevillon, B Rousseau and DDS Meneses. Radiative thermal rectification between SiC and SiO 2. Optics express, 23(24), A1388-A1397 (2015).

[347] A Ghanekar, J Ji and Y Zheng. High-rectification near-field thermal diode using phase change periodic nanostructure. Applied Physics Letters, 109(12), 123106 (2016).

[348] A Fiorino et al. A thermal diode based on nanoscale thermal radiation. ACS nano, 12(6), pp. 5774-5779 (2018).

[349] PR Gaddam, ST Huxtable and WA Ducker. A liquid-state thermal diode. International Journal of Heat and Mass Transfer, 106, pp. 741-744 (2017).

[350] D Sawaki, W Kobayashi, Y Moritomo, I Terasaki. Thermal rectification in bulk materials with asymmetric shape, Appl. Phys. Lett. 98 (8) 081915 (2011).

[351] Z Zhang, Y Chen, Y Xie and S Zhang. Transition of thermal rectification in silicon nanocones. Applied Thermal Engineering, 102, pp. 1075-1080 (2016).

[352] H Wang, Y Yang, H Chen, N Li and L Zhang. Thermal rectification induced by geometrical asymmetry: A two-dimensional multiparticle Lorentz gas model. Phys. Rev. E, 99(6), 062111 (2019).

[353] M Criado-Sancho, FX Alvarez and D Jou. Thermal rectification in inhomogeneous nanoporous Si devices. JAP 114(5), 053512 (2013).

[354] R Dettori, C Melis, R Rurali and L Colombo. Thermal rectification in silicon by a graded distribution of defects. JAP 119, 215102 (2016).

[355] S Fumeron, B Berche, F Moraes, F Santos, E Rodrigues. Geometrical optics limit of phonon transport in a channel of disclinations. Eur. Phys. J. B 90 (2017).

[356] II Smalyukh, BI Senyuk, SV Shiyanovskii, OD Lavrentovich, AN Kuzmin, AV Kachynski and PN Prasad. Optical Trapping, Manipulation, and 3D Imaging of Disclinations in Liquid Crystals and Measurement of their Line Tension. Mol. Cryst. Liq. Cryst. 450(1), pp. 279-295 (2006).

[357] H Zhang, G Lee and K Cho. Thermal transport in graphene and effects of vacancy defects. PRB 84, 115460 (2011)

[358] PS Letelier, Spacetime defects: von Kármán vortex street like configurations, Class. Quantum Grav. 17, pp. 3639-3643 (2001).

[359] A Akhiezer, V Truten, N Shul'ga. Phys. Rep. 203(5), pp. 289–343 (1991).

[360] B Berche, S Fumeron, F Moraes. On the energy of topological defect lattices. Condensed Matter Physics 23(2), pp. 1–7 (2020). `https://arxiv.org/pdf/2001.10066.pdf`.

[361] R Sorkin. Time-evolution problem in regge calculus. Phys. Rev. D 12 pp. 385–396 (1975). Erratum: Phys. Rev. D 23, 565 (1981)

[362] UR Fischer and M Visser. Riemannian geometry of irrotational vortex acoustics, Phys. Rev. Lett. **88**, 110201 (2002).

[363] S Fumeron, B Berche and F Moraes. Improving student understanding of electrodynamics: The case for differential forms. American Journal of Physics. Am. J. Phys. 88, 1083 (2020). A series of lectures given on electrodynamics and exterior algebra can also be found at `https://lpct.univ-lorraine.fr/seminaires/seminaire.php?&titre=Electrodynamics\%20reloaded`.

[364] FJ Dyson. Why is Maxwell's theory so hard to understand ? James Clerk Maxwell commemorative booklet: James Clerk Maxwell Foundation, Edinburgh (1999).

[365] M Born and E Wolf. Principles of Optics, Cambridge University Press, Cambridge (1999).

[366] JD Jackson. Classical Electrodynamics, John Wiley & Sons, New-York (1999).

[367] J Gratus, P Kinsler and MW McCall. Maxwell's (D, H) excitation fields: lessons from permanent magnets, European Journal of Physics 40, 025203 (2019).

[368] DJ Griffith. Introduction to Electrodynamics, Cambridge University Press, Cambridge (2017).

[369] A Zangwill. Modern electrodynamics, Cambridge University Press, Cambridge (2013).

[370] J Van Kranendonk and JE Sipe. Foundations of the macroscopic electromagnetic theory of dielectric media, Progress in Optics 15 pp. 245-350 (1977).

[371] AJ Ward and JB Pendry. Refraction and geometry in Maxwell's equations, Journal of Modern Optics 43, pp. 773-793 (1996).

[372] M Kitano. Reformulation of electromagnetism with differential forms, Trends in Electromagnetism—From Fundamentals to Applications; V. Barsan and R.P. Lungu Eds. IntechOpen (2012).

[373] GA Deschamps. Electromagnetics and differential forms, Proceedings of the IEEE 69, pp. 676-696 (1981).

[374] N Schleifer. Differential forms as a basis for vector analysis—with applications to electrodynamics, Am J Phys 51, pp. 1139-1145 (1983).

[375] Y Hoshino. An elementary application of exterior differential forms in quantum mechanics, Am J Phys 46, pp. 1148-1150 (1978).

[376] H Amar. Elementary application of differential forms to electromagnetism, Am J Phys 48, pp. 252-252 (1980).

[377] D Baldomir. Differential forms and electromagnetism in 3-dimensional Euclidean space R^3, IEE Proceedings A-Physical Science, Measurement and Instrumentation, Management and Education-Reviews 133, pp. 139-143 (1986).

[378] A Bossavit. Differential forms and the computation of fields and forces in electromagnetism. European Journal of Mechanics B 10, pp. 474-488 (1991).

[379] FL Teixeira and WC Chew. Differential forms, metrics, and the reflectionless absorption of electromagnetic waves, Journal of Electromagnetic Waves and Applications 13, pp. 665-686 (1999).

[380] KF Warnick and PH Russer. Differential forms and electromagnetic field theory, Progress In Electromagnetics Research 148, pp. 83-112 (2014).

[381] W Thirring. *A Course in Mathematical Physics 2: Classical Field Theory.* Springer-Verlag New York (1978).

[382] WL Burke. *Applied differential geometry.* Cambridge University Press, Cambridge (1985).

[383] J Baez and JP Muniain. Gauge fields, knots and gravity. World Scientific Publishing Company, Singapore (1994).

[384] H Flanders. Differential Forms with Applications to the Physical Sciences. Dover Publication Inc., New-York (1989).

[385] I.V. Lindell. Differential forms in electromagnetics. John Wiley & Sons (2004)

[386] T Frankel. The geometry of physics: an introduction. Cambridge University Press, Cambridge (2011).

[387] B Felsager. Geometry, Particles and Fields. Springer, New-York (1998).

[388] D Bachman. A geometric approach to differential forms. Birkhäuser, Boston (2012).

[389] T Dray. Differential forms and the geometry of general relativity. CRC Press, Boca Raton (2014).

[390] A Zee. Quantum Field Theory in a Nutshell. Princeton University Press, Princeton (2003).

[391] M Göckeler and T Schücker. Differential Geometry, gauge theories, and gravity. Cambridge University Press, Cambridge (1987).

[392] B Schutz. Geometrical methods of mathematical physics. Cambridge University Press, Cambridge (1980).

[393] MD Spivak. A comprehensive introduction to differential geometry. Publish or perish Inc., Houston (1970).

[394] A Robinson. Non-standard analysis. Princeton landmarks in mathematics and physics, Princeton University Press, Princeton (1996).

[395] FW Hehl and YN Obukhov. Foundations of classical electrodynamics: Charge, flux, and metric. Birhäuser, Boston (2003).

[396] WL Burke. Div, grad, curl are dead (1995). Available at `https://people.ucsc.edu/~rmont/papers/Burke_DivGradCurl.pdf`

[397] Y Choquet-Bruhat and C DeWitt-Morette, with M Dillard-Bleick. Analysis, manifolds and physics. North Holland,Amsterdam (1982).

[398] R Heras. The Helmholtz theorem and retarded fields. European Journal of Physics 37, 065204 (2016).

[399] S Carroll. Spacetime and geometry: An introduction to general relativity. Pearson, Harlow (2003).

[400] RH Price. General relativity primer. American Journal of Physics 50, pp. 300-329 (1982).

[401] M Gasperini. Theory of Gravitational interactions. Springer, Milan (2013).

[402] M Fecko. Differential geometry and Lie groups for physicists. Cambridge University Press, Cambridge (2006).

[403] DH Kobe. Helmholtz's theorem revisited. American Journal of Physics 54, pp. 552-554 (1986).

[404] FW Hehl and YN Obukhov. A gentle introduction to the foundations of classical electrodynamics: The meaning of the excitations (D, H) and the field strengths (E, B). arXiv preprint physics/0005084 (2000).

[405] EJ Post. Sagnac effect. Reviews of Modern Physics 39, 475 (1967).

[406] V Guillemin and S Sternberg. Symplectic techniques in physics. Cambridge university Press, Cambridge (1990).

[407] JC Maxwell. A treatise on electricity and magnetism. Clarendon press, Oxford (1881).

[408] H. Weber. Die partiellen Differential-Gleichungen der mathematischen Physik nach Riemann's Vorlesungen bearb. F. Vieweg & Sohn (1919).

[409] I Bialynicki-Birula and Z Bialynicka-Birula. The role of the Riemann-Silberstein vector in classical and quantum theories of electromagnetism. Journal of Physics A: Mathematical and Theoretical 46, 053001 (2013).

[410] F Kottler. Maxwellsche Gleichungen und Metrik, Sitzungsber. Akad. Wiss. Wien, Math.-Naturw. Klasse, Abt. IIa, 131, pp. 119–146 (1922). English translation by D Delphenich at `http://www.neo-classical-physics.info/`.

[411] D van Dantzig. The fundamental equations of electromagnetism, independent of metrical geometry, Proc. Cambridge Phil. Soc. 30, pp. 421–427 (1934).

[412] FW Hehl, Y Itin and YN Obukhov. On Kottler's path: Origin and evolution of the premetric program in gravity and in electrodynamics. International Journal of Modern Physics D, 25(11), 1640016 (2016).

[413] E Whittaker, A History of the Theories of Aether and Electricity, Vol. 2: The Modern Theories 1900-1926 (1953). Reprintedin Humanities Press, New York (1973).

[414] P Ehrenfest. Welche Rolle spielt die Dreidimensionalität des Raumes in den Grundgesetzen der Physik ? Ann. Physik, 61, pp. 440-446 (1920).

[415] FR Tangherlini. Schwarzschild field inn dimensions and the dimensionality of space problem. Nuovo Cim. 27 636 (1963).

[416] J Gonzalez-Ayala, R Cordero and F Angulo-Brown. Is the (3+ 1)-d nature of the universe a thermodynamic necessity?. EPL (Europhysics Letters), 113(4), 40006 (2016).

[417] A Berera et al. Knotty inflation and the dimensionality of spacetime. The European Physical Journal C, 77 (10), pp. 1-7 (2017).

[418] GF Rubilar. Linear pre-metric electrodynamics and deduction of the lightcone, Ph.D. Thesis, University of Cologne (2002); see Ann. Phys. (Leipzig) 11 pp. 717-782 (2002).

[419] YN Obukhov, T Fukui and GF Rubilar. Wave propagation in linear electrodynamics. Phys. Rev. D, 62(4), 044050 (2000).

[420] PA Ade and Polarbear Collaboration. POLARBEAR constraints on cosmic birefringence and primordial magnetic fields. Phys. Rev. D, 92(12), 123509 (2015).

[421] Y Itin. Nonbirefringence conditions for spacetime. Phys. Rev. D, 72(8), 087502 (2005).

[422] FW Hehl, YN Obukhov and GF Rubilar. Spacetime metric from linear electrodynamics II. arXiv preprint gr-qc/9911096 (1999).

[423] Y Itin, FW Hehl and YN Obukhov. Premetric equivalent of general relativity: Teleparallelism. Phys. Rev. D, 95(8), 084020 (2017).

[424] JW Maluf. The teleparallel equivalent of general relativity. Annalen der Physik, 525(5), pp. 339-357 (2013).

[425] ES Whittaker. On electric phenomena in gravitational fields. Proceedings of the Royal Society of London. Series A, 116 pp. 720-735 (1927).

[426] S Liberati, S Sonego S and M Visser. Scharnhorst effect at oblique incidence. Phys. Rev. D 63, 085003 (2001).

[427] KF Warnick, RH Selfridge and DV Arnold. Teaching electromagnetic field theory using differential forms. IEEE Transactions on education 40, pp. 53-68 (1997).

[428] HJ Eysenck. Genius: The natural history of creativity. Cambridge University Press, Cambridge (1995).

[429] MC Marchetti et al. Hydrodynamics of soft active matter. Reviews of Modern Physics, 85(3), 1143 (2013).

[430] S Ramaswamy. Active matter. Journal of Statistical Mechanics: Theory and Experiment, 2017(5), 054002 (2017).

[431] D Needleman and Z Dogic. Active matter at the interface between materials science and cell biology. Nature reviews materials, 2(9), pp. 1-14 (2017).

[432] P Provenzano et al. Collagen reorganization at the tumor-stromal interface facilitates local invasion. BMC medicine, 4(1), pp. 1-15 (2006).